

DOKUZ EYLÜL UNIVERSITY
GRADUATE SCHOOL OF NATURAL AND APPLIED SCIENCES

**ELECTRONIC STRUCTURE OF PARABOLIC
CONFINING QUANTUM WIRES WITH RASHBA
AND DRESSELHAUS SPIN-ORBIT COUPLING IN A
PERPENDICULAR MAGNETIC FIELD**

by

Sevil SARIKURT

August, 2013

İZMİR

**ELECTRONIC STRUCTURE OF PARABOLIC
CONFINING QUANTUM WIRES WITH RASHBA
AND DRESSELHAUS SPIN-ORBIT COUPLING IN A
PERPENDICULAR MAGNETIC FIELD**

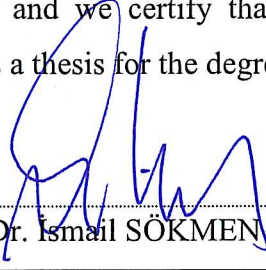
**A Thesis Submitted to the
Graduate School of Natural And Applied Sciences of Dokuz Eylül University
In Partial Fulfillment of the Requirements for the Degree of Doctor of
Philosophy in Physics**

**by
Sevil SARIKURT**


**August, 2013
İZMİR**

Ph.D. THESIS EXAMINATION RESULT FORM


We have read the thesis entitled “ELECTRONIC STRUCTURE OF PARABOLIC CONFINING QUANTUM WIRES WITH RASHBA AND DRESSELHAUS SPIN-ORBIT COUPLING IN A PERPENDICULAR MAGNETIC FIELD” completed by SEVİL SARIKURT under supervision of PROF. DR. İSMAİL SÖKMEN and we certify that in our opinion it is fully adequate, in scope and in quality, as a thesis for the degree of Doctor of Philosophy.


Prof. Dr. İsmail SÖKMEN


Supervisor


Prof. Dr. C. Cengiz ÇELİKOĞLU

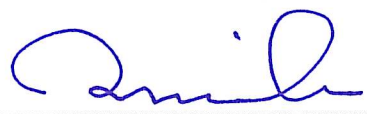
Thesis Committee Member


Yrd.Doç.Dr. Kadir AKGÜNGÖR

Thesis Committee Member


Prof. Dr. Yüksel ERGÜN

Examining Committee Member


Prof. Dr. Doğan DEMİRHAN

Examining Committee Member


Prof. Dr. Ayşe OKUR
Director

Graduate School of Natural and Applied Sciences

ACKNOWLEDGEMENTS

It is a great pleasure for me to thank all these people who play an important role in the successful completion of this work.

Firstly, I would like to express my deepest gratitude to my supervisor Prof. Dr. İsmail Sökmen for giving me the opportunity to do this thesis, providing his excellent guidance, continuous support and encouragement during the development of this thesis. He continually gave me detailed explanation with patience. I'm especially indebted to him for his faith in me during the period of this work.

I sincerely appreciate Assoc. Prof. Dr. Serpil Şakiroğlu for her motivation, endless support, useful comments about thesis, and sharing of her expertise. She deserves many thanks for her invaluable time and constant interest in my thesis and also contributions especially in preparation of the publications. This work would not have become possible without her courage and invaluable help.

I would like to explicitly express my sincere gratitude to Asst. Prof. Dr. Kadir Akgüngör for his support, endless help and sharing his knowledge and experience about high performance computing. I also want to thank Assoc. Prof. Dr. Tuğrul Hakioglu for suggesting spin-orbit coupling as a topic of my research and supporting me as a special student at Bilkent University during the spring semester 2007 – 2008. And I would like to say that I consider myself extremely lucky to have met such a large number of great people with summer schools and conferences which held under the chairmanship of him at Institute of Theoretical and Applied Physics (ITAP).

I would like to thank the Scientific and Technological Research Council of Turkey (TÜBİTAK) for five-year financial support within National Scholarship Programme for PhD Students (BİDEB-2211). Project that related to my PhD research is funded by Scientific Research Fund (SRF) of Dokuz Eylül University (DEU-BAP:2009183).

Many special thanks should also be delivered to Dr. Ümit Akıncı for always being a big brother to me and always giving me invaluable support. I would like to express my special thanks to Cem Çelik and Asst. Prof. Dr. Celal Cem Sarioğlu who helped me by providing a L^AT_EX template of thesis. I'm also thankful to all members of our working group: Zeynep Demir, Mehmet Batı, Aslı Çakan, Bircan Gişi, Dilek Polat Ulaş, Yenal Karaaslan, Dilara Gül and all people in the Physics department for their friendship and support. I would like to express my immense gratitude to all of my closer friends for all the great times that we have shared. Each of them has been very supportive to my efforts. Great thanks to one of my best friends, Özgün Koşaner for proofreading this dissertation.

Last but not least, I would like to thank my mother Keziban for helping me grow and becoming the person I am today. Thanks for everything you have done for me throughout my whole life. My special thanks also go to my sister Sevgi for providing me with invaluable emotional support. Your ceaseless love has been my foundation. I love you both so much and appreciate your patience, continual encouragement and showing me such dedication no matter what. Their generosity made it possible for me to bring this project into life. All the thanks in the world!...

I like to dedicate this thesis to my dear grandmother Ayşe Yalçın and grandaunt Gülşen Ülkütaş who are no long with us. I thank them for taking care of me during my childhood and during the weekdays while my parents were at work. Their roles in my life were immense. They will always be in my heart...

Sevil SARIKURT

ELECTRONIC STRUCTURE OF PARABOLIC CONFINING QUANTUM WIRES WITH RASHBA AND DRESSELHAUS SPIN-ORBIT COUPLING IN A PERPENDICULAR MAGNETIC FIELD

ABSTRACT

In this thesis, we have investigated theoretically the effect of spin-orbit coupling on the energy level spectrum and spin texturing of a quantum wire with parabolic confining potential subjected to perpendicular magnetic field. Additionally we have also taken into account exchange-correlation contribution. We have used finite element method to get numerical solutions of Schrödinger equation with high accuracy.

Our results have been revealed that the interplay of the spin-orbit coupling with effective magnetic field considerably modifies the band structure, producing additional subband extrema and energy gaps. In addition to these, we have obtained that the magnitude of spin splitting between energy subbands depends on the strength of the magnetic field. We have also found that spin orientation strongly depends on the applied external magnetic field and the strengths of SO couplings. Competing effects between external magnetic field and spin-orbit coupling terms have introduced complex features in spin texturing owing to couplings in energy subbands. We have seen that spatial modulation of spin density along the wire width can be considerably modified by spin-orbit coupling strength, magnetic field and charge carrier concentration. We have observed that the presence of exchange-correlation contribution leads to a softening behavior in the local maxima at subbands and shifts all energy subbands to lower energy values. We have also obtained that the combined effect of exchange-correlation and spin-orbit coupling produces asymmetry in the dispersion relations.

Keywords: Spin-orbit coupling, quantum wire, spin texture, density functional theory, exchange-correlation effect.

DİK MANYETİK ALAN ALTINDA RASHBA VE DRESSELHAUS SPİN YÖRÜNGE ETKİLEŞİMLİ PARABOLİK KUŞATILMIŞ KUANTUM TELİNİN ELEKTRONİK YAPISI

ÖZ

Bu tezde, spin-yörünge çiftleniminin dik manyetik alan altındaki parabolik hapsedme potansiyeline sahip kuantum telinin enerji spektrumu ve spin dağılımları üzerine etkisini teorik olarak inceledik. Buna ek olarak, deęiřtokuř-korelasyon katkısını içeren spin-yörünge sistemlerini de inceledik. Sonlu elemanlar yöntemini kullanarak Schrödinger denkleminin nümerik çözümlerini yüksek hassasiyetle elde ettik.

Elde ettięimiz sonuçlar, spin-yörünge çiftlenimi ile etkin manyetik alan arasındaki etkileşimlerin band yapısını önemli derecede deęiřtirdiğini, ek altband uçdeęerleri ve enerji aralıkları oluşturduğunu ortaya koymaktadır. Bu sonuçlara ek olarak enerji altbandları arasındaki spin ayrılmalarının büyüklüğünün manyetik alanın şiddetine baęlı olduğunu elde ettik. Ayrıca spin dağılım desenlerinin uygulanan manyetik alana ve spin-yörünge çiftleniminin şiddetine güçlü bir şekilde baęlı olduęu sonucunu elde ettik. Dış manyetik alan ve spin-yörünge çiftlenim terimleri arasındaki yarışmacı etkileşim enerji altbandlarındaki çiftlenimlerden dolayı spin dağılımında karmaşık özellikleri ortaya çıkarmaktadır. Kuantum telinin genişlięi boyunca spin yoğunluğunun uzaysal dağılımının spin-yörünge çiftleniminin kuvveti, manyetik alan ve yük taşıyıcı yoğunluęu aracılıęı ile önemli ölçüde deęiřtirilebildiğini gördük. Deęiřtokuř-korelasyon katkısının altbandların yerel maksimumları civarında bandın düzleşen bir davranışa sebep olduğunu ve bütün enerji altbandlarını daha düşük enerji deęerlerine kaydırduğunu gözlemledik. Ayrıca, deęiřtokuř-korelasyon ve spin-yörünge çiftleniminin enerji dağılımında asimetriye neden olduęu sonucunu elde ettik.

Anahtar Sözcükler : Spin-yörünge çiftlenimi, kuantum teli, spin yönelimi, yoğunluk fonksiyoneli teorisi, deęiřtokuř-korelasyon etkisi.

CONTENTS

	Page
THESIS EXAMINATION RESULT FORM.....	ii
ACKNOWLEDGEMENTS	iii
ABSTRACT	v
ÖZ.....	vi
LIST OF FIGURES	xiii
LIST OF TABLES.....	xiv
CHAPTER ONE – INTRODUCTION.....	1
CHAPTER TWO – LOW-DIMENSIONAL SYSTEMS & SPIN-ORBIT COUPLING	5
2.1 Two Dimensional Electron Gases.....	5
2.1.1 Quantum Wire	7
2.2 Semiconductor Spintronics	9
2.3 Origin of Spin-Orbit Coupling	10
2.4 Spin-Orbit Interaction and Inversion Asymmetry	13
2.4.1 Dresselhaus Spin-Orbit Coupling	15
2.4.2 Rashba Spin-Orbit Coupling	16
2.5 Zeeman Effect	18
CHAPTER THREE – THEORETICAL BACKGROUND	20
3.1 The Electronic Structure Problem.....	20
3.1.1 Born-Oppenheimer Approximation	21
3.2 Hartree and Hartree-Fock Approximation	23
3.3 Density Functional Theory	25
3.3.1 Hohenberg-Kohn Theorems	26
3.3.2 Kohn-Sham Equations.....	27
3.4 Exchange-Correlation Energy Functional	30

3.4.1 Local Density Approximation.....	31
3.4.2 Local Spin Density Approximation	32
3.5 Numerical Methodology: Finite Element Method	34
3.5.1 Area Coordinates and Linear Basis Functions in 1D	35
3.5.1.1 Linear Basis Functions in 1D.....	37
3.5.1.2 High Order Basis Functions in 1D	39
3.5.2 Solution of the Confined Quantum Mechanical Systems with FEM.....	44
3.5.3 Solution of Coupled Systems with FEM.....	52
CHAPTER FOUR – FORMALISM OF THE PHYSICAL SYSTEM	67
4.1 Introduction.....	67
4.2 Hamiltonian of the Physical System.....	68
4.3 Dimensionless Form of Hamiltonian.....	70
4.3.1 Kohn-Sham Hamiltonian and Exchange-Correlation Potential.....	74
4.3.1.1 Non-collinear Local-Spin Density Approximation.....	76
4.4 Spin Orientation.....	80
CHAPTER FIVE – RESULTS AND DISCUSSIONS	83
5.1 Numerical Results	83
5.1.1 Energy Bands	83
5.1.1.1 Without Magnetic Field.....	84
5.1.1.2 With Magnetic Field	87
5.1.2 Wave Functions.....	90
5.1.3 Spin Orientation.....	93
5.1.3.1 Without Spin-Orbit Interaction.....	94
5.1.3.2 Without External Magnetic Field.....	95
5.1.3.3 In The Presence of Both Spin-Orbit Interaction and External Magnetic Field.....	96
5.1.4 Effects of Exchange-Correlation Energy	99
5.1.4.1 Energy Bands Without Magnetic Field	100
5.1.4.2 Energy Bands With Magnetic Field	103

5.1.4.3 Spin Orientation Without Spin-Orbit Interaction	109
5.1.4.4 Spin Orientation Without Magnetic Field.....	111
5.1.4.5 Spin Orientation In The Presence of Both Spin-Orbit Interaction and Magnetic Field	112
CHAPTER SIX – CONCLUSION	115
REFERENCES.....	118

LIST OF FIGURES

	Page
Figure 2.1 Energy bands of two components of a GaAs/AlGaAs heterojunction ..	6
Figure 2.2 Schematic representation of quantum confinement structures.....	7
Figure 2.3 Schematical view of a QWR that was fabricated by cleaved-edge overgrowth method	8
Figure 2.4 The schematic band profile of 2DEG quantum well	17
Figure 2.5 The Rashba SO interaction in a system with SIA along the \hat{z} direction. (a) The effective field from the Rashba term is linear in k and always perpendicular to \mathbf{k} (b) Energy dispersion of Rashba spin-split subbands for a one- dimensional system. (c) Energy subbands for two-dimensional system	18
Figure 3.1 Schematic representation of the self-consistent solution of Kohn- Sham Equation.....	31
Figure 3.2 Global element, local element and element nodes in 1D	35
Figure 3.3 Schematic representation of the problem domain in 1D	36
Figure 3.4 (a) Work space which is divided into global elements. (b) Global element which has two nodes (1D).	37
Figure 3.5 One dimensional shape functions with two nodes ($N_{ngen} = 2$) in a global element	39
Figure 3.6 Area coordinates and positions of nodes in a global element.....	39
Figure 3.7 One dimensional shape functions with three nodes ($N_{ngen} = 3$) in a global element	41
Figure 3.8 Area coordinates and positions of nodes in a global element.....	41
Figure 3.9 One dimensional shape functions with four nodes ($N_{ngen} = 4$) in a global element	42
Figure 3.10 A global element with five nodes in (1D)	43
Figure 3.11 One dimensional shape functions with five nodes ($N_{ngen} = 5$) in a global element	44
Figure 4.1 Schematic representation of the wire system.....	67

Figure 4.2 A representation for intersection points between the Fermi energy and $E - k_y$ curve.	81
Figure 5.1 Quantum-wire energy dispersions with no Dresselhaus SO interaction term at zero magnetic field for three different Rashba SO strengths	85
Figure 5.2 Subband energy spectra of QWR for various Rashba and Dresselhaus SO coupling strengths at $B = 0$	86
Figure 5.3 (a) Energy spectrum at $k_y = 0$ as a function of ω_c/ω_0 . (b)-(c) Energy dispersion of a QWR subjected to external magnetic field in the absence of SO interactions ($\omega_c/\omega_0 = 0.5$ and $\omega_c/\omega_0 = 2$, respectively)	88
Figure 5.4 Energy dispersion of the spin-split subbands under the influence of external magnetic field and Rashba SO interaction	89
Figure 5.5 (a) Energy subband dispersion at $B = 0$ with Rashba ($\Delta_{so}^R/\hbar\omega_0 = 0.5$) and Dresselhaus ($\Delta_{so}^D/\hbar\omega_0 = 0.25$) SO coupling effect (b) Energy spectrum at $k_y = 0$ as a function of ω_c/ω_0 . (c) Energy dispersion of the wire at a finite magnetic field ($\omega_c/\omega_0 = 2$)	90
Figure 5.6 (a) Energy subband dispersion at $B = 0$ with the equal strength of Rashba and Dresselhaus SO interaction ($\Delta_{so}^R/\hbar\omega_0 = \Delta_{so}^D/\hbar\omega_0 = 0.25$) (b) Energy spectrum at $k_y = 0$ as a function of ω_c/ω_0 . (c) Energy dispersion of the wire at a finite magnetic field ($\omega_c/\omega_0 = 2$).	91
Figure 5.7 Real and imaginary parts of the spinor wave function as a function of x/l_0 in the first subband for the case of strong magnetic field and the absence of SO interaction	92
Figure 5.8 Real and imaginary parts of the spinor wave function as a function of x/l_0 in the first subband when the QWR is under the effect of Rashba SO interaction and external magnetic field	92
Figure 5.9 Spinor wave function components as a function of x/l_0 for the lowest spin-split level in the presence of weak Dresselhaus SO interaction and strong magnetic field	93
Figure 5.10 The components of the spinor wave function when both SO interaction and external magnetic field are present	93

Figure 5.11 Spin density components in the absence of Rashba and Dresselhaus SO interactions at $\hbar\omega_0 = 2 \text{ meV}$	94
Figure 5.12 Spin densities under the influence of weak SO couplings at $\omega_c/\omega_0 = 0$ and $\hbar\omega_0 = 2 \text{ meV}$	96
Figure 5.13 Spatial variation of spin density components in the presence of weak Rashba and Dresselhaus SO coupling strengths at different magnetic fields	97
Figure 5.14 Spin texture for the strong Rashba and Dresselhaus SO couplings. Magnetic field is varied from weak to strong limit.....	98
Figure 5.15 Spin texture for the case when both spin-split branches of the lowest subband are occupied. Strong Rashba and Dresselhaus SO couplings case is considered for three different values of magnetic field.....	100
Figure 5.16 Exchange-correlation effect on the energy subband structure of the QWR in the absence of Dresselhaus SO interaction term at zero magnetic field for low density regime.....	101
Figure 5.17 Energy dispersion relations of the subbands for weak and strong SO interactions at $B = 0$	102
Figure 5.18 Energy subband dispersion at $\rho_{1D}l_0 \simeq 0.43$ with strong regime of Rashba SO coupling and zero Dresselhaus SO coupling. The strength of the magnetic field is varied from weak to strong limit	104
Figure 5.19 Energy subband dispersion at $\rho_{1D}l_0 \simeq 0.43$ with zero Rashba SO coupling and strong regime of Dresselhaus SO coupling for two different values of magnetic field	105
Figure 5.20 Subband energy spectra of the QWR with no Dresselhaus SO interaction term at strong magnetic field and low electron density. Rashba SO coupling strength is varied from weak to strong regime	106
Figure 5.21 Subband energy spectra of QWR with no Rashba SO interaction term at strong magnetic field and low electron density for two different values of Dresselhaus SO coupling strength.....	107
Figure 5.22 Energy dispersion of the spin-split subbands at $\rho_{1D}l_0 \simeq 0.43$ for two different values of magnetic field when Rashba SO interaction is strong and Dresselhaus SO interaction is weak	107

Figure 5.23 Energy subband dispersion for weak strength of Rashba and Dresselhaus SO interactions at a finite magnetic field.....	108
Figure 5.24 Energy subband dispersion for equal strength of weak and strong SO interactions at a finite magnetic field.....	109
Figure 5.25 Energy subband dispersion for different mechanism of Rashba and Dresselhaus SO interactions.....	110
Figure 5.26 Subband energy spectra of QWR with strong SO coupling strengths for two density limits at a finite magnetic field.....	111
Figure 5.27 Spin density components in the absence of both SO coupling terms at $\omega_c/\omega_0 = 1$ for different density limits. (a) low-density limit (b) high-density limit.....	112
Figure 5.28 Spin densities under the influence of exchange-correlation and weak SO couplings at $\omega_c/\omega_0 = 0$ and $\hbar\omega_0 = 2 \text{ meV}$	112
Figure 5.29 Spatial variation of spin density components for the case of different SO coupling strengths at a finite magnetic field value and low density regime in the absence/presence of the exchange-correlation contribution.....	113
Figure 5.30 Spin texture for the strong Rashba and Dresselhaus SO couplings in the absence/presence of the exchange-correlation effect. Magnetic field is varied from weak to strong limit.....	114

LIST OF TABLES

	Page
Table 3.1 Matrix representations in FEM notation	45
Table 3.2 Mathematical notation of matrices for coupled systems	53

CHAPTER ONE

INTRODUCTION

In recent years, spintronics (short for **spin** transport **electronics** or **spin**-based **electronics**) has become an ever-evolving research field of magnetic electronics which uses the spin of electrons rather than its charge to store information (Bader & Parkin, 2010). The aim of this multidisciplinary field is to understand the interaction between the particle's spin and its solid-state environment, to investigate spin transport in electronic materials and to produce useful electronic devices (e.g. spin-FETs (field effect transistor), MRAM (magnetoresistive random-access memory), etc.) based on the quantum properties of the electron (Fabian, Matos-Abiaguea, Ertlera, Stano, & Zutic, 2007, Zutic, Fabian, & Sarma, 2004).

In spin-based semiconductor devices, spin-orbit (SO) interaction is considered as an important tool for controlling and manipulating of the spin orientation (Malet, Pi, Barranco, Serra, & Lipparini, 2007, Zhang, Liang, Zhang, Zhang, & Liu, 2006, Knobbe & Schäpers, 2005). For a two-dimensional electron gas (2DEG), confined in a semiconductor heterostructure, two major SO terms are usually present. The first one is Rashba SO coupling (Rashba, 1960) arising due to structure inversion asymmetry along the growth direction in quantum heterostructures where 2DEG is realized. The other term is Dresselhaus SO coupling (Dresselhaus, 1955) which is due to bulk inversion asymmetry of the lattice (Winkler, 2003). The strengths of the SO terms are difficult to measure independently, but a full understanding of their strengths is crucial (Schliemann, Egues, & Loss, 2003) for investigations of spin dependent phenomena in low dimensional structures (Debald & Kramer, 2005, Serra, Sanchez, & Lopez, 2005, Giglberger, Golub, Bel'kov, Danilov, Schuh, Gerl, & et al., 2007).

Spin density modulation emerged in quantum confined systems known as "spin texturing effect" is important for spintronics due to the fact that it provides information about the spatial distribution of the effective magnetic field in the presence of SO interaction (Upadhyaya, Pramanik, Bandyopadhyay, & Cahay, 2008b, Gujarathi, Alam, & Pramanik, 2012). In recent years, investigations of SO coupling effects in

low-dimensional systems have attracted a considerable amount of interest. There are many theoretical (Governale & Zülicke, 2002, Upadhyaya et al., 2008b, Governale & Zülicke, 2004) and experimental (Meier, Salis, Shorubalko, Gini, Schön, & Ensslin, 2007, Guzenko, Bringer, Knobbe, Hardtdegen, & Schäpers, 2007, Schäpers, Guzenko, Bringer, Akabori, Hagedorn, & Hardtdegen, 2009, Quay, Hughes, Sulpizio, Pfeiffer, Baldwin, West, & et al., 2010) studies which survey extensively the effects of SO coupling on the electronic and transport properties of these systems. Moroz & Barnes (1999, 2000) and Mireles & Kirczenow (2001) theoretically calculated the influence of Rashba SO interaction on the band structure and transport at low temperature of quasi-one-dimensional (1D) electron systems. Perroni, Bercioux, Ramaglia, & Cataudella (2007) discussed spectral and the transport properties of a quasi-1D quantum wire (QWR) with hard-wall boundaries in the presence of Rashba SO interaction while Pramanik, Bandyopadhyay, & Cahay (2007) numerically calculated the energy dispersion relations and spatial variation of spin components of InAs QWR in the presence of both SO interactions. More recently Gujarathi et al. (2012) reported the subband structure and spatial modulation of spin density in a QWR with hard-wall confinement for a wide range of magnetic field, Dresselhaus SO coupling strength and carrier concentration. The electronic structure of Rashba spin-split QWR that is parabolically confined under the influence of perpendicular magnetic field has been studied by Knobbe & Schäpers (2005) and Debald & Kramer (2005). Furthermore Zhang, Liang & et al. (2006) obtained the energy band structure of QWRs described by a parabolic confinement potential and subjected to an external magnetic field taking into account both Rashba and Dresselhaus SO interaction. In Ref. Zhang, Zhao, & Li (2009), researchers reported that the interplay of Rashba, Dresselhaus and the lateral SO interaction as well as applied magnetic field in a parabolic QWR leads to rather complex electrosubbands. An analytical approximation schemes suitable for obtaining the energy spectrum of quasi-1D QWR with SO coupling has been developed by Erlingsson, Egues, & Loss (2010) and Gharaati & Khordad (2012). Experimental works have been performed by several researchers. The effect of Rashba SO coupling in InGaAs/InP QWR structures has been discussed in Refs. Guzenko et al. (2007), Schäpers, Knobbe, Guzenko, & van der Hart (2004b) and Schäpers, Knobbe,

& Guzenko (2004a). On the other hand, in Ref. Schäpers, Guzenko & et al. (2009) the effect of both SO coupling terms in 2DEG and QWR structures have been investigated.

Although there are several studies related to Rashba and Dresselhaus SO interactions in quantum confined systems, to our knowledge, less attention has been paid on the spin texture calculations for parabolically confined QWRs in an external magnetic field. Detailed investigation of electrosubbands and spin density modulation could be useful for identification of spin polarization in zinc-blende QWRs.

In this thesis, we focus on the Rashba and Dresselhaus SO couplings and external magnetic field extensively. We calculate the energy spectrum of spin-split subbands and spin orientations of a parabolically confined QWR considering various strengths of Rashba and/or Dresselhaus SO couplings in the existence or absence of perpendicular magnetic field for different carrier concentrations. We also study the exchange-correlation effects to the energy band with Rashba and/or Dresselhaus SO coupling for different strengths of magnetic field.

This work is organized as follows: In Chapter 2 general knowledge about 2DEG and semiconductor QWRs is presented. And then a brief description of SO coupling and Zeeman effect is given. Both types of SO coupling terms (Rashba and Dresselhaus) are also presented concisely. A short statement about the theoretical fundamental theorems and numerical solution methods which are used in this thesis are given in Chapter 3. We identify the Schrödinger equation and also finite element method formalism of the physical system in Chapter 4. We derive the analytical formulations for the solution of total Hamiltonian which includes SO coupling contribution, Zeeman effect and additional potentials (e.g. confinement potential, exchange-correlation potential). Afterwards, in Chapter 5 we present numerical results for analyzing how the SO coupling and externally applied magnetic field affects the energy subband dispersion and spin-texturing of a parabolically confined quasi-1D QWR. We examine several cases with the presence or absence of a uniform magnetic field. Based on these results we discuss the interplay between different SO interaction contributions and various strengths of external magnetic field. We also investigate the spin orientation for various

SO coupling strengths. We then present numerical results that indicate the influence of exchange-correlation potential on energy band structure of the quasi-1D QWR. The conclusions and discussions of the thesis are summarized in Chapter 6.

CHAPTER TWO

LOW-DIMENSIONAL SYSTEMS & SPIN-ORBIT COUPLING

In this chapter we briefly introduce the physics of low-dimensional systems and then give information about spin-based electronics substantially.

In section 2.1.1, a short description of quantum wire is given exclusively. Section 2.2 includes a brief information about spintronics. Fundamental studies of spintronics include understanding spin dynamics and spin relaxation. It is important to mention that, SO interactions have major influences on the emerging field of spintronics by virtue of the fact that these interactions provide means to manipulate spins without the use of magnetic fields (Bin, 2010). In section 2.3, we review the basic physical concepts that needed to understand the physics of SO interaction. We give a brief introduction of Rashba and Dresselhaus SO coupling under Section 2.4.

2.1 Two Dimensional Electron Gases

Semiconductor heterostructures are now tremendously used in electronics and optoelectronics. Heterostructures are primarily used to confine electrons and holes and to produce low-dimensional electronic systems (Singh, 2003).

A heterojunction is made by growing materials with similar lattice constants but different band gaps. One of the most widely used heterostructure systems is that formed from the compound semiconductor GaAs and the semiconductor alloy $\text{Al}_x\text{Ga}_{1-x}\text{As}$. Their lattice constants are nearly identical and also this semiconductor pair is well lattice-matched at any alloy composition x (Shik, 1998). The difference between their band gaps are considerable and also the Fermi energy in the widegap AlGaAs layer is higher than that in the narrow gap GaAs layer (see Fig. 2.1) (Datta, 1995).

When AlGaAs and GaAs layers are brought in contact with each other, electrons flow from the higher potential in the AlGaAs into the GaAs, leaving behind positively-

charged donors. This space charge gives rise to an electrostatic potential that leads the bands edges to bend near the interface. Due to the discontinuities in the bands, a narrow triangle-like potential well occurs in the GaAs layer at the GaAs/ $\text{Al}_x\text{Ga}_{1-x}\text{As}$ interface as it is illustrated in Fig. 2.1. And thus, electrons are confined by this triangular potential. The electrons are free to move in the plane parallel to the heterojunction but restricted in the confinement direction that perpendicular to the interface. Hereby a two-dimensional electron gas is formed (Schöll, 1998).

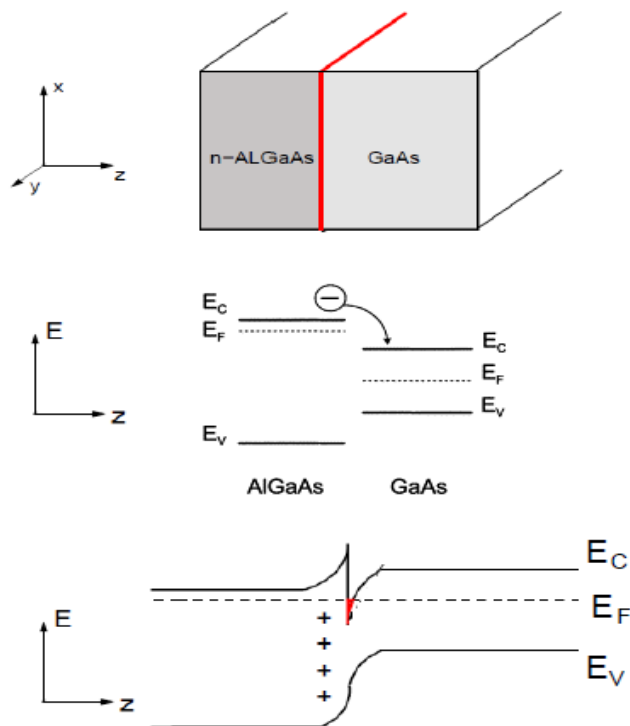


Figure 2.1 Energy bands of two components of a GaAs/AlGaAs heterojunction. By mixing layers of materials with different band gaps it is possible to restrict electron movement to the interface between the materials. As a result 2DEG is formed at the interface between two semiconductors.

The quantum confinement restricts the motion of electrons in one or more directions. Depending on whether the confinement occurs in one, two or even all three spatial directions, the electrons can move only in the remaining two, one or zero directions, respectively (Fig. 2.2). And these structures can be quantum wells (2D), quantum wires (1D), or quantum dots (0D). A quantum well (QW) is formed when the motion of electrons is restricted only one direction. In the case of QWRs, the electrons have only one free dimension to move, the other two dimensions are restricted.

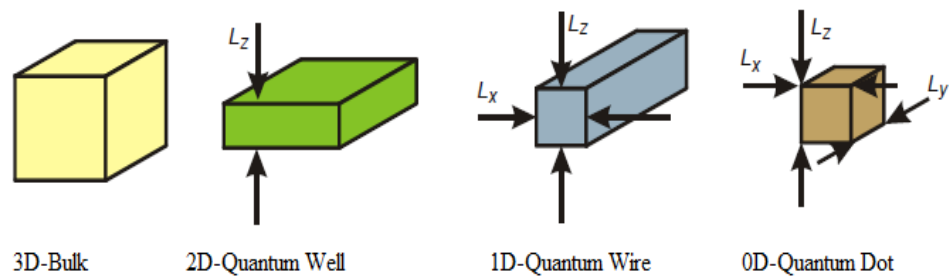


Figure 2.2 Schematic representation of quantum confinement structures. In bulk semiconductor materials, the electrons move freely in all directions. As the dimensions of the material restrict, the effect of quantum confinement arises.

Additional confinement in the remaining direction completely confines the motion of electrons. Such systems are called quantum dots (QD). It is beneficial to indicate that aforementioned situation of the electron motion exhibits quantum effects which is a powerful way in the design of electronic devices (Weisbuch & Vinter, 1991).

2.1.1 Quantum Wire

In the past few years, a great deal of attention has been focused on the physics of low-dimensional semiconductor structures such as QWs, QWRs, and QDs since nowadays electronic devices have been intentionally approaching ever smaller size and therefore reduced physical dimensionalities. Extensive research on the quantum mechanical nature of restricted semiconductor systems exhibit fascinating new electronic and optical properties that permit improvement in the performance of electronic devices (Khordad, 2013).

QWRs of all these low-dimensional semiconductor structures have shown noteworthy optical, electronic, magnetic, and mechanical properties that have a wide range of applications in future technologies such as conducting nanowire in quantum computing devices (Banerjee, Dan, & Chakravorty, 2002, Kumar, Lahon, Jha, & Mohan, 2013).

Semiconductor QWRs (or quasi-1D electron gases), which are realized by applying split gates on top of a 2DEG in a semiconductor heterostructure, have been studied

intensively for a wide spectrum of materials. Most QWRs fabricated and studied experimentally are of GaAs/Al_xGa_{1-x}As heterostructures (Sun, 1995).

The most widespread used methods for fabrication of QWR structures rely on the growth of heterostructures by molecular-beam epitaxy (MBE) (Herman, 1994) or metal-organic chemical vapor deposition (MOCVD) (Thompson, 1997) and afterwards lateral restriction of the electron motion either by gates, or by lithography in conjunction with etching techniques (Weisbuch & Vinter, 1991).

In 1982, Petro, Gossard, Logan, & Wiegmann reported for the first time the fabrication of GaAs/AlGaAs quantum well-wires using MBE growth method combined with electron-beam lithography and wet/dry chemical etching. Kash and his coworkers (Kash, Scherer, M. Worklock, Craighead, & Tamargo, 1986) manufactured QWRs in a different way which was based on the direct processing of QWs into QWRs using the same growth technique. Refs. Asahi (1997) and Wang & Voliotis (2006) involve an overview of the growth methods and formation of various QWR structures extensively. A QWR sample that fabricated from GaAs/AlGaAs heterostructures using the cleaved-edge overgrowth (CEO) technique by de Picciotto and his coworkers (Picciotto, Stormer, Pfeiffer, Baldwin, & West, 2001) is demonstrated in Fig. 2.3.

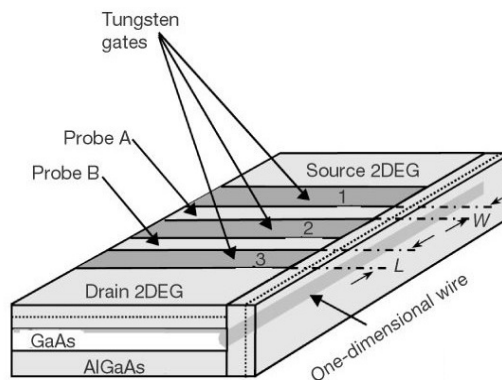


Figure 2.3 Schematic view of a QWR that was fabricated by cleaved-edge over-growth method. The fabrication starts with a high-quality 2DEG created by epitaxial growth of a unilaterally doped GaAs quantum well onto a GaAs substrate. The pre-fabricated tungsten gate electrodes (for example, gate 1) are used to separate the 2DEG from the wire.

This thesis is about semiconductor QWRs that presents theoretical studies of the electronic structure of QWRs under the effects of both type of SO coupling and externally applied magnetic field.

2.2 Semiconductor Spintronics

Spintronics, which offer a new generation of information storage and manufacturing of electronic equipments, refers to manipulate and control the electron spin in quantum-electronic devices. This is usually achieved by applying an external magnetic field to rotate the spin, and one can control the spin electronically in the presence of SO coupling. In recent years, there has been fascinating improvement in this field, both in experiment and in developing theoretical concepts. On account of the fact that the aims of spintronics are considerably intriguing, research is developing along several fields (Rashba, 2007). This spin-based electronics characterizes electrical, optical, and magnetic properties of solids. Fundamental studies of spintronics include exploration of spin polarization and spin transport in electronic materials, as well as of spin dynamics and spin relaxation (Fabian et al., 2007).

The Giant Magneto-Resistive (GMR) effect, which is discovered in 1988 by French and German physicists, is considered as the beginning of the spintronics. This effect is the primary operating principle behind current hard-drive technology and also the subject of the 2007 Nobel Prize in physics (Fert, 2007, Grünberg, 2007).

The comprising spin of electrons besides its charge contributes to the electronic devices to gain new functionalities and one of the most ambitious goals of spintronics is accomplishing quantum computing with electron spins (Fabian et al., 2007, Rashba, 2007).

Semiconductor spintronics combines semiconductor microelectronics with spin dependent effects that arise from the interaction between the spin of a charge carrier and the magnetic properties of the materials. In spintronic devices, the spin degree

of freedom of the electron which provides functionality in addition to the charge of the electron plays an important role. Adding the spin degree of freedom to conventional charge-based electronics or using the spin degree of freedom alone will add more capability and performance to electronic products (Wolf, Awschalom, Buhrman, Daughton, von Molnár, Roukes, & et al., 2001).

2.3 Origin of Spin-Orbit Coupling

“Spin-orbit” coupling is described as the interaction between an electron’s spin and its motion through the electromagnetic field of the nucleus, which shifts atomic energy levels. The SO interaction can remove the degeneracy of electron energy levels in many atoms, molecules and solids. Doubly degenerated bands split into spin-up and spin-down levels in the presence of SO coupling.

SO interaction can be included as a relativistic correction to the Schrödinger equation. To obtain a representation for the SO interaction, we need to start with the Dirac equation which is the main equation for electronic systems. This equation describes the electron spin and involves its relativistic feature.

The derivation of the SO interaction has been taken from J. J. Sakurai (Sakurai, 1967) and R. Winkler (Winkler, 2003).

Time-dependent Schrödinger equation is known as

$$i\hbar \frac{\partial \Psi}{\partial t} = \mathcal{H}\Psi \quad (2.3.1)$$

For a free particle the Dirac Hamiltonian can be written in the form:

$$\mathcal{H} = c\boldsymbol{\alpha} \cdot \mathbf{p} + \beta mc^2 + \mathbb{V} \quad (2.3.2)$$

where m is the free electron mass, c is the speed of light, \mathbf{p} is the momentum operator,

\mathbb{V} is arbitrary scalar potential

$$\mathbb{V} = V \cdot I = \begin{pmatrix} V & 0 \\ 0 & V \end{pmatrix}$$

and α, β are four-dimensional matrices:

$$\alpha = \begin{pmatrix} 0 & \boldsymbol{\sigma} \\ \boldsymbol{\sigma} & 0 \end{pmatrix} \quad \beta = \begin{pmatrix} \mathbb{I} & 0 \\ 0 & -\mathbb{I} \end{pmatrix} \quad (2.3.3)$$

Here, \mathbb{I} is the two-by-two identity matrix and $\boldsymbol{\sigma} = (\sigma_x, \sigma_y, \sigma_z)$ are the well known Pauli spin matrices.

$$\sigma_x = \begin{pmatrix} 0 & 1 \\ 1 & 0 \end{pmatrix} \quad \sigma_y = \begin{pmatrix} 0 & -i \\ i & 0 \end{pmatrix} \quad \sigma_z = \begin{pmatrix} 1 & 0 \\ 0 & -1 \end{pmatrix} \quad (2.3.4)$$

With using Eqs. (2.3.1) and (2.3.2), the Dirac equation can be introduced by

$$i\hbar \frac{\partial \Psi}{\partial t} = (c\boldsymbol{\alpha} \cdot \mathbf{p} + \beta mc^2 + V)\Psi \quad (2.3.5)$$

Here, Ψ is the solution of Dirac equation and this wave function denotes a four-component spinor which can be defined by two component spinors ψ_A (upper spinor) and ψ_B (lower spinor):

$$\Psi = \begin{pmatrix} \psi_A \\ \psi_B \end{pmatrix} \quad (2.3.6)$$

With using the definition of the matrices α and β (Eq. (2.3.3)), an expression for the coupled equations can be written in terms of two-component spinors ψ_A and ψ_B as in the following equations:

$$(\boldsymbol{\sigma} \cdot \mathbf{p}) \psi_B = \frac{1}{c}(E' - V)\psi_A \quad (2.3.7a)$$

$$(\boldsymbol{\sigma} \cdot \mathbf{p}) \psi_A = \frac{1}{c}(E' - V + 2mc^2)\psi_B \quad (2.3.7b)$$

Consequently, Dirac equation becomes a set of coupled equations for ψ_A and ψ_B . We assume that $E' = E - mc^2$ to study the non-relativistic limit of the Dirac equation. Using the second equation (Eq. (2.3.7b)) we obtain lower spinor ψ_B in terms of upper spinor

ψ_A .

$$\psi_B = \boldsymbol{\sigma} \cdot \mathbf{p} \left[\frac{c}{(E' - V + 2mc^2)} \right] \psi_A \quad (2.3.8)$$

Substituting this expression of ψ_B into Eq. (2.3.7a) we can get

$$(\boldsymbol{\sigma} \cdot \mathbf{p}) (\boldsymbol{\sigma} \cdot \mathbf{p}) \left[\frac{c^2}{(E' - V + 2mc^2)} \right] \psi_A = (E' - V) \psi_A \quad (2.3.9)$$

We can expand the energy denominator $[E' - V + 2mc^2]^{-1}$ in the non-relativistic limit ($(E' - V)/2mc^2 \ll 1$), into

$$\frac{c^2}{E' - V + 2mc^2} = \frac{1}{2m} \left(1 + \frac{E' - V}{2mc^2} \right)^{-1} \approx \frac{1}{2m} \left[1 - \frac{E' - V}{2mc^2} + \dots \right] \quad (2.3.10)$$

If we neglected the terms of order $(v/c)^2$ we would get the Pauli equation. Keeping only the first term in this expansion (Eq. (2.3.10)) we get ψ_B as follows:

$$\psi_B \approx \frac{1}{2mc} (\boldsymbol{\sigma} \cdot \mathbf{p}) \psi_A \quad (2.3.11)$$

And inserting the above equation into Eq. (2.3.9) we simply obtain the non-relativistic limit of the Dirac equation, or the Pauli equation

$$\left[\frac{1}{2m} (\boldsymbol{\sigma} \cdot \mathbf{p})^2 + V \right] \psi_A = E' \psi_A \quad (2.3.12)$$

This eigenvalue equation can be thought as the time-dependent Schrödinger equation for ψ_A . Due to the fact that, ψ_A itself does not satisfy the normalization requirement we cannot identify ψ_A as a full wave function. The probabilistic interpretation of the Dirac theory requires that

$$\int d^3r \Psi^\dagger \Psi = \int d^3r (\psi_A^\dagger \psi_A + \psi_B^\dagger \psi_B) = 1 \quad (2.3.13)$$

With using the definition of ψ_B in terms of ψ_A we can rewrite the normalization

requirement as in the following equation

$$\int d^3r \psi_A^\dagger \left(1 + \frac{\mathbf{p}^2}{4m^2c^2}\right) \psi_A = 1 \quad (2.3.14)$$

Here, we also use this equality:

$$(\boldsymbol{\sigma} \cdot \mathbf{X})(\boldsymbol{\sigma} \cdot \mathbf{Y}) = \mathbf{X} \cdot \mathbf{Y} + i\boldsymbol{\sigma} \cdot [\mathbf{X} \times \mathbf{Y}] \Rightarrow (\boldsymbol{\sigma} \cdot \mathbf{p})^2 = \mathbf{p}^2$$

Eq. (2.3.14) suggests that we should work with a new two-component wave function Ψ defined by

$$\Psi = \left(1 + \frac{\mathbf{p}^2}{8m^2c^2}\right) \psi_A$$

which is correctly normalized to unity.

Replacing ψ_A in Eq. (2.3.9) by $\psi_A = [1 + \mathbf{p}^2/(8m^2c^2)]^{-1} \Psi$ and using the expansion Eq. (2.3.10), we obtain after some rearrangement (Sakurai, 1967) the Pauli equation, or the non-relativistic limit of Dirac equation,

$$\left[\frac{\mathbf{p}^2}{2m} + V - \frac{\mathbf{p}^4}{8m^3c^2} - \frac{\hbar}{4m^2c^2} \boldsymbol{\sigma} \cdot [\mathbf{p} \times \nabla V] + \frac{\hbar^2}{8m^2c^2} \nabla^2 V \right] \Psi = E\Psi \quad (2.3.15)$$

The first and second term on the left hand side are the non-relativistic kinetic and potential energy, respectively. The third term is the relativistic correction to the kinetic energy and the fourth is the SO coupling term. The last term is called the Darwin term and it gives a shift in energy.

2.4 Spin-Orbit Interaction and Inversion Asymmetry

SO interaction leads to a coupling between the spin of a particle and its orbital motion. SO coupling lifts the spin degeneracy of the conduction band electrons of III-V compound semiconductor heterostructures without any external magnetic field.

The general form of the SO interaction in a single particle Hamiltonian is given by

Pauli equation (Eq. (2.3.15)):

$$\mathcal{H}_{so} = -\frac{\hbar}{4m^2 c^2} \boldsymbol{\sigma} \cdot [\mathbf{p} \times \nabla V] \quad (2.4.1)$$

where V is the electric potential.

A moving electron in an electric field feels an effective magnetic field even in the absence of external magnetic field. The spin magnetic moment of the electron is influenced by this effective magnetic field (Sugahara & Nitta, 2010). The principle of SO interaction is based on these effects. In analogy to Zeeman Hamiltonian, $\mathcal{H}_Z = \mu_B \boldsymbol{\sigma} \cdot \mathbf{B}$, the strength of effective magnetic field of the SO interaction is

$$\mathbf{B}_{eff} = \frac{\mathbf{p} \times \mathbf{E}}{2mc^2} \quad (2.4.2)$$

This equation indicates that the direction of this effective magnetic field is perpendicular to both the electron momentum and the electric field.

In III-V semiconductor heterostructures, spin-splitting in energy subbands results from the lack of inversion symmetries namely bulk inversion asymmetry (BIA) and structural inversion asymmetry (SIA).

The inversion symmetry in space and time change the wave vector \mathbf{k} into $-\mathbf{k}$, and furthermore, the time inversion also flips the orientation of the spin.

$$\text{Behavior under time reversal} \quad \Rightarrow \quad E(\mathbf{k}, \uparrow) = E(-\mathbf{k}, \downarrow)$$

$$\text{Behavior under spatial inversion} \quad \Rightarrow \quad E(\mathbf{k}, \uparrow) = E(-\mathbf{k}, \uparrow)$$

$$\text{Result} \quad \Rightarrow \quad E(\mathbf{k}, \uparrow) = E(\mathbf{k}, \downarrow)$$

Here, \uparrow and \downarrow label spin-up and spin-down projections, respectively. In III-V zinc blende semiconductors, there is no inversion symmetry ($E(\mathbf{k}, \uparrow) \neq E(\mathbf{k}, \downarrow)$) and thus for $k \neq 0$ the spin bands can be split in energy. Spatial inversion asymmetry in crystal structures leads to coupling between the motion of a charge carriers and its spin states, and thus it results in spin-splitting of the energy band.

Inversion asymmetry properties of low-dimensional systems give rise to the Dresselhaus (Dresselhaus, 1955) and Rashba (Rashba, 1960, Bychkov & Rashba, 1960) SO couplings. The SO coupling caused by bulk inversion asymmetry of the crystal structure is known as the Dresselhaus SO coupling. The structural inversion asymmetry of the confinement potential of electrons in a semiconductor heterostructure leads to Rashba type SO coupling.

2.4.1 Dresselhaus Spin-Orbit Coupling

The moving electrons through the lattice of III-V zinc-blende semiconductor structures experience an asymmetric crystal potential which is defined as bulk inversion asymmetry. This asymmetry causes a spin-depending energy splitting in k-space that was investigated theoretically by Dresselhaus (Dresselhaus, 1955).

The Hamiltonian that represent the Dresselhaus SO coupling for a bulk zinc blende structure is given as (Schäpers et al., 2009)

$$\mathcal{H}_D = \gamma_D \sum_{c.p.(x,y,z)} \{ \sigma_x \mathcal{K}_x, \mathcal{K}_y^2 - \mathcal{K}_z^2 \} \quad (2.4.3)$$

where γ_D is known as cubic Dresselhaus SO coupling parameter that depends on width and thickness of the QWR (Pramanik et al., 2007, Zhang et al., 2009). And here $\mathcal{K} = (\mathbf{p} + e\mathbf{A})$ is the canonical momentum where \mathbf{A} is the vector potential. The curly brackets represent the anticommutation relation: $\{A, B\} = \frac{1}{2}(AB + BA)$.

If we consider that the thickness of the QWR is so small such that $\langle p_z^2 \rangle \gg \langle p_y^2 \rangle, \langle p_x^2 \rangle$, with using the components of canonical momentum we can get Dresselhaus SO Hamiltonian as in the following form:

$$\mathcal{H}_D = \frac{\beta}{\hbar} [\sigma_y \mathcal{K}_y - \sigma_x \mathcal{K}_x] + \gamma_D [\sigma_x \{ \mathcal{K}_x, \mathcal{K}_y^2 \} - \sigma_y \{ \mathcal{K}_y, \mathcal{K}_x^2 \}] \quad (2.4.4)$$

where $\beta = \hbar \gamma_D \langle k_z^2 \rangle$ is the linear Dresselhaus SO coupling constant with k_z being the wave number. The strength of Dresselhaus SO interaction (β) is considered to be a

material constant parameter because it depends on the material band parameters and the thickness of the 2DEG. Correspondingly, the Dresselhaus SO coupling contribution can be tuned by sample thickness or electron density (Schäpers et al., 2009, Chang, Chu, & Mal'shukov, 2009).

In heterostructures, where electrons are confined in one direction (generally assumed along \hat{z} direction) to a 2DEG (in the $\hat{x} - \hat{y}$ plane), expectation value of the momenta vanishes ($\langle p_z \rangle = 0$) and the term $\langle p_z^2 \rangle = \hbar^2 \langle k_z^2 \rangle$ has a finite value. Accordingly, the Hamiltonian in Eq. (2.4.4) is reduced to the linear form

$$\mathcal{H}_D = \frac{\beta}{\hbar} \left[\sigma_y (p_y + eA_y) - \sigma_x (p_x + eA_x) \right] \quad (2.4.5)$$

The bulk inversion asymmetry leads to an effective electric field inside the crystal. According to the relativistic effect, the electric field is seen as an effective magnetic field by moving electrons. This relativistically generated pseudo-magnetic field known as effective Dresselhaus pseudo-magnetic field (\mathbf{B}_D).

2.4.2 Rashba Spin-Orbit Coupling

The second important SO coupling is the Rashba SO coupling which is caused by the structural inversion asymmetry. It is known that the Rashba SO coupling term is dominant over the Dresselhaus SO coupling term in heterostructures consisting of narrow-gap semiconductors (Kaneko, Koshino, & Ando, 2008).

When the potential of 2D electron system is symmetric, the Rashba SO interaction caused by an electric field in this system is zero and spin states are degenerated. As shown in Fig. 2.4, by applying an external gate bias voltage on the top of the quantum well, the potential has an asymmetric profile that leads to a finite Rashba SO interaction. This asymmetric potential profile in the heterostructure lifts the spin degeneracy since the internal electric field is finite.

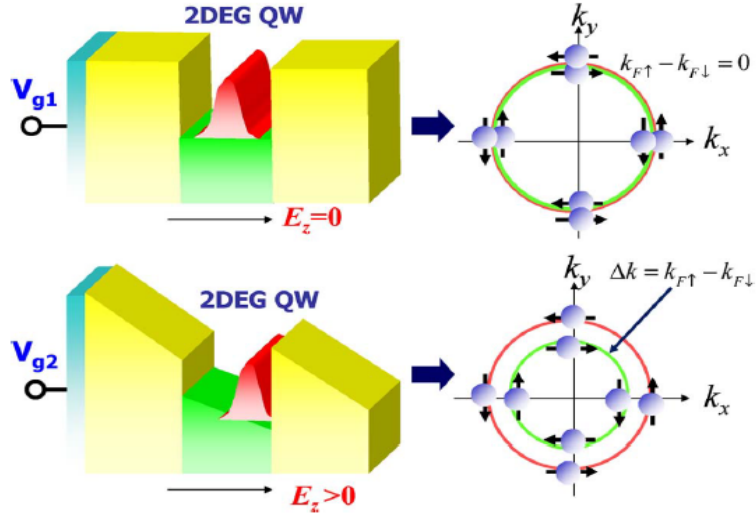


Figure 2.4 The schematic band profile of 2DEG quantum well. The spin configuration at Fermi energy is shown in right bottom figure. Fermi momentum difference between spin-up and spin-down is proportional to the Rashba SO interaction parameter α (Sugahara & Nitta, 2010).

Bychkov and Rashba (Bychkov & Rashba, 1960) described the Rashba SO interaction Hamiltonian as in the following equation

$$\mathcal{H}_R = \frac{\alpha}{\hbar} [\boldsymbol{\sigma} \times (\mathbf{p} + e\mathbf{A})]_z \quad (2.4.6)$$

in which α is the Rashba SO coupling coefficient. The strength of the Rashba SO coupling, the magnitude of α , can be tuned by changing the gate voltage (Nitta, Akazaki, Takayanagi, & Enoki, 1997). The electrical control of the Rashba SO interaction is represented in Fig. 2.4.

If the confining potential is along the \hat{z} direction, electrons move freely in the other two spatial coordinates and accordingly the Rashba Hamiltonian can be written as

$$\mathcal{H}_R = \frac{\alpha}{\hbar} [\sigma_x (p_y + eA_y) - \sigma_y (p_x + eA_x)] \quad (2.4.7)$$

Unlike the Dresselhaus SO coupling term, the Rashba SO contribution only has a linear dependency in k .

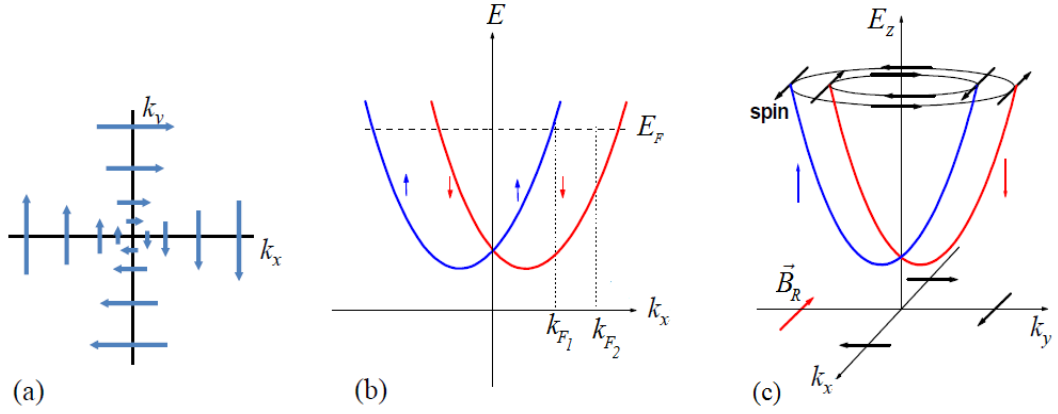


Figure 2.5 The Rashba SO interaction in a system with SIA along the \hat{z} direction. (a) The effective field from the Rashba term is linear in \mathbf{k} and always perpendicular to \mathbf{k} (b) Energy dispersion of Rashba spin-split subbands for a one-dimensional system. The internal magnetic field in the Hamiltonian will shift the two spin sub-bands of the conduction band. In addition spin-up and spin-down electrons move with different velocities. (c) Energy subbands for two-dimensional system. Arrows denote the direction of the spin eigenstates (Stern, 2008, Rahman, 2007).

The effective Rashba pseudo-magnetic field (\mathbf{B}_R) that generated by the electric field is directed along the plane of the 2DEG and is perpendicular to both the direction of electric field and the electron's velocity vector. In the absence of external magnetic field, the spin of the moving electron precesses around the direction of \mathbf{B}_R , similar to the Larmor-precession around an external magnetic field. The Rashba SIA term is extremely important in gated heterostructures where there is an electric field out-of-plane in the \hat{z} direction (Fig. 2.5).

2.5 Zeeman Effect

The splitting of the energy levels of an atom by an externally applied magnetic field is known as “*Zeeman effect*”. It was first observed in 1896 by Pieter Zeeman. Energy band is doubly-degenerated at zero magnetic field. In the presence of Zeeman effect, each atomic level is split into two sublevels which correspond to spin-up and spin-down electrons. The splitting occurs because of the interaction of the magnetic moment $\boldsymbol{\mu}$ of the atom with an externally applied magnetic field \mathbf{B} slightly shifts the energy of the atomic levels by an amount $\Delta E = -\boldsymbol{\mu} \cdot \mathbf{B}$. This energy shift depends on

the relative orientation of the magnetic moment and the magnetic field.

In general, there are two type of magnetic moment. The first one is electron's magnetic moment that arises from orbital angular momentum, and the other one is the magnetic moment of the electron spin which occurs due to the intrinsic spin angular momentum (\mathbf{S}) of the electrons. The spin of an electron can be assumed to have two values $\pm\hbar/2$. Traditional approaches to using electron spin are based on the alignment of a spin (either "up" or "down") relative to a reference such as an applied magnetic field (Wolf et al., 2001).

If an atom has only a single electron and the electron has only intrinsic spin angular momentum, the Zeeman Hamiltonian can be written as follows:

$$\mathcal{H}_Z = -\boldsymbol{\mu} \cdot \mathbf{B} = g^* \mu_B \mathbf{S} \cdot \mathbf{B} \quad (2.5.1)$$

where g^* is the effective Lande-g factor of electron ($g \approx 2$ for free electrons) and $\mu_B = e\hbar/2m^*$ is the Bohr magneton. Here, the magnetic moment $\boldsymbol{\mu}$ is defined in terms of μ_B and S such as $\boldsymbol{\mu} = -g^* \mu_B \mathbf{S}$.

The interaction of the spin with magnetic fields (applied externally or inherent in a material) is the underlying mechanism of spintronics devices (Nix, 2006).

CHAPTER THREE

THEORETICAL BACKGROUND

In this chapter we give a brief overview of approximation methods which are used to calculate the electronic structures of atoms and molecules. Owing to electronic structure we can obtain information about physical, chemical and optical properties of materials.

In the first section, some fundamental approximations which are necessary in order to solve Schrödinger equation are presented. In the next section, the physical interpretation of the density functional theory (DFT) and all approximations that are used to simplify DFT are described and the formal derivations are given. In the other section, approximations for exchange and correlation are introduced briefly: The local density approximation (LDA), which is the simplest and most successful approximation within DFT, and local spin density approximation (LSDA) which is the spin-scaled generalization of LDA.

In the following section, Finite Element Method (FEM) and its formulations are introduced (Section 3.5). And then the application steps of the method are discussed. In this thesis, we employ the FEM to obtain the solution of Schrödinger equation which identifies the physical system numerically. This numerical technique has been known as one of the major numerical solution techniques and employs the philosophy of constructing piecewise approximations of solutions to problems described by differential equations (Reddy, 1993).

3.1 The Electronic Structure Problem

Most of the electronic structure properties of atoms, molecules and solids can be obtained by solving the nonrelativistic time-independent many-electron Schrödinger equation:

$$\mathcal{H}\Psi(\mathbf{R}, \mathbf{r}) = E\Psi(\mathbf{R}, \mathbf{r}) \quad (3.1.1)$$

\mathcal{H} is the Hamiltonian operator consisting of the kinetic energy, mutual Coulomb interaction and external confinement operators. $\Psi(\mathbf{R}, \mathbf{r})$ is a many-electron wave function that depends on the nuclear coordinates ($\{\mathbf{R} = \mathbf{R}_I\}$, $I = 1, \dots, N_n$) and the positions of the electrons ($\{\mathbf{r} = \mathbf{r}_i\}$, $i = 1, \dots, N_e$).

Such physical systems consist not only of electrons but also of nuclei and each of these particles moves in the field generated by the others. Hamiltonian of the system that includes N_e electrons and N_n nuclei can be written as

$$\mathcal{H} = - \sum_{I=1}^{N_n} \frac{\hbar^2}{2M_I} \nabla_I^2 - \sum_{i=1}^{N_e} \frac{\hbar^2}{2m} \nabla_i^2 - \sum_{I=1}^{N_n} \sum_{i=1}^{N_e} \frac{Z_I e^2}{|\mathbf{R}_I - \mathbf{r}_i|} + \frac{1}{2} \sum_{\substack{i,j=1 \\ i \neq j}}^{N_e} \frac{e^2}{|\mathbf{r}_i - \mathbf{r}_j|} + \frac{1}{2} \sum_{\substack{I,J=1 \\ I \neq J}}^{N_n} \frac{Z_I Z_J e^2}{|\mathbf{R}_I - \mathbf{R}_J|} \quad (3.1.2)$$

The indices i and j refers to the electrons, I and J denote the nuclei, m is the electron mass and M_I is the mass of each different nuclei. The first two terms are the operators for kinetic energies of all the electrons and nuclei, respectively. The third term describes the attractive electrostatic interaction (Coulomb attraction) between the electrons and nuclei. The last two terms describe the electron-electron and nucleus-nucleus repulsion energy operators, respectively.

Eq. (3.1.1) is deceptively simple by its form but insuperably complex to solve, even for a simple two electron system such as helium atom or hydrogen molecule, because of the electrostatic correlations between each component. Accordingly, there occurs a need to use approximation methods for reducing this complexity. Born-Oppenheimer approximation is the first approximation to simplify the Schrödinger equation.

3.1.1 Born-Oppenheimer Approximation

The first important approximation is Born-Oppenheimer approximation which is based on the great difference of mass between the nuclei and electrons ($m_e/M \simeq 10^{-3} - 10^{-5}$). Due to the fact that nuclei are much heavier than the electrons, they move at much slower speeds compared to the speed at which electrons move. Therefore, one can consider that the nuclei do not move and the interacting electrons move in the field

of static nuclei (Born & Oppenheimer, 1927).

In consideration of this approximation, the first term of Eq. (3.1.2), the kinetic energy of the nuclei, can be ignored and the final term of Eq. (3.1.2), the repulsion between the nuclei, can be considered to a constant for a fixed configuration of the nuclei. Any constant added to an operator only adds to the operator eigenvalues and has no effect on the operator eigenfunctions. The remaining terms in Eq. (3.1.2) are called the “*electronic Hamiltonian*”. This Hamiltonian describes the motion of N_e electrons in the field generated by N_n point charges and reduces to

$$\mathcal{H}_e = - \sum_{i=1}^{N_e} \frac{\hbar^2}{2m} \nabla_i^2 - \sum_{I=1}^{N_n} \sum_{i=1}^{N_e} \frac{Z_I e^2}{|\mathbf{R}_I - \mathbf{r}_i|} + \frac{1}{2} \sum_{\substack{i,j=1 \\ i \neq j}}^{N_e} \frac{e^2}{|\mathbf{r}_i - \mathbf{r}_j|} \quad (3.1.3)$$

We may write this equation more compactly as

$$\mathcal{H}_e = \mathcal{T} + \mathcal{V}_{ext} + \mathcal{V}_{ee} \quad (3.1.4)$$

Due to this approach, Schrödinger equation is given by

$$\mathcal{H}_e \Psi_e(\mathbf{R}, \mathbf{r}) = E_e \Psi_e(\mathbf{R}, \mathbf{r}) \quad (3.1.5)$$

where E_e is the electronic energy and $\Psi_e(\mathbf{R}, \mathbf{r}) = \Psi_e(\mathbf{R}_1, \mathbf{R}_2, \dots, \mathbf{R}_{N_n}, \mathbf{r}_1, \mathbf{r}_2, \dots, \mathbf{r}_{N_e})$ is the electronic wavefunction. There is a parametric dependence of the electronic wavefunction on the set of nuclear coordinates \mathbf{R} , hence we can conceal the fixed configuration of nuclei.

The third term of Eq. (3.1.3) contains the interactions between the electrons and all many-body quantum effects. Consequently this many-body problem is still too difficult to solve. There exist several ways of approximating the eigenfunctions of the Hamiltonian (Eq. (3.1.3)). There are two major categories of these methods: wave function based methods such as Hartree-Fock approximation and density based methods (e.g. Density Functional Theory).

3.2 Hartree and Hartree-Fock Approximation

In the beginning of the age of quantum mechanics (in 1928), first approximation was proposed by Hartree. It assumes that N-electron wave function can be written as product of one-electron wave functions each of which satisfies one-particle Schrödinger equation in an effective potential (Hartree, 1928).

$$\Psi(\mathbf{r}_1, \mathbf{r}_2, \dots, \mathbf{r}_n) = \prod_{i=1}^N \phi_i(\mathbf{r}_i) \quad (3.2.1)$$

The coordinates \mathbf{r}_i of electron i comprise space coordinates \mathbf{x}_i and spin coordinates σ_i :

$$\mathbf{r}_i = (\mathbf{x}_i, \sigma_i)$$

The Hartree approximation describes a state of the system where the motion of each electron is independent of the motion of other electrons and it takes no account of the indistinguishability of electrons. It implies that the Hartree approximation does not include the influence of interchange of the space and spin coordinates of any two electrons (which is known as exchange terms) and also correlation terms which are created by the motion of the other electrons on the energy of each electron.

Many-electron wave function must obey to Pauli exclusion principle, which states that two fermions (etc. electrons) cannot occupy the same quantum state, and accordingly wave function should be antisymmetric with respect to the interchange of the coordinate \mathbf{r} (both space and spin) of any two fermions:

$$\Psi(\mathbf{r}_1, \dots, \mathbf{r}_i, \dots, \mathbf{r}_j, \dots, \mathbf{r}_n) = -\Psi(\mathbf{r}_1, \dots, \mathbf{r}_j, \dots, \mathbf{r}_i, \dots, \mathbf{r}_n) \quad (3.2.2)$$

Since Hartree approximation does not take into account the fermionic structure of electrons, V. Fock (1930) and J. C. Slater (1928) improved this approximation by including the Pauli exclusion principle. This approximation is known as Hartree-Fock (HF) approximation which considers the many-electron wave functions can

be written as either a single Slater determinant or a linear combination of Slater determinants (Szabo & Ostlund, 1996).

Slater determinant is defined as

$$\Psi(\mathbf{r}_1, \mathbf{r}_2, \dots, \mathbf{r}_n) = \frac{1}{\sqrt{N!}} \begin{vmatrix} \psi_1(\mathbf{x}_1, \sigma_1) & \psi_2(\mathbf{x}_1, \sigma_2) & \dots & \psi_N(\mathbf{x}_1, \sigma_N) \\ \psi_1(\mathbf{x}_2, \sigma_1) & \psi_2(\mathbf{x}_2, \sigma_2) & \dots & \psi_N(\mathbf{x}_2, \sigma_N) \\ \vdots & \vdots & & \vdots \\ \psi_1(\mathbf{x}_N, \sigma_1) & \psi_2(\mathbf{x}_N, \sigma_2) & \dots & \psi_N(\mathbf{x}_N, \sigma_N) \end{vmatrix} \quad (3.2.3)$$

where the factor $1/\sqrt{N!}$ is a normalization factor. In Eq. (3.2.3), the rows of an N-electron Slater determinant are labeled by spatial coordinates and the columns are labeled by spin orbitals. Interchanging the spatial and spin coordinates of two electrons corresponds to commute two rows of the Slater determinant, as a consequence of that the determinant changes sign and therefore Slater determinants meet the requirement of the antisymmetry principle. Having two electrons occupying the same spin orbital corresponds to having two columns of the determinant equal, which makes the determinant zero. Thus no more than one electron can occupy a spin orbital and this corresponds to Pauli exclusion principle (Szabo & Ostlund, 1996).

The procedure for solving Hartree-Fock equation is called the self-consistent-field (SCF). The self consistency iterative procedure is carried out as follows: By making a initial guess at the spin orbitals, one can calculate the Hartree potential (average field seen by each electron) and then solve the Schrödinger equation with this potential for a new set of spin orbitals which are used in turn to construct a new potential. This process is repeated over and over until convergence is achieved (Szabo & Ostlund, 1996, Thijssen, 1999).

HF approximation contains exchange terms and treats electrons as if they were moving independently of each other, this means correlation terms not taken into account in HF formalism. As a consequence of that HF approximation is assumed as a starting point for more accurate approximations which include the effects of electron correlation.

3.3 Density Functional Theory

The limitation of the HF approximation is that only the systems which have small number of electrons can be investigated, many-body wave function is not necessarily well-represented by a single Slater determinant. The systems with a large number of electrons can be examined by DFT.

In DFT, the electron density is used instead of the many-body wave function to describe the ground state properties of interacting system. The electron density corresponds to number of electrons and so we can get information about all groundstate electronic properties of system by means of electron density . Density is a function of only spatial coordinates ($\mathbf{r} = (x,y,z)$) while the wavefunction of a system with N electrons is dependent on $3N$ variables (three spatial variables for each of the N electrons).

DFT starts with Thomas-Fermi (TF) model (Thomas, 1927, Fermi, 1928) which defines the total energy of electrons as a functional of the electron density instead of wavefunction. The electron density ($\rho(\mathbf{r})$), which determines the probability of finding any of the N electrons within volume element $d\mathbf{r}$, is defined by following equation

$$\rho(\mathbf{r}) = N \int \dots \int |\Psi(\mathbf{r}, \mathbf{r}_2, \dots, \mathbf{r}_N)|^2 d\sigma d\mathbf{r}_2 \dots d\mathbf{r}_N \quad (3.3.1)$$

The integral of the electron density over all space gives the total number of electrons,

$$\int \rho(\mathbf{r}) d\mathbf{r} = N \quad (3.3.2)$$

They assumed a uniform gas of noninteracting electrons (homogeneous electron gas) in order to derive a representation of the kinetic energy in terms of the density. They neglected all exchange energy and correlation effects and thereby, the total energy functional involves only the direct Coulomb repulsion (Hartree energy) and the coupling to the external potential terms.

Considerable effort was expended in order to enhance this TF theory. It was initially improved by Dirac in 1930 with the inclusion of exchange term (Dirac, 1930). In other respects, first correlation contributions were introduced by Wigner in 1934 (Wigner, 1934). Later Slater (Slater, 1951b,a), Gáspár (Gáspár, 1954) and other researchers improved the Thomas-Fermi theory with the use of an approximate exchange potential.

The assumption that only electron density is sufficient to describe all observable quantities of the system by itself is contributed by Hohenberg-Kohn theorem (Hohenberg & Kohn, 1964).

3.3.1 Hohenberg-Kohn Theorems

The original Thomas-Fermi theory is formally completed by Hohenberg-Kohn theorem (Hohenberg & Kohn, 1964). In 1964, P. Hohenberg and W. Kohn showed that if the ground state particle density is known, all properties of the system with many-electron can be determined. Shortly following in 1965, W. Kohn and L. J. Sham (Kohn & Sham, 1965) suggested a general method to solve the many-body problem uncomplicatedly.

The Hohenberg-Kohn (HK) theory, which forms the basis of DFT, is described by two theorems:

The first HK theorem states that the ground state electron density ($\rho_0(\mathbf{r})$) for any system of interacting particles determines the external potential ($V_{ext}(\mathbf{r})$) uniquely. In other words, the external potential is a unique and well-defined functional of the electron density. The electron density alone is enough to determine all observable quantities of the system.

The second HK theorem, which provides the energy Variational Principle, indicating that the energy of an electron distribution can be described as a functional($F[\rho]$) of the electron density. This functional is a minimum for the ground state density.

The ground state energy could be obtained by solving the Schrödinger equation directly or from the Rayleigh-Ritz minimal principle:

$$E = \min \frac{\langle \Psi | \mathcal{H} | \Psi \rangle}{\langle \Psi | \Psi \rangle} \quad (3.3.3)$$

For systems without degenerate ground states, there is only unique electron density which corresponds to external potential and the minimum energy is obtained with this ground state density. The ground state energy is given by this equation:

$$E_0[\rho] = \langle \Psi[\rho] | (\mathcal{T} + \mathcal{V}_{ee} + \mathcal{V}_{ext}) | \Psi[\rho] \rangle = F_{HK}[\rho] + \int d(\mathbf{r}) \rho(\mathbf{r}) \mathcal{V}_{ext}(\mathbf{r}) \quad (3.3.4)$$

where

$$F_{HK}[\rho] = \langle \Psi[\rho] | (\mathcal{T} + \mathcal{V}_{ee}) | \Psi[\rho] \rangle$$

is a universal functional of electron density $\rho(\mathbf{r})$.

The first HK theorem can be defined as “*presence theory*” and the second one is “*uniqueness theorem*”. The below diagram denotes the Hohenberg-Kohn theorem briefly.

$$\begin{array}{ccc} \mathcal{V}_{ext}(\mathbf{r}) & \xleftrightarrow{HK} & \rho_0(\mathbf{r}) \\ \Downarrow & & \Uparrow \\ \Psi_i(\mathbf{r}) & \Rightarrow & \Psi_0(\mathbf{r}) \end{array}$$

Mean of the short arrows is the usual solution of the Schrödinger equation where the potential $\mathcal{V}_{ext}(\mathbf{r})$ determines all the states of the system $\Psi_i(\mathbf{r})$, including the ground state $\Psi_0(\mathbf{r})$ and ground state density $\rho_0(\mathbf{r})$. The long arrow labeled “HK” indicates the Hohenberg-Kohn theorem, which completes the loop (Martin, 2004).

3.3.2 Kohn-Sham Equations

W. Kohn and L. Sham (1965) turned original many-body problem into an independent electron problem. They proposed that kinetic energy of an interacting system can be replaced with that of an equivalent non-interacting system with same density as the

real system. With this assumption the ground state electron density of an interacting system can be defined in terms of single electron wave functions of non-interacting system.

$$\rho(\mathbf{r}) = \sum_{i=1}^{N_e} |\Psi_i(\mathbf{r})|^2 \quad (3.3.5)$$

These orbitals are called Kohn-Sham orbitals.

Due to theory of Kohn-Sham, minimization of total energy functional provides us to obtain the ground state electron density and energy. So then self-consistent solutions of Schrödinger equation need to be performed. Kohn-Sham ansatz can be described by the following scheme.

$$\begin{array}{ccccccc} \mathcal{V}_{ext}(\mathbf{r}) & \xleftrightarrow{HK} & \rho_0(\mathbf{r}) & \left[\xleftrightarrow{KS} \right] & \rho_0(\mathbf{r}) & \xleftrightarrow{HK_0} & \mathcal{V}_{KS}(\mathbf{r}) \\ \downarrow & & \uparrow & & \uparrow & & \downarrow \\ \Psi_i(\{\mathbf{r}\}) & \Rightarrow & \Psi_0(\{\mathbf{r}\}) & & \Psi_{i=1, N_e}(\mathbf{r}) & \Leftarrow & \Psi_i(\mathbf{r}) \end{array}$$

In this scheme, HK_0 represents the HK theorem applied to the non-interacting problem. The connection between the many-body and independent particle systems is indicated with two sided KS arrow which attaches any point to other point. Accordingly, solution of the independent particle Kohn-Sham problem determines all properties of the full many-body system (Martin, 2004).

Kohn-Sham formulation states that instead of the full many-electron system we can consider an auxiliary system of single-electron orbitals that have the same ground state density as the real system (Toffoli, 2009). Therefore the kinetic energy of the Kohn-Sham orbitals can be written as

$$\mathcal{T}_S[\rho] = \sum_{i=1}^{N_e} \langle \Psi_i(\mathbf{r}) | -\frac{\hbar^2}{2m} \nabla^2 | \Psi_i(\mathbf{r}) \rangle \quad (3.3.6)$$

The kinetic energy of the real system can be defined with a correction term

$$\mathcal{T}[\rho] = \mathcal{T}_S[\rho] + \Delta \mathcal{T}[\rho] \quad (3.3.7)$$

There is a correction term in electron-electron repulsive potential energy also.

$$\mathcal{V}_{ee}[\rho] = \frac{1}{2} \int \int d\mathbf{r} d\mathbf{r}' \frac{\rho(\mathbf{r}) \rho(\mathbf{r}')}{|\mathbf{r} - \mathbf{r}'|} + \Delta \mathcal{V}_{ee}[\rho] \quad (3.3.8)$$

The total ground state energy which is defined in Eq. (3.3.4) can be rewritten as

$$\begin{aligned} E_{KS}[\rho] = & \sum_{i=1}^{N_e} \langle \Psi_i(\mathbf{r}) | -\frac{\hbar^2}{2m} \nabla^2 | \Psi_i(\mathbf{r}) \rangle + \int d(\mathbf{r}) \rho(\mathbf{r}) \mathcal{V}_{ext}(\mathbf{r}) \\ & + \frac{1}{2} \int \int d\mathbf{r} d\mathbf{r}' \frac{\rho(\mathbf{r}) \rho(\mathbf{r}')}{|\mathbf{r} - \mathbf{r}'|} + \Delta \mathcal{T}[\rho] + \Delta \mathcal{V}_{ee}[\rho] \end{aligned} \quad (3.3.9)$$

The sum of last two correction terms (the difference between the exact kinetic energy and T_S , the nonclassical part of $\mathcal{V}_{ee}[\rho]$ respectively) are known as exchange-correlation energy term. As can be seen in the above equation this energy contains all the unknown correlation contributions.

$$E_{xc}[\rho] = \Delta \mathcal{T}[\rho] + \Delta \mathcal{V}_{ee}[\rho] \quad (3.3.10)$$

The main reason of this term is the difference between a system of N_e interacting and non-interacting particles.

$$\begin{aligned} E_{KS}[\rho] = & \sum_{i=1}^{N_e} \langle \Psi_i(\mathbf{r}) | -\frac{\hbar^2}{2m} \nabla^2 | \Psi_i(\mathbf{r}) \rangle + \int d(\mathbf{r}) \rho(\mathbf{r}) \mathcal{V}_{ext}(\mathbf{r}) \\ & + \frac{1}{2} \int \int d\mathbf{r} d\mathbf{r}' \frac{\rho(\mathbf{r}) \rho(\mathbf{r}')}{|\mathbf{r} - \mathbf{r}'|} + E_{xc}[\rho] \end{aligned} \quad (3.3.11)$$

In this equation the first term denotes the kinetic energy of noninteracting electrons and it can be calculated with the help of derivation of Kohn-Sham orbitals from ground state density. The second and third terms can be obtained if ground state density is known. The last term, which includes all the effects of the many-body character of the true electron system, is the ‘‘exchange-correlation’’ term. To evaluate this unknown functional, there should be a proper method.

Kohn-Sham equation:

$$\mathcal{H}_{KS} \Psi = E_{KS} \Psi \quad (3.3.12)$$

For non-degenerate ground states, the Kohn-Sham ground state wavefunction is a single Slater determinant

$$\Psi = \frac{1}{\sqrt{N!}} \det[\psi_1(\mathbf{r}_1, \sigma_1) \dots \psi_N(\mathbf{r}_{N_e}, \sigma_{N_e})] \quad (3.3.13)$$

Kohn-Sham equation can be rewritten in terms of the single-particle orbitals as follow

$$\left[-\frac{\hbar^2}{2m} \nabla^2 + \mathcal{V}_{eff}(\mathbf{r}) \right] \psi_i = \varepsilon_i \psi_i \quad (3.3.14)$$

The total energy of the system is:

$$E_{KS} = \sum_i \varepsilon_i \quad (3.3.15)$$

$$\mathcal{V}_{eff}(\mathbf{r}) = \mathcal{V}_{ext}(\mathbf{r}) + \int d\mathbf{r}' \frac{\rho(\mathbf{r}')}{|\mathbf{r} - \mathbf{r}'|} + \mathcal{V}_{xc}(\mathbf{r}) \quad (3.3.16)$$

Solution of the Kohn-Sham equation is summarized in the Fig. (3.1)

3.4 Exchange-Correlation Energy Functional

Hartree, Hartree-Fock and Kohn-Sham theories provide one electron equations for describing many-body electronic systems. The Kohn-Sham theory is distinguished from the Hartree-Fock theory on account of the fact that it includes the exchange-correlation effect of electrons.

Exact functionals for exchange and correlation are known only for the homogeneous (uniform) electron gas. If $E_{xc}[\rho]$ is known obviously by the help of any successive better approximation, electron density and total energy can be obtained exactly (Parr & Yang, 1989). The most widely used approximation is local density approximation. The spin-density-dependent version of LDA is known as local spin-density approximation-LSDA. And this approximation is used whenever spin-polarization is present.

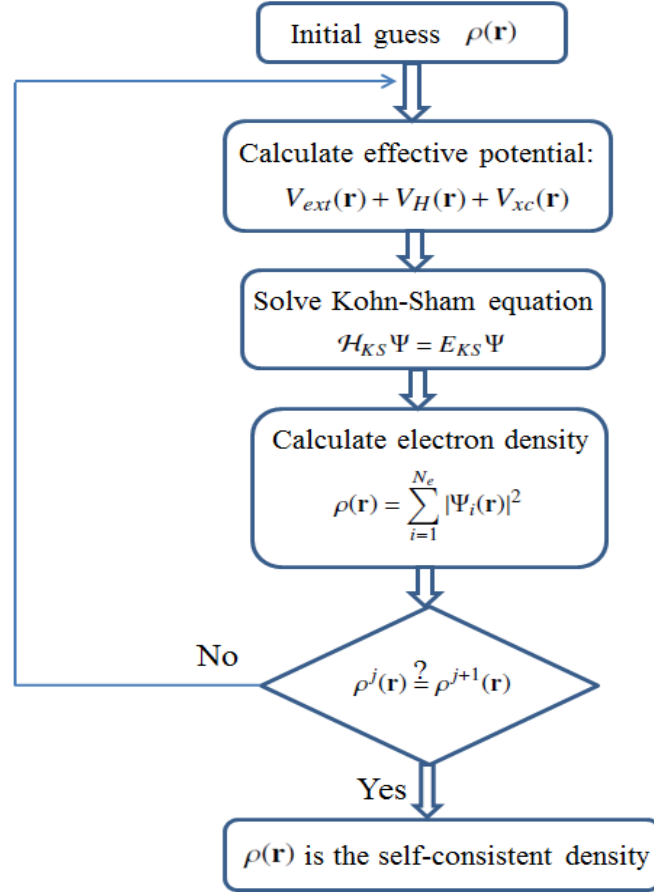


Figure 3.1 Schematic representation of the self-consistent solution of Kohn-Sham Equation

3.4.1 Local Density Approximation

The local density approximation introduced by Kohn and Sham in 1965, has been the cornerstone of all approximations to exchange-correlation energy functionals. And this approximation is valid for homogenous 2D electrons and also for systems with small variation in electron density.

The exchange-correlation potential is a functional derivative of the exchange correlation energy with respect to the local density. And for a homogeneous electron gas, this will depend on the value of the electron density.

$$V_{xc}(\mathbf{r}) = \frac{\delta E_{xc}[\rho(\mathbf{r})]}{\delta \rho(\mathbf{r})} \quad (3.4.1)$$

The main idea of LDA is the assumption that the functional is the same with the model of homogeneous electron gas. In other words, the energy depends on only the local density at the point where the functional is evaluated (Kohn & Sham, 1965). In this approximation, total exchange-correlation energy can be derived from the following integration

$$E_{xc}^{LDA}[\rho] = \int \rho(\mathbf{r}) \varepsilon_{xc}^{LDA}(\rho(\mathbf{r})) d\mathbf{r} \quad (3.4.2)$$

Here $\varepsilon_{xc}(\rho(\mathbf{r}))$ is the local exchange-correlation energy per particle with density $\rho(\mathbf{r})$. LDA assumes that this local exchange-correlation energy per particle is equal to the local exchange-correlation energy per particle of a homogeneous electron gas within the same density which is numerically known.

$$\varepsilon_{xc}^{LDA}(\rho(\mathbf{r})) = \varepsilon_{xc}^{hom}(\rho(\mathbf{r})) \quad (3.4.3)$$

Corresponding exchange-correlation potential is defined as

$$\mathcal{V}_{xc}^{LDA}(\mathbf{r}) = \frac{\delta E_{xc}^{LDA}[\rho(\mathbf{r})]}{\delta \rho(\mathbf{r})} = \varepsilon_{xc}(\rho(\mathbf{r})) + \rho(\mathbf{r}) \frac{\partial \varepsilon_{xc}(\rho(\mathbf{r}))}{\partial \rho(\mathbf{r})} \quad (3.4.4)$$

And the Kohn-Sham equation can be rewritten as follows:

$$\left[-\frac{\hbar^2}{2m} \nabla^2 + \mathcal{V}_{ext}(\mathbf{r}) + \int d\mathbf{r}' \frac{\rho(\mathbf{r}')}{|\mathbf{r} - \mathbf{r}'|} + \mathcal{V}_{xc}^{LDA}(\mathbf{r}) \right] \psi_i = \varepsilon_i \psi_i \quad (3.4.5)$$

3.4.2 Local Spin Density Approximation

Local Spin Density Approximation in which the functional is written in terms of spin density is the extension of the LDA to spin-polarized systems.

In LDA formalism, the total energy is written as a functional of density alone and this energy does not depend on spin densities. In the local spin density approximation the exchange-correlation energy not only depends on the density but also on the spin polarization. If the functional is expressed in terms of the spin densities, the

corresponding LSDA can be expressed as

$$E_{xc}^{LSDA}[\rho_{\uparrow}(\mathbf{r}), \rho_{\downarrow}(\mathbf{r})] = \int \rho(\mathbf{r}) \varepsilon_{xc}^{LSDA}(\rho(\mathbf{r}), \zeta(\mathbf{r})) d\mathbf{r} \quad (3.4.6)$$

where $\varepsilon_{xc}^{LSDA}(\rho(\mathbf{r}), \zeta(\mathbf{r}))$ is the exchange and correlation energy per particle of a homogeneous, spin-polarized electron gas with spin-up ($\rho_{\uparrow}(\mathbf{r})$) and spin-down ($\rho_{\downarrow}(\mathbf{r})$) densities, $\zeta(\mathbf{r})$ represents the spin polarization

$$\zeta(\mathbf{r}) = \frac{(\rho_{\uparrow} - \rho_{\downarrow})}{\rho(\mathbf{r})} \quad (3.4.7)$$

The total density $\rho(\mathbf{r})$ is defined by $\rho(\mathbf{r}) = \rho_{\uparrow}(\mathbf{r}) + \rho_{\downarrow}(\mathbf{r})$.

ε_{xc} can be divided into exchange and correlation energy parts:

$$\varepsilon_{xc}(\rho) = \varepsilon_x(\rho) + \varepsilon_c(\rho) \quad (3.4.8)$$

There are various parametrizations for determining the exchange-correlation energy which are based on Quantum Monte Carlo simulations. The most commonly used parametrizations in the literature for the exchange-correlation energy are that of von Barth and Hedin which was mainly interested with intrinsically spin polarized systems such as transition metals and non-singlet atoms for intermediate polarizations (Barth & Hedin, 1972), that of Ceperley and Alder in 3D for the non-polarized ($\zeta(\mathbf{r}) = 0$) and ferromagnetic ($\zeta(\mathbf{r}) = 1$) cases (Ceperley & Alder, 1980), and that of Tanatar and Ceperley for electronic systems confined in 2D (Tanatar & Ceperley, 1989). The recent parametrization is defined by Attaccalite and co-workers (Attaccalite, Moroni, Gori-Giorgi, & Bachelet, 2002, 2003). The last one performed for the whole range of spin polarization ($0 \leq \zeta \leq 1$) and wide range of electron densities ($1 < r_s < 40$) (Räsänen, 2004). This new parametrization satisfies the complete results at the low and high-density limits in the 2DEG (Gori-Giorgi, Attaccalite, Moroni, & Bachelet, 2003). The exchange-correlation energy formulation of Attaccalite and coworkers is given

by (Attaccalite et al., 2002)

$$\varepsilon_{xc}(r_s, \zeta) = \varepsilon_x(r_s, \zeta) + (e^{-\beta r_s} - 1)\varepsilon_x^6(r_s, \zeta) + \alpha_0(r_s) + \alpha_1(r_s)\zeta^2 + \alpha_2(r_s)\zeta^4 \quad (3.4.9)$$

where the exchange energy is equal to

$$\varepsilon_x(r_s, \zeta) = -\frac{2\sqrt{2}}{3\pi r_s} [(1 + \zeta)^{3/2} + (1 - \zeta)^{3/2}] \quad (3.4.10)$$

In these equations, $r_s = 1/\sqrt{\pi n}$ is the density parameter for the 2DEG with an electron number density n at zero temperature, α 's are density-dependent functions of the generalized Perdew-Wang form (Perdew & Wang, 1992), the parameter β is equal to 1.3386, and $\varepsilon_x^6(r_s, \zeta)$ is the Taylor expansion of ε_x beyond the fourth order in ζ at $\zeta = 0$.

The parametrization of Attaccalite and coworkers (Attaccalite et al., 2002) is considerably more accurate than the form of Tanatar and Ceperley (Tanatar & Ceperley, 1989) in zero magnetic field case (Räsänen, 2004).

3.5 Numerical Methodology: Finite Element Method

Finite Element Method (FEM) is a powerful computational technique devised to evaluate differential and integral equations that arise in various fields of engineering and applied sciences (Hutton, 2004, Zieliński, 2012). This method based on the discretization of the physical region and the representation of the wavefunction by piecewise polynomials (Ram-Mohan, 2002). This discretization has two advantages. It allows accurate representation of complex geometries and inclusion of dissimilar materials. It enables accurate representation of the solution within each element, to bring out local effects (Reddy, 1993).

The advantages of FEM are numerous and important. One of the major advantages of FEM is that it is applicable to any field problem (e.g. heat transfer, stress analysis, magnetic fields etc.) and to the various kinds of problems with any complex shape simply. Also, it can be applied to the systems which have different boundary conditions

on different portions of the boundary. With ease using the finite element method, different elements (behaviour and mathematical descriptions) can be combined in a single finite element model. The main advantage of FEM is that the results can be obtained with a very high accuracy (Kwon & Bang, 1997, Ram-Mohan, 2002, Hutton, 2004).

3.5.1 Area Coordinates and Linear Basis Functions in 1D

In FEM, the domain of the problem is represented by a collection of subdomains and each subdomain is called a “*global element*”. Therefore, the problem domain consists of many global element patches. When one of these global elements is discretized into subdomains, we get “*local element*”. In other words, total of the local elements in related subdomain generate each global element. To connect the local elements and impose continuity of the solution at nodes common to elements, the endpoints of each element are known as “*element nodes*” (Reddy, 1993, Kwon & Bang, 1997).

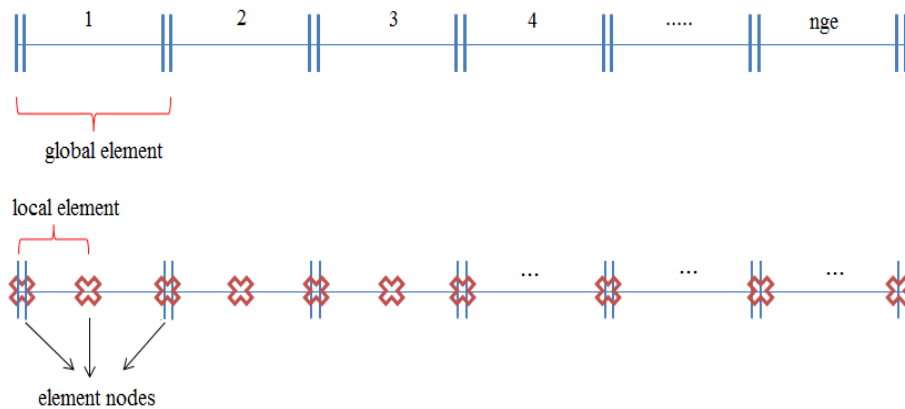


Figure 3.2 Global element, local element and element nodes in 1D

The abbreviations that are used for the analytical derivation of FEM and also in Fig. (3.3) represent for the terms as follows:

- n_{gen} : Number of **global element nodes**
- n_{ge} : Number of **global element**
- n_{tn} : Number of **total nodes** ($n_{tn} = n_{ge} \cdot (n_{gen} - 1) + 1$)
- $N(x)$: Global element basis functions
- $\mathbb{N}(x)$: Whole space basis functions

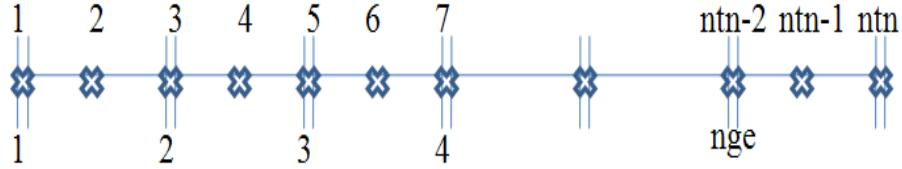


Figure 3.3 Schematic representation of the problem domain in 1D

If we represent the number of sub-domains and global element nodes with N_{nge} and N_{ngen} respectively, number of basis functions in the work space will be $N_{nge} \cdot N_{ngen}$. But due to the fact that there is a degeneracy at the point $N_{nge} - 1$, the total number of basis functions will be $[N_{nge} \cdot N_{ngen} - (N_{nge} - 1)]$.

Subdividing a geometrically complex domain into parts that allow the evaluation of desired quantities is a practical approach. Approximation of the solution over each element of the domain is simpler than its approximation over the entire domain. Better results can be obtained by the use of more elements and also through the use of higher order interpolation functions (Reddy, 1993).

Approximate solution over the work space is assumed to be a linear combination of appropriately chosen approximation functions $\mathbb{N}_i(x)$ and undetermined coefficients c_i

$$\psi(x) = \sum_{i=1}^{N_{tn}} c_i \mathbb{N}_i(x) \quad (3.5.1)$$

In FEM, the approximation functions $\mathbb{N}_i(x)$ are called “*basis functions*” (also shape functions or interpolation functions) which span the whole space. These basis functions in FEM are often polynomials that are derived using interpolation theory. We choose the “Lagrange Polynomials” as the basis functions for the polynomial space basis functions (Pask, Klein, Sterne, & Fong, 2001).

Basis functions have to satisfy the condition below.

$$\mathbb{N}_i(x_j) = \delta_{ij} \quad (3.5.2)$$

where \mathbb{N}_i is the i th parent basis function and x_j is the j th node. Each basis function has a value of 1 at its own node and zero at all other nodes (Pask et al., 2001).

3.5.1.1 Linear Basis Functions in 1D

We can define the basis functions with using area coordinates. Let us consider a finite element such as in Fig. (3.4(a)) and take two nodes for each global element (Fig. (3.4(b))):

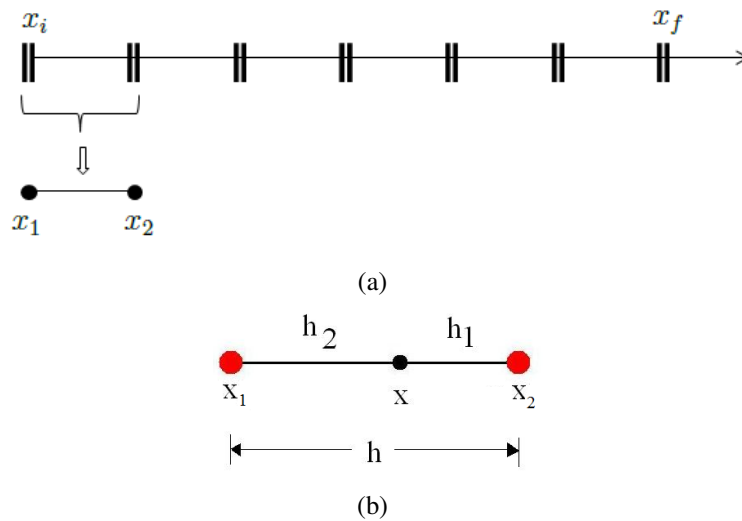


Figure 3.4 (a) Work space which is divided into global elements. (b) Global element which has two nodes (1D).

Here x_1 and x_2 are coordinates at each nodes and h represents the element size.

$$h = x_2 - x_1$$

$$h_1 = x - x_1 \quad h_2 = x_2 - x$$

$$h = h_1 + h_2 \Rightarrow 1 = \frac{h_1}{h} + \frac{h_2}{h}$$

$$1 = \frac{(x_2 - x)}{x_2 - x_1} + \frac{(x - x_1)}{x_2 - x_1}$$

Consequently area coordinates (L_1, L_2) can be defined with the following equation

$$L_1(x) = \frac{(x_2 - x)}{x_2 - x_1} \quad L_2(x) = \frac{(x - x_1)}{x_2 - x_1} \quad (3.5.3)$$

It is important to note that area coordinates have to satisfy the condition

$$L_i(x_j) = \delta_{i,j} \quad (3.5.4)$$

as in basis functions (Eq. 3.5.2).

So we can define a boundary condition for the area coordinates:

$$L_1(x) + L_2(x) = 1 \quad (3.5.5)$$

Basis functions can be defined in terms of area coordinates which span only global elements. The interpolation functions in terms of area coordinates in one dimensional space:

$$\begin{aligned} N_1(x) &= L_1(x) \\ N_2(x) &= L_2(x) \end{aligned} \quad (3.5.6)$$

If we take the node coordinates such as $x_1 = 0$ and $x_2 = 1$, we can obtain the interpolation functions from Eq. (3.5.3)

$$N_1(x) = L_1(x) = 1 - x \quad N_2(x) = L_2(x) = x \quad (3.5.7)$$

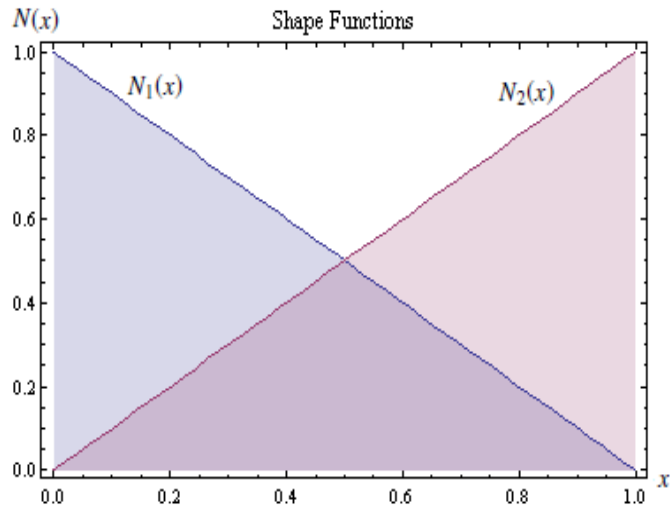


Figure 3.5 One dimensional shape functions with two nodes ($N_{ngen} = 2$) in a global element

3.5.1.2 High Order Basis Functions in 1D

If number of nodes is equal to three ($N_{ngen} = 3$), area coordinates need to comply with a following condition:

$$(L_1 + L_2)^2 = L_1^2 + 2L_1L_2 + L_2^2 = 1 \quad (3.5.8)$$

This condition gives information about which area coordinates can we use to determine the interpolation functions. The first one and the last one of the interpolation function consists of two L_1 and two L_2 area coordinates respectively. The second one includes both of L_1 and L_2 area coordinates.

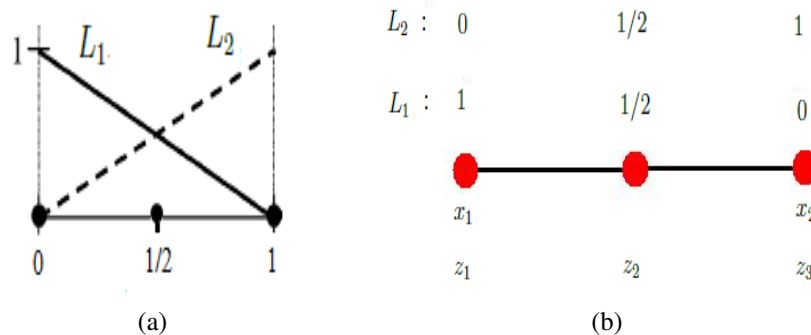


Figure 3.6 Area coordinates and positions of nodes in a global element

To determine the first interpolation function, we need to envelop first node point.

Afterwards an equation is written which makes the area coordinate L_1 zero at the other node points. That is to say, L_1 itself equals zero at z_3 and $L_1 - (1/2)$ comes up to zero at z_2 .

Consequently, we can define first interpolation function with the following equation:

$$N_1(x) = CL_1 \left(L_1 - \frac{1}{2} \right) \quad (3.5.9)$$

where C is a normalization constant that can be obtained with boundary condition (Eq. 3.5.4). In other words the value of C is to provide unity value for $N_1(x)$ at node z_1 .

$$N_1(x=0) = 1 \Rightarrow 1 = C \cdot 1 \cdot \frac{1}{2} \Rightarrow C = 2$$

$$N_1(x) = 2L_1 \left(L_1 - \frac{1}{2} \right) \quad (3.5.10)$$

To obtain a formulation for the second interpolation function we take the second node point z_2 as a reference which is a degenerate point for L_1 and L_2 . At z_2 , area coordinates has the same value $L_1 = L_2 = 1/2$. L_1 and L_2 are equal to zero at the right hand side and the left hand side of the related point respectively.

Therefore;

$$N_2(x) = C \cdot L_1 \cdot L_2$$

$$N_2(x=1/2) = 1 \Rightarrow 1 = C \cdot \frac{1}{2} \cdot \frac{1}{2} \Rightarrow C = 4$$

$$N_2(x) = 4L_1L_2 \quad (3.5.11)$$

We use the node point z_3 for the last interpolation function which involve only L_2 area coordinate. According to condition $N_i(x_j) = \delta_{ij}$ for related interpolation function, L_2 itself and $L_2 - (1/2)$ have a value of zero at node z_2 and z_1 node points respectively.

$$N_3(x) = C \cdot L_2 \left(L_2 - \frac{1}{2} \right)$$

$$N_3(x=1) = 1 \Rightarrow 1 = C \cdot 1 \cdot \frac{1}{2} \Rightarrow C = 2$$

So, result formulation for the interpolation function is written as

$$N_3(x) = 2L_2 \left(L_2 - \frac{1}{2} \right) \quad (3.5.12)$$

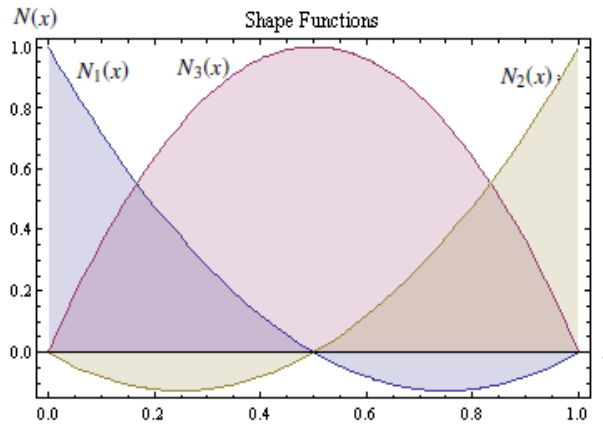


Figure 3.7 One dimensional shape functions with three nodes ($N_{ngen} = 3$) in a global element

When the number of nodes is $N_{ngen} = 4$, related formulations can be derived such as below equations similarly.

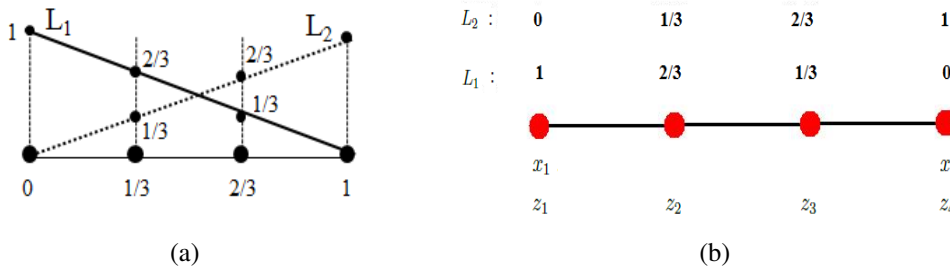


Figure 3.8 Area coordinates and positions of nodes in a global element

$$(L_1 + L_2)^{N_0-1} = 1 \Rightarrow (L_1 + L_2)^3 = 1$$

$$(L_1 + L_2)^3 = L_1^3 + 3L_1^2L_2 + 3L_1L_2^2 + L_2^3 \quad (3.5.13)$$

Due to this equation; N_1 has three of L_1 area coordinates, N_2 has two of L_1 and one of L_2 , N_3 has one of L_1 and two of L_2 , the last one N_4 has three of L_2

area coordinates. These interpolation functions can be obtained using the boundary condition (Eq. (3.5.4)) as mentioned before.

$$N_1 = C \cdot L_1 \cdot \left(L_1 - \frac{1}{3}\right) \cdot \left(L_1 - \frac{2}{3}\right)$$

$$1 = C \cdot 1 \cdot \left(1 - \frac{1}{3}\right) \left(1 - \frac{2}{3}\right) \Rightarrow C = \frac{9}{2}$$

$$N_1(x) = \frac{9}{2} L_1 \left(L_1 - \frac{1}{3}\right) \left(L_1 - \frac{2}{3}\right) \quad (3.5.14)$$

$$N_2(x) = C \cdot L_1 \cdot \left(L_1 - \frac{1}{3}\right) \cdot L_2$$

$$1 = C \cdot \frac{2}{3} \cdot \left(\frac{2}{3} - \frac{1}{3}\right) \cdot \frac{1}{3} \Rightarrow C = \frac{27}{2}$$

$$N_2(x) = \frac{27}{2} L_1 \left(L_1 - \frac{1}{3}\right) L_2 \quad (3.5.15)$$

$$N_3(x) = \frac{27}{2} L_1 \left(L_2 - \frac{1}{3}\right) L_2 \quad (3.5.16)$$

$$N_4(x) = \frac{9}{2} L_2 \left(L_2 - \frac{1}{3}\right) \left(L_2 - \frac{2}{3}\right) \quad (3.5.17)$$

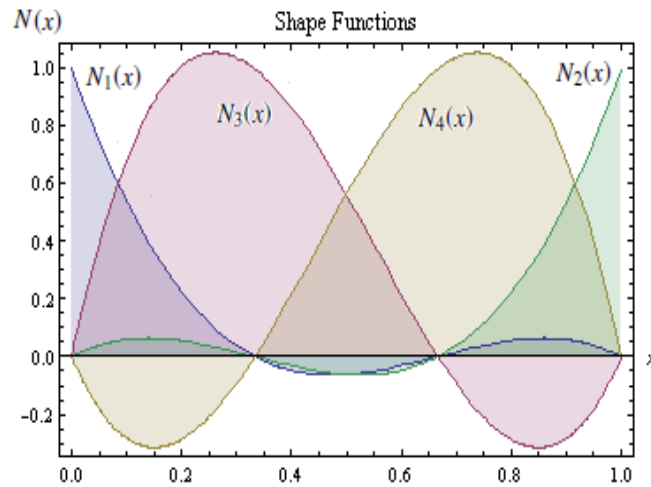


Figure 3.9 One dimensional shape functions with four nodes ($N_{ngen} = 4$) in a global element

If there are $N_{ngen} = 5$ node points in one global element, definition of interpolation functions in terms of area coordinates are given with the following equations:

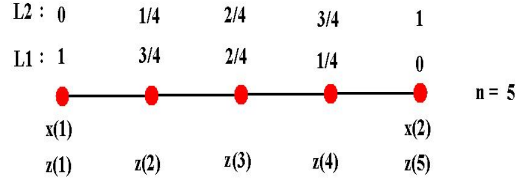


Figure 3.10 A global element with five nodes in (1D)

The interpolation functions are given as

$$(L_1 + L_2)^4 = L_1^4 + 4L_1^3L_2 + 6L_1^2L_2^2 + 4L_1L_2^3 + L_2^4$$

$$N_1(x) = L_1 \left(L_1 - \frac{1}{4} \right) \left(L_1 - \frac{2}{4} \right) \left(L_1 - \frac{3}{4} \right) \frac{64}{6}$$

$$N_2(x) = L_1 \left(L_1 - \frac{1}{4} \right) \left(L_1 - \frac{2}{4} \right) L_2 \frac{64 \cdot 4}{6}$$

$$N_3(x) = L_1 \left(L_1 - \frac{1}{4} \right) \left(L_2 - \frac{1}{4} \right) L_2 \frac{64 \cdot 4}{4} \quad (3.5.18)$$

$$N_4(x) = L_1 \left(L_2 - \frac{2}{4} \right) \left(L_2 - \frac{2}{4} \right) L_2 \frac{64 \cdot 4}{6}$$

$$N_5(x) = \left(L_2 - \frac{3}{4} \right) \left(L_2 - \frac{2}{4} \right) \left(L_2 - \frac{1}{4} \right) L_2 \frac{64}{6}$$

Each interpolation function has value of unity at its associated node and value zero at the other nodes (Fig. 3.11).

In this thesis, we derive interpolation functions for maximum $N_{ngen} = 10$ node points in one global element.

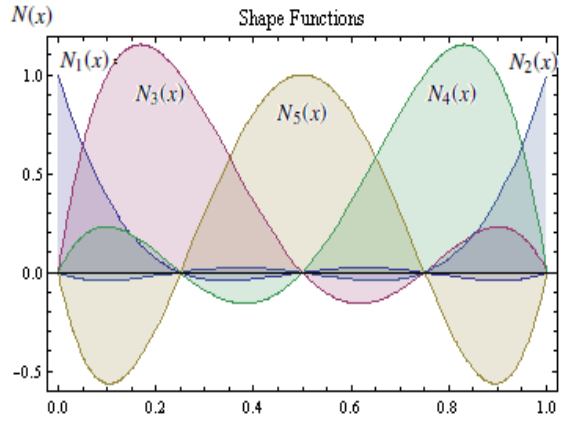


Figure 3.11 One dimensional shape functions with five nodes ($N_{ngen} = 5$) in a global element

3.5.2 Solution of the Confined Quantum Mechanical Systems with FEM

The Hamiltonian of a particle moving in a confinement potential $V(\mathbf{r})$ is

$$\mathcal{H} = -\frac{\hbar^2}{2m}\nabla^2 + V(\mathbf{r}) \quad (3.5.19)$$

We can use the Bohr radius and effective Hartree energy with intent to get the dimensionless form of Hamiltonian.

$$\mathcal{H} = -\frac{1}{2}\nabla_d^2 + V(\mathbf{r}) \quad (3.5.20)$$

where the subscript “ d ” stands for the dimension of the system. The eigenvalue equation is known as in the following form:

$$\mathcal{H}\Psi(\mathbf{r}) = E\Psi(\mathbf{r}) \quad (3.5.21)$$

Due to the variational principle we need to start with a suggestion for the trial wave function which describes the physical system. Using our experience with the wave function we next write down the Schrödinger equation and then solve this equation via the minimization principle to obtain a set of wave functions. Accordingly, the Schrödinger equation is described with this trial wave function $\psi(\mathbf{r})$ instead of the

wave function $\Psi(\mathbf{r})$:

$$\begin{aligned} \Psi(\mathbf{r}) \rightarrow \psi(\mathbf{r}) \quad \Rightarrow \quad \mathcal{H}\psi(\mathbf{r}) = E\psi(\mathbf{r}) \\ (\mathcal{H} - E)\psi(\mathbf{r}) \cong 0 \end{aligned} \quad (3.5.22)$$

As a first step to derive the solution of the Schrödinger equation (Eq. 3.5.22), the physical region is divided into subregions. Therefore, wave function can be defined as a complete set of basis functions which span the related domain

$$\psi(\mathbf{r}) = \sum_{i=1}^{N_{nm}} \psi_i \mathbb{N}_i(\mathbf{r}) \quad (3.5.23)$$

where N_{nm} is the number of total nodes in discretized solution space.

The representation of square matrix, column and row matrices which is used in FEM can be seen in Table (3.1).

Table 3.1 Matrix representations in FEM notation

		FEM
Matrix	$X = \begin{pmatrix} * & * & * \\ * & * & * \\ * & * & * \end{pmatrix}$	$\{X\}$
Column Matrix	$X = \begin{pmatrix} * \\ * \\ * \end{pmatrix}$	$\{X\}$
Row Matrix	$X = \begin{pmatrix} * & * & * \end{pmatrix}$	$\{X\}^T$

Matrix notation of the wave function over all the nodes in the solution space can be written as

$$\psi(\mathbf{r}) = \sum_{i=1}^{N_{nm}} \psi_i \mathbb{N}_i(\mathbf{r}) = \left\{ \psi_1 \quad \psi_2 \quad \dots \quad \psi_{N_{nm}} \right\} \cdot \begin{pmatrix} \mathbb{N}_1(\mathbf{r}) \\ \mathbb{N}_2(\mathbf{r}) \\ \vdots \\ \mathbb{N}_{N_{nm}}(\mathbf{r}) \end{pmatrix} = \{\psi\}^T \{\mathbb{N}(\mathbf{r})\} \quad (3.5.24)$$

$$\psi(\mathbf{r}) = \{\mathbb{N}(\mathbf{r})\}^T \cdot \{\psi\} \quad (3.5.25)$$

where

$$\{\mathbb{N}(\mathbf{r})\}^T = (\mathbb{N}_1(\mathbf{r}), \mathbb{N}_2(\mathbf{r}), \mathbb{N}_3(\mathbf{r}), \dots, \mathbb{N}_{N_{nm}}(\mathbf{r})) \quad (3.5.26)$$

$$\{\psi\}^T = (\psi_1, \psi_2, \psi_3, \dots, \psi_{N_{nm}}) \quad (3.5.27)$$

The hermitian conjugate of wave function is

$$\psi^\dagger(\mathbf{r}) = \{\psi\}^\dagger \cdot \{\mathbb{N}(\mathbf{r})\} \quad (3.5.28)$$

To derive variational parameters $(\psi_i(\mathbf{r}))$ “*Galerkin’s Method*” can be used. We can describe the mathematical procedure such as: Firstly the Schrödinger equation is written with searched wave function $\psi(\mathbf{r})$. Then the equation is multiplied by hermitian conjugate of the wave function on the left hand side and integral is taken of this outcome equality over the associated solution space to obtain the expression which makes the variation parameters minimum.

$$\mathcal{G} = \int_{\Omega} \psi^\dagger(\mathbf{r})(\mathcal{H} - E\mathbf{I})\psi(\mathbf{r}) d\Omega \quad (3.5.29)$$

where \mathbf{I} is the unitary matrix ($N \times N$). With using the definitions of the wave function (Eq. 3.5.25) and it’s hermitian conjugate (Eq. 3.5.28) in Eq. (3.5.29) the following equation is obtained.

$$\mathcal{G} = \{\psi\}^\dagger \cdot \left[\int_{\Omega} \{\mathbb{N}\}(\mathcal{H} - E\mathbf{I})\{\mathbb{N}\}^T d\Omega \right] \cdot \{\psi\} \quad (3.5.30)$$

We can use the variational method to determine the wave function by minimizing the \mathcal{G} expression. A set of wave functions which minimize the integration of \mathcal{G} also minimize the energy of the system.

$$\frac{\partial \mathcal{G}}{\partial \psi^\dagger} = 0 \quad \Rightarrow \quad \left[\int_{\Omega} \{\mathbb{N}\}(\mathcal{H} - E\mathbf{I})\{\mathbb{N}\}^T d\Omega \right] \cdot \{\psi\} = 0 \quad (3.5.31)$$

When the Hamiltonian expression Eq. (3.5.20) is written in Eq. (3.5.31)

$$\left[\int_{\Omega} d\Omega \left[-\frac{1}{2} \{\mathbb{N}\} \cdot \nabla_d^2 \{\mathbb{N}\}^T + \{\mathbb{N}\} V(\mathbf{r}) \{\mathbb{N}\}^T \right] \right] \cdot \{\psi\} = E \left[\int_{\Omega} d\Omega \{\mathbb{N}\} \{\mathbb{N}\}^T \right] \cdot \{\psi\} \quad (3.5.32)$$

The first term which includes the kinetic energy can be written as

$$- \int_{\Omega} \{\mathbb{N}\} \cdot \nabla_d^2 \{\mathbb{N}\}^T d\Omega = \int_{\Omega} \nabla_d \{\mathbb{N}\} \cdot \nabla_d \{\mathbb{N}\}^T d\Omega - \int_{\Omega} \nabla_d (\{\mathbb{N}\} \cdot \nabla_d \{\mathbb{N}\}^T) d\Omega \quad (3.5.33)$$

The second integration term of this equation can be turned into a surface integral by *Gauss Theorem*:

$$\int_{\Omega} \nabla_d (\{\mathbb{N}\} \cdot \nabla_d \{\mathbb{N}\}^T) d\Omega = \int_{\partial\Omega} \{\mathbb{N}\} (\nabla_d \{\mathbb{N}\}^T) \cdot d\mathbf{S} \quad (3.5.34)$$

According to the boundary conditions of the confined physical system, the wave function and its conjugate must be zero on the surface of the solution space. This condition is valid for exact solution $\psi(\mathbf{r})$ and also trial wave function. Therefore Eq. (3.5.34) equals to zero.

Consequently we can rearrange the Eq. (3.5.32) with using Eqs. (3.5.33) and (3.5.34).

$$\left[\int_{\Omega} d\Omega \left[\frac{1}{2} \nabla_d \{\mathbb{N}\} \cdot \nabla_d \{\mathbb{N}\}^T + \{\mathbb{N}\} V(\mathbf{r}) \{\mathbb{N}\}^T \right] \right] \cdot \{\psi\} = E \left[\int_{\Omega} d\Omega \{\mathbb{N}\} \{\mathbb{N}\}^T \right] \cdot \{\psi\} \quad (3.5.35)$$

In the matrix notation this equation is described with the following equation

$$\{\{K\}\} \cdot \{\psi\} = E \{\{M\}\} \cdot \{\psi\} \quad (3.5.36)$$

where $\{\{K\}\}$ is “*Stiffness Matrix*” and $\{\{M\}\}$ is “*Mass Matrix*”. Eq. (3.5.36) is a representation of generalized eigenvalue equation of the system. To calculate the energy eigenvalues of the system we need to solve this eigenvalue equation.

The stiffness matrix ($\{\{K\}\}$) is a coefficient matrix whose elements do not include

the energy term. This matrix is defined with the below equation explicitly

$$\{\{K\}\} = \int_{\Omega} d\Omega \left[\frac{1}{2} \nabla_d \{\mathbb{N}\} \cdot \nabla_d \{\mathbb{N}\}^T + \{\mathbb{N}\} V(\mathbf{r}) \{\mathbb{N}\}^T \right] \quad (3.5.37)$$

The mass matrix ($\{\{M\}\}$) is a coefficient matrix also but this coefficients consist of the energy term and explicit form of the mass matrix is

$$\{\{M\}\} = \int_{\Omega} d\Omega \{\mathbb{N}\} \{\mathbb{N}\}^T \quad (3.5.38)$$

If we discretize the solution space, summation of the integrals over the divided solution space elements is equal to integrals over the whole solution space

$$\int_{\Omega} d\Omega = \sum_{e=1}^{N_e} \int_{\Omega_e} d\Omega_e \quad (3.5.39)$$

where N_e represents the number of global elements. Consequently we can re-describe the stiffness and mass matrices in the discretized solution space:

$$\{\{K\}\} = \sum_{e=1}^{N_e} \{\{k_e\}\} \quad (3.5.40a)$$

$$\{\{k_e\}\} = \int_{\Omega_e} d\Omega_e \left[\frac{1}{2} \nabla_d \{N\} \cdot \nabla_d \{N\}^T + \{N\} V(\mathbf{r}) \{N\}^T \right] \quad (3.5.40b)$$

$\{\{k_e\}\}$ matrix includes both of the kinetic energy term and potential energy term.

$$\{\{k_e\}\} = \{\{k_{e,kin}\}\} + \{\{k_{e,pot}\}\}$$

$$\{\{k_{e,kin}\}\} = \int_{\Omega_e} d\Omega_e \left[\frac{1}{2} \nabla_d \{N\} \nabla_d \{N\}^T \right] \quad (3.5.41)$$

$$\{\{k_{e,pot}\}\} = \int_{\Omega_e} d\Omega_e \left[\{N\} V \{N\}^T \right] \quad (3.5.42)$$

$$\{\{M\}\} = \sum_{e=1}^{N_e} \{\{m_e\}\} \quad (3.5.43a)$$

$$\{\{m_e\}\} = \int_{\Omega_e} d\Omega_e \{N\}\{N\}^T \quad (3.5.43b)$$

In these equations $\{N\}$ and $\{\mathbb{N}\}$ represent the global element basis function and the whole space basis functions respectively. Integration over each elements can be performed since basis functions are known functions.

By making a transformation for global elements which constitute the parts of discretized space, we can pass through to area coordinates from global element coordinates. So we need to write shape functions as a function of area coordinates.

In a d -dimensional space following transformation can be done for the transition from its self coordinates to area coordinates

$$d\Omega_e = \prod_{i=1}^d dx_i$$

$$\{N\}^T = \left(N_1 \quad N_2 \quad \cdots \quad N_{d+1} \right)$$

$$d\Omega_e = J_e dL_1 dL_2 \cdots dL_d$$

where J_e is the Jacobi Determinant. It describes the transformation matrix between the coordinates. Boundary condition for the area coordinates is as follows:

$$1 = L_1 + L_2 + \dots + L_d + L_{d+1}$$

The matrix elements which belong the kinetic part of the stiffness matrix (Eq. (3.5.41)) can be written obviously as in the following equations

$$\{\{k_{e,kin}\}\} = \int_{\Omega_e} d\Omega_e \left[\frac{1}{2} \nabla_d \{N\} \nabla_d \{N\}^T \right]$$

$$\nabla_d \{N\} \nabla_d \{N\}^T = \sum_{i=1}^d \frac{\partial \{N\}}{\partial x_i} \frac{\partial \{N\}^T}{\partial x_i}$$

$$\{\{k_{e,kin}\}\} = \sum_{i=1}^d \int_{\Omega_e} d\Omega_e \frac{1}{2} \left(\frac{\partial\{N\}}{\partial x_i} \right) \left(\frac{\partial\{N\}^T}{\partial x_i} \right)$$

The derivative of global element basis function is defined in terms of area coordinates such as

$$\frac{\partial\{N\}}{\partial x_i} = \begin{pmatrix} \frac{\partial N_1}{\partial x_i} \\ \frac{\partial N_2}{\partial x_i} \\ \frac{\partial N_3}{\partial x_i} \\ \vdots \\ \frac{\partial N_{ngen}}{\partial x_i} \end{pmatrix} = \sum_{j=1}^d \left(\frac{\partial L_j}{\partial x_i} \right) \left(\frac{\partial\{N\}}{\partial L_j} \right)$$

where the abbreviation “ngen” expresses the number of global element nodes.

And we can write the transpose of this expression similarly

$$\frac{\partial\{N\}^T}{\partial x_i} = \sum_{k=1}^d \left(\frac{\partial L_k}{\partial x_i} \right) \left(\frac{\partial\{N\}^T}{\partial L_k} \right)$$

$$\{\{k_{e,kin}\}\} = \sum_{i=1}^d \sum_{j=1}^d \sum_{k=1}^d \int_{\Omega_e} d\Omega_e \frac{1}{2} \left(\frac{\partial L_j}{\partial x_i} \frac{\partial\{N\}}{\partial L_j} \right) \left(\frac{\partial L_k}{\partial x_i} \frac{\partial\{N\}^T}{\partial L_k} \right)$$

$$\begin{aligned} \{\{k_{e,kin}\}\} &= \sum_{i=1}^d \sum_{j=1}^d \sum_{k=1}^d \frac{1}{2} \left(\frac{\partial L_j}{\partial x_i} \right) \left(\frac{\partial L_k}{\partial x_i} \right) \cdot J_e \\ &\cdot \int_0^1 dL_1 \int_0^{1-L_1} dL_2 \int_0^{1-L_1-L_2} dL_3 \cdots \int_0^{1-L_1-L_2-\cdots-L_{d-1}} dL_d \left(\frac{\partial\{N(L)\}}{\partial L_j} \right) \left(\frac{\partial\{N(L)\}^T}{\partial L_k} \right) \end{aligned}$$

(l, m) th matrix element can be written as

$$(k_{e,kin})_{lm} = \sum_{i=1}^d \sum_{j=1}^d \sum_{k=1}^d \frac{1}{2} \left(\frac{\partial L_j}{\partial x_i} \right) \left(\frac{\partial L_k}{\partial x_i} \right) \cdot J_e \cdot \int_0^1 dL_1 \int_0^{1-L_1} dL_2 \int_0^{1-L_1-L_2} dL_3 \cdots \int_0^{1-L_1-L_2-\cdots-L_{d-1}} dL_d \left(\frac{\partial N_l(L)}{\partial L_j} \right) \left(\frac{\partial N_m^T(L)}{\partial L_k} \right) \quad (3.5.44)$$

$$(k_{e,kin})_{lm} = \sum_{i=1}^d \sum_{j=1}^d \sum_{k=1}^d \frac{1}{2} \left(\frac{\partial L_j}{\partial x_i} \right) \left(\frac{\partial L_k}{\partial x_i} \right) \cdot J_e \cdot (k_{inv})_{lm} \quad (3.5.45)$$

$$\{\{k_{e,kin}\}\} \rightarrow J_e \{\{k_{inv}\}\}$$

where $\{\{k_{inv}\}\}$ is an invariant matrix and J_e contains the information about coordinates of node.

$$\{\{k_{inv}\}\} = \sum_{l=1}^{ngen} \sum_{m=1}^{ngen} \int_0^1 dL_1 \int_0^{1-L_1} dL_2 \int_0^{1-L_1-L_2} dL_3 \cdots \int_0^{1-L_1-L_2-\cdots-L_{d-1}} dL_d \left(\frac{\partial N_l(L)}{\partial L_j} \right) \left(\frac{\partial N_m^T(L)}{\partial L_k} \right)$$

The matrix elements of potential terms in $\{\{K\}\}$:

$$\{\{k_{e,pot}\}\} = \int_{\Omega_e} d\Omega_e [\{N\} V \{N\}^T]$$

$$V = \sum_{k=1}^{ngen} V_k \cdot N_k$$

(i, j) th matrix element for potential part of k_e can be written as

$$\left(k_{e,pot} \right)_{ij} = \sum_{k=1}^{ngen} V_k \cdot J_e \int_0^1 dL_1 \int_0^{1-L_1} dL_2 \int_0^{1-L_1-L_2} dL_3 \cdots \int_0^{1-L_1-L_2-\cdots-L_{d-1}} dL_d N_i(L) N_k(L) N_j(L) \quad (3.5.46)$$

$$(k_{e,pot})_{ij} = \sum_{k=1}^{ngen} V_k \cdot J_e((k_{e,pot})_k)_{ij} \quad (3.5.47)$$

And the matrix elements of m_e in terms of area coordinates can be defined as in the following equation

$$\{\{m_e\}\} = \int_{\Omega_e} d\Omega \{N\} \{N\}^T$$

(i, j) th matrix element of m_e

$$(m_e)_{ij} = J_e \int_0^1 dL_1 \int_0^{1-L_1} dL_2 \int_0^{1-L_1-L_2} dL_3 \cdots \int_0^{1-L_1-L_2-\cdots-L_{d-1}} dL_d N_i(L) N_j(L) \quad (3.5.48)$$

$$(m_e)_{ij} = J_e (m_{inv})_{ij}$$

$$\{\{m_e\}\} = J_e \{\{m_{inv}\}\}$$

where $\{\{m_{inv}\}\}$ represents the invariant matrix

$$\{\{m_{inv}\}\} = \sum_{i=1}^{ngen} \sum_{j=1}^{ngen} \int_0^1 dL_1 \int_0^{1-L_1} dL_2 \int_0^{1-L_1-L_2} dL_3 \cdots \int_0^{1-L_1-L_2-\cdots-L_{d-1}} dL_d N_i(L) N_j(L)$$

3.5.3 Solution of Coupled Systems with FEM

In Table (3.2) mathematical notation of matrices for coupled systems which we use in finite element analysis is described.

The classical Hamiltonian representation for coupled systems is given by

$$\overline{\overline{\mathcal{H}}} = \overline{\overline{\mathcal{H}}}_A + \overline{\overline{\mathcal{H}}}_{BP_\xi} + \overline{\overline{\mathcal{H}}}_{CP_\xi^2} \quad (3.5.49)$$

where $p_\xi = -i \frac{\partial}{\partial \xi}$ is the dimensionless canonical momentum operator. The Hamiltonian

Table 3.2 Mathematical notation of matrices for coupled systems

		FEM	Coupled System
Square Matrix	$X = \begin{pmatrix} * & * & * \\ * & * & * \\ * & * & * \end{pmatrix}$	$\{\{X\}\}$	$\overline{\overline{X}}$
Column Matrix	$X = \begin{pmatrix} * \\ * \\ * \end{pmatrix}$	$\{X\}$	\overline{X}
Row Matrix	$X = (* \ * \ *)$	$\{X\}^T$	\overline{X}^T

of coupled systems in quantum mechanical formulation can be written as

$$\overline{\overline{\mathcal{H}}} = \sum_{n=0}^{\infty} \left\{ \frac{1}{n!} \frac{\partial^n \overline{\overline{\mathcal{H}}}}{\partial p_{\xi}^n} \Big|_{p_{\xi}=0}, p_{\xi}^n \right\} = \{\overline{\overline{\mathcal{H}}}_A, 1\} + \{\overline{\overline{\mathcal{H}}}_B, p_{\xi}\} + \{\overline{\overline{\mathcal{H}}}_C, p_{\xi}^2\} \quad (3.5.50)$$

where \mathcal{H}_A is a part of the total Hamiltonian which does not contain the canonical momentum operator p_{ξ} . \mathcal{H}_B and \mathcal{H}_C contain the canonical momentum operator p_{ξ} and the square of it p_{ξ}^2 , respectively.

$$\{\overline{\overline{\mathcal{H}}}_A, 1\} = \frac{1}{2} (\overline{\overline{\mathcal{H}}}_A \cdot 1 + 1 \cdot \overline{\overline{\mathcal{H}}}_A) = \overline{\overline{\mathcal{H}}}_A \quad (3.5.51)$$

$$\{\overline{\overline{\mathcal{H}}}_B, p_{\xi}\} = \frac{1}{2} (\overline{\overline{\mathcal{H}}}_B p_{\xi} + p_{\xi} \overline{\overline{\mathcal{H}}}_B) \quad (3.5.52)$$

$$\begin{aligned} \{\overline{\overline{\mathcal{H}}}_C, p_{\xi}^2\} &= \frac{1}{2} (\overline{\overline{\mathcal{H}}}_C p_{\xi}^2 + p_{\xi}^2 \overline{\overline{\mathcal{H}}}_C) \\ &= \frac{1}{2} \left((p_{\xi} \overline{\overline{\mathcal{H}}}_C + [\overline{\overline{\mathcal{H}}}_C, p_{\xi}]) p_{\xi} + p_{\xi} (\overline{\overline{\mathcal{H}}}_C p_{\xi} - [\overline{\overline{\mathcal{H}}}_C, p_{\xi}]) \right) \\ \{\overline{\overline{\mathcal{H}}}_C, p_{\xi}^2\} &= p_{\xi} \overline{\overline{\mathcal{H}}}_C p_{\xi} + \frac{1}{2} [[\overline{\overline{\mathcal{H}}}_C, p_{\xi}], p_{\xi}] \end{aligned} \quad (3.5.53)$$

If we use these definitions in Eq. (3.5.50), we can get

$$\overline{\overline{\mathcal{H}}} = \overline{\overline{\mathcal{H}}}_A + \frac{1}{2} \left(\overline{\overline{\mathcal{H}}}_B p_\xi + p_\xi \overline{\overline{\mathcal{H}}}_B \right) + p_\xi \overline{\overline{\mathcal{H}}}_C p_\xi + \frac{1}{2} \left[\overline{\overline{\mathcal{H}}}_C, p_\xi \right], p_\xi \quad (3.5.54)$$

If the $\overline{\overline{\mathcal{H}}}_C$ contains only the terms which depend on spatial coordinates, the last term in Eq. (3.5.54) can be added to the $\overline{\overline{\mathcal{H}}}_A$ Hamiltonian expression as a correction term. And in this consideration we can rearrange the Hamiltonian expression such as

$$\overline{\overline{\mathcal{H}}} = \overline{\overline{\mathcal{H}}}_A + \frac{1}{2} \left(\overline{\overline{\mathcal{H}}}_B p_\xi + p_\xi \overline{\overline{\mathcal{H}}}_B \right) + p_\xi \overline{\overline{\mathcal{H}}}_C p_\xi \quad (3.5.55)$$

Within FEM's compass, approximate solution is searched in the finite-size function space where this function space is discretized into finite number of subregion or element. The function space is often known as "solution region".

The wave function for nc coupled band system can be defined as

$$\overline{\overline{\mathcal{X}}}(\xi) = \begin{pmatrix} \mathcal{X}_1(\xi) \\ \mathcal{X}_2(\xi) \\ \vdots \\ \mathcal{X}_{nc}(\xi) \end{pmatrix}$$

where nc is the measurement of coupling.

And the wave function of the set of basis functions can be written in a serial form

as follows

$$\begin{aligned}
 \mathcal{X}_1(\xi) &= \sum_{i=1}^{ntn} \mathcal{X}_{i1} \mathbb{N}_i(\xi) \\
 \mathcal{X}_2(\xi) &= \sum_{i=1}^{ntn} \mathcal{X}_{i2} \mathbb{N}_i(\xi) \\
 &\vdots \\
 \mathcal{X}_{nc}(\xi) &= \sum_{i=1}^{ntn} \mathcal{X}_{i(nc)} \mathbb{N}_i(\xi)
 \end{aligned} \tag{3.5.56}$$

The wave function, which we want to achieve, can be shown in matrix notation over the nodes of related space.

$$\bar{\mathcal{X}}(\xi) = \begin{pmatrix} \mathbb{N}_1(\xi) & 0 & \dots & 0 & | & \mathbb{N}_2(\xi) & 0 & \dots & 0 & | & \mathbb{N}_{nm}(\xi) & 0 & \dots & 0 \\ 0 & \mathbb{N}_1(\xi) & \dots & 0 & | & 0 & \mathbb{N}_2(\xi) & \dots & 0 & | & 0 & \mathbb{N}_{nm}(\xi) & \dots & 0 \\ \vdots & \dots & \ddots & \vdots & | & \vdots & \dots & \ddots & \vdots & | & \vdots & \dots & \ddots & \vdots \\ 0 & \dots & 0 & \mathbb{N}_1(\xi) & | & 0 & \dots & 0 & \mathbb{N}_2(\xi) & | & 0 & \dots & 0 & \mathbb{N}_{nm}(\xi) \end{pmatrix} \cdot \begin{pmatrix} \mathcal{X}_{11} \\ \mathcal{X}_{12} \\ \vdots \\ \mathcal{X}_{1(nc)} \\ \hline \mathcal{X}_{21} \\ \mathcal{X}_{22} \\ \vdots \\ \mathcal{X}_{2(nc)} \\ \hline \vdots \\ \vdots \\ \hline \mathcal{X}_{nm1} \\ \mathcal{X}_{nm2} \\ \vdots \\ \mathcal{X}_{nm(nc)} \end{pmatrix} \tag{3.5.57}$$

$$\bar{\mathcal{X}}(\xi) = \left(\bar{\mathbb{N}}_1 \cdot \bar{\mathbb{I}}_{nc \times nc}, \bar{\mathbb{N}}_2 \cdot \bar{\mathbb{I}}_{nc \times nc}, \bar{\mathbb{N}}_3 \cdot \bar{\mathbb{I}}_{nc \times nc}, \dots, \bar{\mathbb{N}}_{ntn} \cdot \bar{\mathbb{I}}_{nc \times nc} \right) \begin{pmatrix} \bar{\mathcal{X}}_1 \\ \bar{\mathcal{X}}_2 \\ \vdots \\ \bar{\mathcal{X}}_{ntn} \end{pmatrix}$$

Thus, we can write the wave function and its hermitian conjugate of it in matrix notation of FEM

$$\bar{\mathcal{X}}(\xi) = \left\{ \bar{\mathbb{N}}(\xi) \bar{\mathbb{I}} \right\}^\dagger \{ \bar{\mathcal{X}} \} \quad (3.5.58)$$

$$\bar{\mathcal{X}}^\dagger(\xi) = \left(\mathcal{X}_1^\dagger(\xi), \mathcal{X}_2^\dagger(\xi), \dots, \mathcal{X}_{nc}^\dagger(\xi) \right) = \{ \bar{\mathcal{X}} \}^\dagger \left\{ \bar{\mathbb{N}}(\xi) \bar{\mathbb{I}} \right\} \quad (3.5.59)$$

And so the unknown variational parameters $\mathcal{X}_{(nc)}$ can be derived with “*Galerkin’s Method*”

$$\mathcal{G} = \int_{\xi_i}^{\xi_f} d\xi \bar{\mathcal{X}}^\dagger(\xi) (\bar{\mathcal{H}} - \varepsilon \bar{\mathbb{I}}) \bar{\mathcal{X}}(\xi) \quad (3.5.60)$$

where $\bar{\mathbb{I}}$ is the unitary matrix ($ngen \times ngen$).

If one can write the wave function and hermitian conjugate of it in matrix notation, the following equation is obtained

$$\mathcal{G} = \{ \bar{\mathcal{X}} \}^\dagger \left[\int_{\xi_i}^{\xi_f} d\xi \left\{ \bar{\mathbb{N}}(\xi) \right\} (\bar{\mathcal{H}} - \varepsilon \bar{\mathbb{I}}) \left\{ \bar{\mathbb{N}}(\xi) \right\}^\dagger \right] \{ \bar{\mathcal{X}} \}$$

We minimize the “ \mathcal{G} ” term with respect to the $(\{ \bar{\mathcal{X}} \}^\dagger)$. As aforementioned (section 3.5.2) $(\{ \bar{\mathcal{X}} \}, \{ \bar{\mathcal{X}} \}^\dagger)$ family is also minimize the energy of the system.

$$\frac{\partial \mathcal{G}}{\partial \{ \bar{\mathcal{X}} \}^\dagger} = 0 \quad (3.5.61)$$

$$\left[\int_{\xi_i}^{\xi_f} d\xi \left\{ \bar{\mathbb{N}}(\xi) \right\} (\bar{\mathcal{H}} - \varepsilon \bar{\mathbb{I}}) \left\{ \bar{\mathbb{N}}(\xi) \right\}^\dagger \right] \{ \bar{\mathcal{X}} \} = 0 \quad (3.5.62)$$

$$\left[\int_{\xi_i}^{\xi_f} d\xi \{\bar{\bar{\mathbf{N}}}(\xi)\} \bar{\bar{\mathcal{H}}} \{\bar{\bar{\mathbf{N}}}(\xi)\}^\dagger \right] \{\bar{\mathcal{X}}\} = \varepsilon \left[\int_{\xi_i}^{\xi_f} d\xi \{\bar{\bar{\mathbf{N}}}(\xi)\} \{\bar{\bar{\mathbf{N}}}(\xi)\}^\dagger \right] \{\bar{\mathcal{X}}\} \quad (3.5.63)$$

The generalized eigenvalue equation of the system can be defined by using the new presentation

$$\{\{\bar{\bar{\mathbf{K}}}\}\} \{\bar{\mathcal{X}}\} = \varepsilon \{\{\bar{\bar{\mathbf{M}}}\}\} \{\bar{\mathcal{X}}\} \quad (3.5.64)$$

where $\{\{\bar{\bar{\mathbf{K}}}\}\}$ represents the “*Stiffness Matrix*” and $\{\{\bar{\bar{\mathbf{M}}}\}\}$ denotes the “*Mass Matrix*” for the coupled system. Explicit forms of these matrix expressions are;

$$\{\{\bar{\bar{\mathbf{K}}}\}\} = \int_{\xi_i}^{\xi_f} d\xi \{\bar{\bar{\mathbf{N}}}(\xi)\} \bar{\bar{\mathcal{H}}} \{\bar{\bar{\mathbf{N}}}(\xi)\}^\dagger \quad (3.5.65)$$

$$\{\{\bar{\bar{\mathbf{M}}}\}\} = \int_{\xi_i}^{\xi_f} d\xi \{\bar{\bar{\mathbf{N}}}(\xi)\} \{\bar{\bar{\mathbf{N}}}(\xi)\}^\dagger \quad (3.5.66)$$

The integrals over the whole solution space can be re-described as the summation of the integrals over the divided solution space elements.

$$\int_{\xi_i}^{\xi_f} d\xi \quad \rightarrow \quad \sum_{e=1}^{nge} \int_{\xi_e}^{\xi_{e+1}} d\xi$$

We can rewrite the stiffness matrix and mass matrix by using the integration of the stiffness matrix and the mass matrix over the each global element

$$\{\{\bar{\bar{\mathbf{K}}}\}\} = \sum_{e=1}^{nge} \{\{\bar{\bar{\mathbf{k}}}_e\}\} \quad (3.5.67)$$

$$\{\{\bar{\bar{\mathbf{k}}}_e\}\} = \int_{\xi_e}^{\xi_{e+1}} d\xi \{\bar{\bar{\mathbf{N}}}(\xi)\} \bar{\bar{\mathcal{H}}} \{\bar{\bar{\mathbf{N}}}(\xi)\}^\dagger \quad (3.5.68)$$

$$\{\{\bar{\mathcal{M}}\}\} = \sum_{e=1}^{nge} \{\{\bar{m}_e\}\} \quad (3.5.69)$$

$$\{\{\bar{m}_e\}\} = \int_{\xi_e}^{\xi_{e+1}} d\xi \{\{\bar{N}_e(\xi)\}\} \{\{\bar{N}_e(\xi)\}\}^\dagger = \int_{\xi_e}^{\xi_{e+1}} d\xi \{\{\bar{N}_e(\xi)\}\} \{\{\bar{N}_e(\xi)\}\}^\dagger \quad (3.5.70)$$

With below transformation we can take place $[0, 1]$ space and then we can generate FEM bases in this space. If we divide the $[0, 1]$ space into n pieces, we get $(n + 1)$ basis functions which are given by n th degree polynomial.

$$\begin{array}{c} \xi_e \quad \xi_{e+1} \rightarrow \quad \frac{s_1}{0} \quad \frac{s_2}{\quad} \quad \cdots \quad \frac{s_j}{\quad} \quad \frac{s_{j+1}}{\quad} \quad \cdots \quad \frac{s_{n-1}}{1} \quad \frac{s_n}{1} \rightarrow s \end{array}$$

$$[0, 1] \rightarrow [s_0, s_1] + [s_1, s_2] + \cdots + [s_k, s_{k+1}] \cdots + [s_{n-1}, s_n] \quad (3.5.71)$$

where $s_0 = 0$ and $s_n = 1$.

$$s = \frac{\xi - \xi_e}{\xi_{e+1} - \xi_e} \quad h_e = \xi_{e+1} - \xi_e \quad (3.5.72)$$

$$\Rightarrow \quad \xi = s \cdot h_e + \xi_e \quad h_e ds = d\xi \quad (3.5.73)$$

$$\int_{\xi_e}^{\xi_{e+1}} d\xi \quad \rightarrow \quad (h_e) \int_0^1 ds \quad (3.5.74)$$

$$\{\{\bar{N}_e(\xi)\}\} \quad \rightarrow \quad \{\{\bar{N}_e(s)\}\} \quad , \quad s \in [0, 1]$$

Therefore Eq. (3.5.70)

$$\{\{\bar{m}_e\}\} = (h_e) \underbrace{\int_0^1 ds \{\bar{N}(s)\} \{\bar{N}(s)\}^\dagger}$$

$\{\{\bar{m}\}\} : (\text{invariant matrix})$

$$\{\{\bar{m}\}\} = \int_0^1 ds \left\{ \begin{array}{c} \bar{N}_1(s) \\ \bar{N}_2(s) \\ \vdots \\ \bar{N}_{ngen}(s) \end{array} \right\} \left\{ \bar{N}_1(s), \bar{N}_2(s), \dots, \bar{N}_{ngen}(s) \right\}$$

$$\{\{\bar{m}\}\} = \int_0^1 ds \left\{ \begin{array}{cccc} N_1(s) & 0 & \dots & 0 \\ 0 & N_1(s) & \dots & 0 \\ \vdots & \vdots & \ddots & \vdots \\ 0 & \dots & 0 & N_1(s) \\ \hline N_2(s) & 0 & \dots & 0 \\ 0 & N_2(s) & \dots & 0 \\ \vdots & \vdots & \ddots & \vdots \\ 0 & \dots & 0 & N_2(s) \\ \hline \vdots & \vdots & \vdots & \vdots \\ \vdots & \vdots & \vdots & \vdots \\ \hline N_{ngen}(s) & 0 & \dots & 0 \\ 0 & N_{ngen}(s) & \dots & 0 \\ \vdots & \vdots & \ddots & \vdots \\ 0 & \dots & 0 & N_{ngen}(s) \end{array} \right\}$$

$$\left(\begin{array}{cccc|cccc|cccc} N_1(s) & 0 & \dots & 0 & N_2(s) & 0 & \dots & 0 & N_{ngen}(s) & 0 & \dots & 0 \\ 0 & N_1(s) & \dots & 0 & 0 & N_2(s) & \dots & 0 & 0 & N_{ngen}(s) & \dots & 0 \\ \vdots & \dots & \ddots & \vdots & \vdots & \dots & \ddots & \vdots & \vdots & \dots & \ddots & \vdots \\ 0 & \dots & 0 & N_1(s) & 0 & \dots & 0 & N_2(s) & 0 & \dots & 0 & N_{ngen}(s) \end{array} \right)$$

$$\{\{\bar{m}\}\} = \int_0^1 ds \left(\begin{array}{cccc} N_1(s) \cdot N_1(s) \cdot \bar{I}, & N_1(s) \cdot N_2(s) \cdot \bar{I}, & \dots, & N_1(s) \cdot N_{ngen}(s) \cdot \bar{I} \\ N_2(s) \cdot N_1(s) \cdot \bar{I}, & N_2(s) \cdot N_2(s) \cdot \bar{I}, & \dots, & N_2(s) \cdot N_{ngen}(s) \cdot \bar{I} \\ \dots & \dots & \dots & \dots \\ N_{ngen}(s) \cdot N_1(s) \cdot \bar{I}, & N_{ngen}(s) \cdot N_2(s) \cdot \bar{I}, & \dots, & N_{ngen}^2(s) \cdot \bar{I} \end{array} \right)$$

$$\bar{\bar{I}} = \begin{pmatrix} 1 & 0 & \dots & \dots & 0 \\ 0 & 1 & \vdots & \vdots & \vdots \\ \vdots & \vdots & \ddots & \vdots & \vdots \\ 0 & \dots & \dots & 0 & 1 \end{pmatrix}_{(nc) \times (nc)}$$

$$\{\{\bar{\bar{m}}\}\} = \int_0^1 ds \begin{pmatrix} N_1(s) \cdot N_1(s), & N_1(s) \cdot N_2(s), & \dots, & N_1(s) \cdot N_{ngen}(s) \\ N_2(s) \cdot N_1(s), & N_2(s) \cdot N_2(s), & \dots, & N_2(s) \cdot N_{ngen}(s) \\ \dots & \dots & \dots & \dots \\ N_{ngen}(s) \cdot N_1(s), & N_{ngen}(s) \cdot N_2(s), & \dots, & N_{ngen}^2(s) \end{pmatrix} \otimes \bar{\bar{I}}$$

$$\{\{\bar{\bar{m}}\}\} = \{\{m\}\} \otimes \bar{\bar{I}} \quad \text{Kronecker Product} \quad (3.5.75)$$

$$\{\{m\}\} = \int_0^1 ds \{N(s)\} \{N(s)\}^\dagger \quad (3.5.76)$$

$$\{\{\bar{\bar{m}}_e\}\} = (h_e) \{\{m\}\} \otimes \bar{\bar{I}} \quad (3.5.77)$$

Eq. (3.5.65);

$$\{\{\bar{\bar{K}}\}\} = \int_{\xi_i}^{\xi_f} d\xi \{\bar{\bar{N}}(\xi)\} \bar{\bar{\mathcal{H}}} \{\bar{\bar{N}}(\xi)\}^\dagger$$

and the Hamiltonian which is given in Eq. (3.5.55)

$$\bar{\bar{\mathcal{H}}} = \bar{\bar{\mathcal{H}}}_A + \frac{1}{2} \left(\bar{\bar{\mathcal{H}}}_B p_\xi + p_\xi \bar{\bar{\mathcal{H}}}_B \right) + p_\xi \bar{\bar{\mathcal{H}}}_C p_\xi$$

After inserting this Hamiltonian expression into stiffness matrix equation we can use

integration by parts for the last two terms. Consequently surface terms appear.

$$\begin{aligned}
\{\{\bar{K}\}\} &= \int_{\xi_i}^{\xi_f} d\xi \{\bar{N}(\xi)\} \bar{\mathcal{H}}_A \{\bar{N}(\xi)\}^\dagger + \int_{\xi_i}^{\xi_f} d\xi \{\bar{N}(\xi)\} \frac{1}{2i} \bar{\mathcal{H}}_B \frac{\partial}{\partial \xi} \{\bar{N}(\xi)\}^\dagger \\
&+ \frac{1}{2i} \underbrace{\{\bar{N}(\xi)\}}_0 \bar{\mathcal{H}}_B \{\bar{N}(\xi)\}^\dagger \Big|_{\xi_i}^{\xi_f} - \int_{\xi_i}^{\xi_f} d\xi \frac{\partial \{\bar{N}(\xi)\}}{\partial \xi} \frac{1}{2i} \bar{\mathcal{H}}_B \{\bar{N}(\xi)\}^\dagger \\
&- \underbrace{\{\bar{N}(\xi)\}}_0 \bar{\mathcal{H}}_C \frac{\partial}{\partial \xi} \{\bar{N}(\xi)\}^\dagger \Big|_{\xi_i}^{\xi_f} + \int_{\xi_i}^{\xi_f} d\xi \frac{\partial}{\partial \xi} \{\bar{N}(\xi)\} \bar{\mathcal{H}}_C \frac{\partial}{\partial \xi} \{\bar{N}(\xi)\}^\dagger
\end{aligned} \tag{3.5.78}$$

If the physical system whose solution is desired to get is confined in a specific region of work space, the wave function of this physical system decay on the surface of the solution space. According to this physical boundary condition, the surface terms in Eq. (3.5.78) do not contribute to the stiffness matrix term.

$$\{\bar{N}(\xi_i)\} = \{\bar{N}(\xi_f)\} = 0$$

$$\begin{aligned}
\{\{\bar{K}\}\} &= \int_{\xi_i}^{\xi_f} d\xi \{\bar{N}(\xi)\} \bar{\mathcal{H}}_A \{\bar{N}(\xi)\}^\dagger + \int_{\xi_i}^{\xi_f} d\xi \{\bar{N}(\xi)\} \frac{1}{2i} \bar{\mathcal{H}}_B \frac{\partial}{\partial \xi} \{\bar{N}(\xi)\}^\dagger \\
&- \int_{\xi_i}^{\xi_f} d\xi \frac{\partial \{\bar{N}(\xi)\}}{\partial \xi} \frac{1}{2i} \bar{\mathcal{H}}_B \{\bar{N}(\xi)\}^\dagger + \int_{\xi_i}^{\xi_f} d\xi \frac{\partial}{\partial \xi} \{\bar{N}(\xi)\} \bar{\mathcal{H}}_C \frac{\partial}{\partial \xi} \{\bar{N}(\xi)\}^\dagger
\end{aligned} \tag{3.5.79}$$

We need to go back to Eqs. (3.5.67) and (3.5.68) to make the transformation which is given in Eqs. (3.5.72) and (3.5.73). By using the expressions in Eqs. (3.5.72) and (3.5.73), we can get the definition of $\{\{\bar{k}_e\}\}$ in terms of s :

$$\begin{aligned}
\{\{\bar{k}_e\}\} &= h_e \int_0^1 ds \{\bar{N}(s)\} \bar{\mathcal{H}}_A(s) \{\bar{N}(s)\}^\dagger \\
&+ \frac{1}{2i} \int_0^1 ds \left(\{\bar{N}(s)\} \bar{\mathcal{H}}_B(s) \frac{\partial}{\partial s} \{\bar{N}(s)\}^\dagger - \frac{\partial}{\partial s} \{\bar{N}(s)\} \bar{\mathcal{H}}_B(s) \{\bar{N}(s)\}^\dagger \right) \quad (3.5.80) \\
&+ \frac{1}{h_e} \int_0^1 ds \frac{\partial}{\partial s} \{\bar{N}(s)\} \bar{\mathcal{H}}_C(s) \frac{\partial}{\partial s} \{\bar{N}(s)\}^\dagger
\end{aligned}$$

The Eq. (3.5.80) can be divided into parts related to Hamiltonian components:

$$\{\{\bar{k}_e\}\} = \{\{\bar{k}_{A,e}\}\} + \left(\{\{\bar{k}_{BR,e}\}\} - \{\{\bar{k}_{BL,e}\}\} \right) + \{\{\bar{k}_{C,e}\}\} \quad (3.5.81)$$

$$\{\{\bar{k}_{A,e}\}\} = h_e \int_0^1 ds \{\bar{N}(s)\} \bar{\mathcal{H}}_A(s) \{\bar{N}(s)\}^\dagger \quad (3.5.82)$$

$$\{\{\bar{k}_{A,e}\}\} = h_e \int_0^1 ds \begin{pmatrix} N_1(s) \cdot N_1(s) \cdot \bar{\mathcal{H}}_A(s), & N_1(s) \cdot N_2(s) \cdot \bar{\mathcal{H}}_A(s), & \dots, & N_1(s) \cdot N_{ngen}(s) \cdot \bar{\mathcal{H}}_A(s) \\ N_2(s) \cdot N_1(s) \cdot \bar{\mathcal{H}}_A(s), & N_2(s) \cdot N_2(s) \cdot \bar{\mathcal{H}}_A(s), & \dots, & N_2(s) \cdot N_{ngen}(s) \cdot \bar{\mathcal{H}}_A(s) \\ \dots & \dots & \dots & \dots \\ N_{ngen}(s) \cdot N_1(s) \cdot \bar{\mathcal{H}}_A(s), & N_{ngen}(s) \cdot N_2(s) \cdot \bar{\mathcal{H}}_A(s), & \dots, & N_{ngen}^2(s) \cdot \bar{\mathcal{H}}_A(s) \end{pmatrix}$$

$$\{\{\bar{k}_{A,e}\}\} = h_e \int_0^1 ds \begin{pmatrix} N_1(s) \cdot N_1(s), & N_1(s) \cdot N_2(s), & \dots, & N_1(s) \cdot N_{ngen}(s) \\ N_2(s) \cdot N_1(s), & N_2(s) \cdot N_2(s), & \dots, & N_2(s) \cdot N_{ngen}(s) \\ \dots & \dots & \dots & \dots \\ N_{ngen}(s) \cdot N_1(s), & N_{ngen}(s) \cdot N_2(s), & \dots, & N_{ngen}^2(s) \end{pmatrix} \otimes (\bar{\mathcal{H}}_A(s)) \quad (3.5.83)$$

$$\bar{\mathcal{H}}_A(s) = \sum_{j=1}^{ngen} \bar{\mathcal{H}}_A(s_j) N_j(s) \quad (3.5.84)$$

$$\bar{\mathcal{H}}_A(s_j) = \bar{\mathcal{H}}_{A,j}$$

$$\{\{\bar{k}_{A,e}\}\} = h_e \sum_{j=1}^{ngen} \left[\int_0^1 ds \left(\{\bar{N}(s)\} N_j(s) \{\bar{N}(s)\}^\dagger \right) \right] \otimes (\bar{\mathcal{H}}_A(s_j)) \quad (3.5.85)$$

$$\{\{\bar{k}_{A,e}\}\} = h_e \sum_{j=1}^{ngen} \{\{k_A\}\} \otimes \bar{\mathcal{H}}_A(s_j) \quad (3.5.86)$$

$$\{\{\bar{k}_{BR,e}\}\} = \frac{1}{2i} \int_0^1 ds \{\bar{N}(s)\} \bar{\mathcal{H}}_B(s) \frac{\partial}{\partial s} \{\bar{N}(s)\}^\dagger \quad (3.5.87)$$

$$\{\{\bar{k}_{BR,e}\}\} = \frac{1}{2i} \int_0^1 ds \left(\begin{array}{cccc} N_1(s) \cdot \frac{\partial N_1(s)}{\partial s}, & N_1(s) \cdot \frac{\partial N_2(s)}{\partial s}, & \dots, & N_1(s) \cdot \frac{\partial N_{ngen}(s)}{\partial s} \\ N_2(s) \cdot \frac{\partial N_1(s)}{\partial s}, & N_2(s) \cdot \frac{\partial N_2(s)}{\partial s}, & \dots, & N_2(s) \cdot \frac{\partial N_{ngen}(s)}{\partial s} \\ \dots & \dots & \dots & \dots \\ N_{ngen}(s) \cdot \frac{\partial N_1(s)}{\partial s}, & N_{ngen}(s) \cdot \frac{\partial N_2(s)}{\partial s}, & \dots, & N_{ngen}(s) \cdot \frac{\partial N_{ngen}(s)}{\partial s} \end{array} \right) \otimes (\bar{\mathcal{H}}_B(s)) \quad (3.5.88)$$

$$\bar{\mathcal{H}}_B(s) = \sum_{j=1}^{ngen} \bar{\mathcal{H}}_B(s_j) N_j(s) \quad (3.5.89)$$

$$\{\{\bar{k}_{BR,e}\}\} = \frac{1}{2i} \sum_{j=1}^{ngen} \left[\int_0^1 ds \left(\{\bar{N}(s)\} N_j(s) \frac{\partial}{\partial s} \{\bar{N}(s)\}^\dagger \right) \right] \otimes (\bar{\mathcal{H}}_B(s_j)) \quad (3.5.90)$$

$$\{\{\bar{k}_{BR,e}\}\} = \frac{1}{2i} \sum_{j=1}^{ngen} \{\{k_{BR}\}\} \otimes \bar{\mathcal{H}}_B(s_j) \quad (3.5.91)$$

$$\{\{\bar{k}_{BL,e}\}\} = \frac{1}{2i} \int_0^1 ds \frac{\partial}{\partial s} \{\bar{N}(s)\} \bar{\mathcal{H}}_B(s) \{\bar{N}(s)\}^\dagger \quad (3.5.92)$$

$$\{\{\bar{k}_{BL,e}\}\} = \frac{1}{2i} \int_0^1 ds \left(\begin{array}{cccc} \frac{\partial N_1(s)}{\partial s} \cdot N_1(s), & \frac{\partial N_1(s)}{\partial s} \cdot N_2(s), & \dots, & \frac{\partial N_1(s)}{\partial s} \cdot N_{ngen}(s) \\ \frac{\partial N_2(s)}{\partial s} \cdot N_1(s), & \frac{\partial N_2(s)}{\partial s} \cdot N_2(s), & \dots, & \frac{\partial N_2(s)}{\partial s} \cdot N_{ngen}(s) \\ \dots & \dots & \dots & \dots \\ \frac{\partial N_{ngen}(s)}{\partial s} \cdot N_1(s), & \frac{\partial N_{ngen}(s)}{\partial s} \cdot N_2(s), & \dots, & \frac{\partial N_{ngen}(s)}{\partial s} \cdot N_{ngen}(s) \end{array} \right) \otimes (\bar{\mathcal{H}}_B(s)) \quad (3.5.93)$$

$$\{\{\bar{k}_{BL,e}\}\} = \frac{1}{2i} \sum_{j=1}^{ngen} \left[\int_0^1 ds \left(\frac{\partial}{\partial s} \{\bar{N}(s)\} N_j(s) \{\bar{N}(s)\}^\dagger \right) \right] \otimes \left(\overline{\overline{\mathcal{H}_B(s_j)}} \right) \quad (3.5.94)$$

$$\{\{\bar{k}_{BL,e}\}\} = \frac{1}{2i} \sum_{j=1}^{ngen} \{\{k_{BL}\}\} \otimes \overline{\overline{\mathcal{H}_B(s_j)}} \quad (3.5.95)$$

$$\{\{k_{BL}\}\} = \{\{k_{BR}\}\}^\dagger \quad (3.5.96)$$

$$\{\{\bar{k}_{C,e}\}\} = \frac{1}{h_e} \int_0^1 ds \frac{\partial}{\partial s} \{\bar{N}(s)\} \overline{\overline{\mathcal{H}_C(s)}} \frac{\partial}{\partial s} \{\bar{N}(s)\}^\dagger \quad (3.5.97)$$

$$\{\{\bar{k}_{C,e}\}\} = \frac{1}{h_e} \int_0^1 ds \left(\begin{array}{cccc} \frac{\partial N_1(s)}{\partial s} \cdot \frac{\partial N_1(s)}{\partial s}, & \frac{\partial N_1(s)}{\partial s} \cdot \frac{\partial N_2(s)}{\partial s}, & \dots, & \frac{\partial N_1(s)}{\partial s} \cdot \frac{\partial N_{ngen}(s)}{\partial s} \\ \frac{\partial N_2(s)}{\partial s} \cdot \frac{\partial N_1(s)}{\partial s}, & \frac{\partial N_2(s)}{\partial s} \cdot \frac{\partial N_2(s)}{\partial s}, & \dots, & \frac{\partial N_2(s)}{\partial s} \cdot \frac{\partial N_{ngen}(s)}{\partial s} \\ \dots & \dots & \dots & \dots \\ \frac{\partial N_{ngen}(s)}{\partial s} \cdot \frac{\partial N_1(s)}{\partial s}, & \frac{\partial N_{ngen}(s)}{\partial s} \cdot \frac{\partial N_2(s)}{\partial s}, & \dots, & \frac{\partial N_{ngen}(s)}{\partial s} \cdot \frac{\partial N_{ngen}(s)}{\partial s} \end{array} \right) \otimes \left(\overline{\overline{\mathcal{H}_C(s)}} \right) \quad (3.5.98)$$

$$\overline{\overline{\mathcal{H}_C(s)}} = \sum_{j=1}^{ngen} \overline{\overline{\mathcal{H}_C(s_j)}} N_j(s) \quad (3.5.99)$$

$$\{\{\bar{k}_{C,e}\}\} = \frac{1}{h_e} \sum_{j=1}^{ngen} \left[\int_0^1 ds \left(\frac{\partial}{\partial s} \{\bar{N}(s)\} N_j(s) \frac{\partial}{\partial s} \{\bar{N}(s)\}^\dagger \right) \right] \otimes \left(\overline{\overline{\mathcal{H}_C(s_j)}} \right) \quad (3.5.100)$$

$$\{\{\bar{k}_{C,e}\}\} = \frac{1}{h_e} \sum_{j=1}^{ngen} \{\{k_C\}\} \otimes \overline{\overline{\mathcal{H}_C(s_j)}} \quad (3.5.101)$$

We use the Eqs. (3.5.86), (3.5.91), (3.5.95) and (3.5.101) to solve eigenvalue equation (Eq. (3.5.64)).

CHAPTER FOUR

FORMALISM OF THE PHYSICAL SYSTEM

In this chapter we give a description of the physical system. We also give information about how we calculate the electronic structure of this physical system.

4.1 Introduction

In this thesis our aim is to investigate theoretically the ground state electronic structure of a confined QWR subjected to a perpendicular magnetic field, including both Rashba and Dresselhaus SO interactions and exchange-correlation effects.

We consider a quasi-1D QWR with SO interaction in a perpendicular magnetic field. We assume that the wire lies in the xy plane with \hat{y} direction parallel to the wire and has a parabolic confinement in the \hat{x} direction $V_{conf}(x) = (m^*/2)\omega_0^2 x^2$. Charge carriers move freely along the y - direction, accordingly translational invariance along this direction exists. The magnetic field is oriented along the growth direction, taken to be \hat{z} , $\mathbf{B} = (0, 0, B)$, with corresponding magnetic vector potential in Landau gauge expressed as $\mathbf{A} = (0, Bx, 0)$.

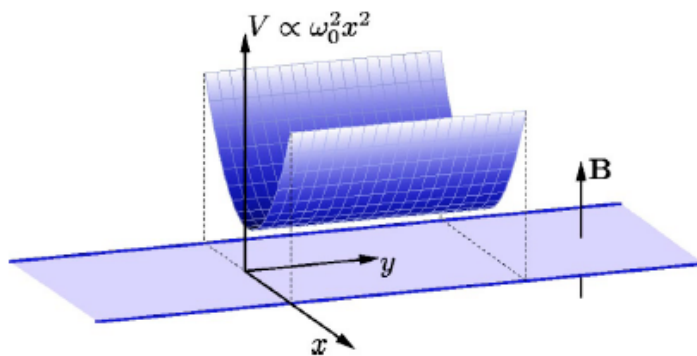


Figure 4.1 Schematic representation of the wire system (Debald & Kramer, 2005).

Translational invariance along \hat{y} direction allows us to decompose the eigenfunction of total Hamiltonian into plane waves in the longitudinal direction and a spinor part

depending on the transverse coordinate x such as

$$\Psi_n(x, y) = e^{ik_y y} \begin{pmatrix} \varphi_{n, k_y}(x, \uparrow) \\ \varphi_{n, k_y}(x, \downarrow) \end{pmatrix} =: e^{ik_y y} \varphi_{n, k_y}(x) \quad (4.1.1)$$

where wave numbers k_y are good quantum numbers of the system, the index n stands for the energy level and $\varphi_{n, k_y}(x, \uparrow (\downarrow))$ defines the spinor function.

4.2 Hamiltonian of the Physical System

The single particle Hamiltonian in quasi-1D with SO coupling is given by

$$\mathcal{H} = \mathcal{H}_0 + \mathcal{H}_Z + \mathcal{H}_{so} \quad (4.2.1)$$

The first term in Eq. (4.2.1) contains kinetic energy and confining potential $V(x)$ contributions,

$$\mathcal{H}_0 = \left(\frac{1}{2m^*} [p_x^2 + (p_y + eBx)^2] + V(x) \right) \sigma_0 \quad (4.2.2)$$

where p_x, p_y are components of electron momentum and σ_0 is the (2×2) unit matrix.

The second term is Zeeman Hamiltonian which is known as:

$$\mathcal{H}_Z = \frac{1}{2} g^* \mu_B \sigma_z B \quad (4.2.3)$$

where g^* is the effective Lande-g factor, μ_B is the Bohr magneton ($\mu_B = e\hbar/(2m_e)$) and σ_z is the z component of Pauli spin matrix. The last term in Eq. (4.2.1), \mathcal{H}_{so} , is total SO Hamiltonian which involves Rashba and Dresselhaus SO couplings. The Dresselhaus term has two components, one linear in the momentum and the other cubic (Dyakonov & Kachorovskii, 1986). Here, we regard only linear Dresselhaus term and neglect the cubic Dresselhaus term which is important for 2D quantum wells (Miller, Zumbühl, Marcus, Lyanda-Geller, Goldhaber-Gordon, Campman, & et al., 2003).

$$\mathcal{H}_{so} = \mathcal{H}_R + \mathcal{H}_D$$

The Rashba SO Hamiltonian is given by

$$\mathcal{H}_R = \frac{\alpha}{\hbar} [\boldsymbol{\sigma} \times (\mathbf{p} + e\mathbf{A})]_z = \frac{\alpha}{\hbar} [\sigma_x(p_y + eBx) - \sigma_y p_x] \quad (4.2.4)$$

whereas Dresselhaus SO Hamiltonian is

$$\mathcal{H}_D = \frac{\beta}{\hbar} [\sigma_y(p_y + eBx) - \sigma_x p_x] \quad (4.2.5)$$

In these Hamiltonians α and β stand for the Rashba and Dresselhaus SO coupling parameters, respectively. σ_x and σ_y denote Pauli spin matrix components.

With the wavefunction ansatz, which is given in Eq. (4.1.1), the Schrödinger equation becomes separable in x and y . So, the explicit form of the \mathcal{H}_0 and \mathcal{H}_{so} Hamiltonians can be written as follows:

$$\mathcal{H}_0 = \left[-\frac{\hbar^2}{2m^*} \frac{d^2}{dx^2} + \frac{1}{2} m^* \omega^2 (x - x_0)^2 + \frac{\omega_0^2 \hbar^2 k_y^2}{\omega^2 2m^*} \right] \sigma_0 \quad (4.2.6)$$

$$\mathcal{H}_{so} = \alpha \left[\sigma_x \left(k_y + \frac{eB}{\hbar} x \right) + i\sigma_y \frac{d}{dx} \right] + \beta \left[\sigma_y \left(k_y + \frac{eB}{\hbar} x \right) + i\sigma_x \frac{d}{dx} \right] \quad (4.2.7)$$

where $\omega = (\omega_0^2 + \omega_c^2)^{1/2}$ is the effective oscillator frequency with the cyclotron frequency

$$\omega_c = \frac{eB}{m^*} \quad (4.2.8)$$

and, x_0 is the center coordinate of the harmonic oscillator

$$x_0 = -\left(\frac{\omega_c}{\omega} \right)^2 \frac{\hbar k_y}{eB} = -\left(\frac{\omega_c \omega_0}{\omega^2} \right) l_0^2 k_y \quad (4.2.9)$$

and l_0 is the harmonic oscillator length.

$$l_0 = \sqrt{\frac{\hbar}{m^* \omega_0}} \quad (4.2.10)$$

4.3 Dimensionless Form of Hamiltonian

We need to scale all parameters in the Schrödinger equation to get solutions. For this purpose, we consider the harmonic oscillator length l_0 as a length scale and consecutively all energies are calculated in terms of $\hbar\omega_0$.

Here are some definitions to get dimensionless form of each Hamiltonian term:

$$x = \xi l_0 \quad \Rightarrow \quad \frac{d}{dx} = \frac{1}{l_0} \frac{d}{d\xi} = \frac{1}{l_0} D_\xi \quad \Rightarrow \quad \frac{d^2}{dx^2} = \frac{1}{l_0^2} D_\xi^2 \quad (4.3.1)$$

$$p_\xi = \frac{1}{i} \frac{\partial}{\partial \xi} = \frac{1}{i} D_\xi \quad \Rightarrow \quad D_\xi = i p_\xi \quad \Rightarrow \quad D_\xi^2 = -p_\xi^2 \quad (4.3.2)$$

$$\mathbb{K}_0 = k_y l_0 \quad \Rightarrow \quad k_y = \frac{1}{l_0} \mathbb{K}_0 \quad (4.3.3)$$

By using Eqs. (4.3.1) - (4.3.3) in \mathcal{H}_0 Hamiltonian term (Eq. (4.2.6)), one can get

$$\mathcal{H}_0 = \frac{\hbar^2}{m^* l_0^2} \left[-\frac{1}{2} D_\xi^2 + \frac{1}{2} \left(\frac{m^* l_0^2}{\hbar^2} \right) m^* \omega^2 l_0^2 (\xi - \xi_0)^2 + \frac{1}{2} \left(\frac{\omega_0}{\omega} \right)^2 \mathbb{K}_0^2 \right] \sigma_0. \quad (4.3.4)$$

By dividing the both sides of the above equation by $\hbar\omega_0$ energy, one can obtain the scaled form of \mathcal{H}_0 Hamiltonian like in the following equation:

$$\frac{\mathcal{H}_0}{\hbar\omega_0} = \left[\frac{1}{2} p_\xi^2 + \frac{1}{2} \left(\frac{\omega}{\omega_0} \right)^2 (\xi - \xi_0)^2 + \frac{1}{2} \left(\frac{\omega_0}{\omega} \right)^2 \mathbb{K}_0^2 \right] \sigma_0. \quad (4.3.5)$$

The frequency ratio (ω/ω_0) expression can be written in terms of cyclotron frequency such as:

$$\omega = \sqrt{\omega_0^2 + \omega_c^2} \quad \Rightarrow \quad \frac{\omega}{\omega_0} = \sqrt{1 + \left(\frac{\omega_c}{\omega_0} \right)^2}. \quad (4.3.6)$$

Zeeman Hamiltonian (Eq. (4.2.3)) can be rewritten in terms of cyclotron frequency using the definition of Bohr magneton (μ_B):

$$\mathcal{H}_Z = \frac{1}{2} g^* \mu_B B \sigma_z = \frac{1}{2} g^* \left(\frac{1}{2} m_0 \hbar \omega_c \right) \sigma_z \quad (4.3.7)$$

where $m_0 = m^*/m_e$.

As a result, the dimensionless form of the Zeeman Hamiltonian can be expressed as in the following equation:

$$\frac{\mathcal{H}_Z}{\hbar\omega_0} = \left[\frac{1}{2} g^* \mathcal{B} \right] \sigma_z \quad (4.3.8)$$

where

$$\mathcal{B} = \frac{1}{2} m_0 \left(\frac{\omega_c}{\omega_0} \right). \quad (4.3.9)$$

By substituting dimensionless parameters that are given in Eqs. (4.3.1) - (4.3.3) into Rashba Hamiltonian expression (first term of Eq. (4.2.7)) one can obtain

$$\mathcal{H}_R = \alpha \left[\sigma_x \left(k_y + \frac{eB}{\hbar} x \right) + i\sigma_y \frac{d}{dx} \right] = \frac{\alpha}{l_0} \left[\sigma_x \left(\mathbb{K}_0 + \frac{l_0^2}{l_B^2} \xi \right) + i\sigma_y D_\xi \right]$$

where l_B is the magnetic length.

$$l_B = \sqrt{\frac{\hbar}{m^* \omega_c}} \quad (4.3.10)$$

After some arrangements, one can get dimensionless expression for Rashba Hamiltonian as follows

$$\frac{\mathcal{H}_R}{\hbar\omega_0} = \eta_R \left[\sigma_x \left(\mathbb{K}_0 + \frac{\omega_c}{\omega_0} \xi \right) - \sigma_y p_\xi \right] \quad (4.3.11)$$

where

$$\eta_R = \frac{\alpha}{l_0 (\hbar\omega_0)} \quad (4.3.12)$$

On the other hand characteristic Rashba SO energy is known as

$$\Delta_{so}^R = \frac{m^* \alpha^2}{2\hbar^2} \quad (4.3.13)$$

$$\Rightarrow \Delta_{so}^R = \frac{m^*}{2\hbar^2} \eta_R^2 (l_0 \hbar\omega_0)^2 = \frac{1}{2} m^* \eta_R^2 \left(\frac{\hbar}{m^* \omega_0} \right) \omega_0^2 \Rightarrow \Delta_{so}^R = \frac{1}{2} \eta_R^2 (\hbar\omega_0)$$

With the help of the above equation, one can write the dimensionless parameter η_R in

terms of characteristic Rashba SO energy:

$$\eta_R = \left[2 \left(\frac{\Delta_{so}^R}{\hbar\omega_0} \right) \right]^{1/2} \quad (4.3.14)$$

Dresselhaus Hamiltonian, which is defined by the last term of Eq. (4.2.7), can also be rewritten in dimensionless form similar to the Rashba Hamiltonian.

$$\begin{aligned} \mathcal{H}_D &= \beta \left[\sigma_y \left(k_y + \frac{eB}{\hbar} x \right) + i\sigma_x \frac{d}{dx} \right] = \frac{\beta}{l_0} \left[\sigma_y \left(\mathbb{K}_0 + \frac{l_0^2}{l_B^2} \xi \right) + i\sigma_x D_\xi \right] \\ \Rightarrow \frac{\mathcal{H}_D}{\hbar\omega_0} &= \eta_D \left[\sigma_y \left(\mathbb{K}_0 + \frac{\omega_c}{\omega_0} \xi \right) - \sigma_x p_\xi \right] \end{aligned} \quad (4.3.15)$$

Here, η_D is given by

$$\eta_D = \frac{\beta}{l_0 (\hbar\omega_0)} \quad (4.3.16)$$

The definition of the characteristic Dresselhaus SO energy is known as follows

$$\Delta_{so}^D = \frac{m^* \beta^2}{2\hbar^2} \quad (4.3.17)$$

In the same way as Eq. (4.3.14), we can write the dimensionless parameter η_D in terms of characteristic Dresselhaus SO energy:

$$\eta_D = \left[2 \left(\frac{\Delta_{so}^D}{\hbar\omega_0} \right) \right]^{1/2} \quad (4.3.18)$$

Consequently, scaled form of total Hamiltonian can be written as in the following equation:

$$\begin{aligned} \frac{\mathcal{H}}{\hbar\omega_0} &= \left[\frac{1}{2} p_\xi^2 + \frac{1}{2} \left(\frac{\omega}{\omega_0} \right)^2 (\xi - \xi_0)^2 + \frac{1}{2} \left(\frac{\omega_0}{\omega} \right)^2 \mathbb{K}_0^2 \right] \sigma_0 + \left[\frac{1}{2} g^* \mathcal{B} \right] \sigma_z \\ &+ \eta_R \left[\sigma_x \left(\mathbb{K}_0 + \frac{\omega_c}{\omega_0} \xi \right) - \sigma_y p_\xi \right] + \eta_D \left[\sigma_y \left(\mathbb{K}_0 + \frac{\omega_c}{\omega_0} \xi \right) - \sigma_x p_\xi \right] \end{aligned} \quad (4.3.19)$$

As mentioned in subsection (3.5.3), we need to write the Hamiltonian in quantum mechanical formulation. This formulation was given in Eq. (3.5.50) previously.

$$\overline{\overline{\mathcal{H}}} = \sum_{n=0}^{\infty} \left\{ \frac{1}{n!} \frac{\partial^n \overline{\overline{\mathcal{H}}}}{\partial p_{\xi}^n} \Big|_{p_{\xi}=0}, p_{\xi}^n \right\} = \{\overline{\overline{\mathcal{H}}}_A, 1\} + \{\overline{\overline{\mathcal{H}}}_B, p_{\xi}\} + \{\overline{\overline{\mathcal{H}}}_C, p_{\xi}^2\}$$

$$\begin{aligned} \overline{\overline{\mathcal{H}}}_A = \overline{\overline{\mathcal{H}}} \Big|_{p_{\xi}=0} &= \hbar\omega_0 \left[\frac{1}{2} \left(\frac{\omega}{\omega_0} \right)^2 (\xi - \xi_0)^2 + \frac{1}{2} \left(\frac{\omega_0}{\omega} \right)^2 \mathbb{K}_0^2 \right] \sigma_0 + \hbar\omega_0 \left[\frac{1}{2} g^* \mathcal{B} \right] \sigma_z \\ &+ \hbar\omega_0 \left[\eta_R \left(\mathbb{K}_0 + \frac{\omega_c}{\omega_0} \xi \right) \sigma_x + \eta_D \left(\mathbb{K}_0 + \frac{\omega_c}{\omega_0} \xi \right) \sigma_y \right] \end{aligned} \quad (4.3.20)$$

$$\overline{\overline{\mathcal{H}}}_B = \frac{\partial \overline{\overline{\mathcal{H}}}}{\partial p_{\xi}} \Big|_{p_{\xi}=0} = \hbar\omega_0 \left[p_{\xi} \sigma_0 - \eta_R \sigma_y - \eta_D \sigma_x \right]_{p_{\xi}=0}$$

$$\overline{\overline{\mathcal{H}}}_B = \hbar\omega_0 \left[-\eta_R \sigma_y - \eta_D \sigma_x \right] \quad (4.3.21)$$

$$\overline{\overline{\mathcal{H}}}_C = \frac{1}{2!} \frac{\partial^2 \overline{\overline{\mathcal{H}}}}{\partial p_{\xi}^2} \Big|_{p_{\xi}=0} = \hbar\omega_0 \left[\frac{1}{2} \sigma_0 \right] \quad (4.3.22)$$

Numerical solution of the Schrödinger equation is performed by Finite Element Method (FEM) which is based on expressing of the wave function as a linear combination of interpolation polynomials multiplied by as-yet-unknown coefficients in each of these elements (Pask et al., 2001, Ram-Mohan, 2002).

Up to now we have not taken into account the exchange-correlation term and now we will mention about noncollinear local-spin density approximation.

4.3.1 Kohn-Sham Hamiltonian and Exchange-Correlation Potential

In the analysis of electronic, structural and optical properties of molecules, solids and other nano-structures, electronic structure calculations that consist in the solution of the Kohn-Sham density functional theory play an important role. The ground-state electron density $\rho(x)$ of an atomistic system can be obtained from the self-consistent solution of the Kohn-Sham equations.

$$\mathcal{H}_{KS}\psi(x) = \varepsilon\psi(x) \quad (4.3.23)$$

where \mathcal{H}_{KS} is the Kohn-Sham Hamiltonian that depends on $\rho(x)$, $\psi(x)$ are the Kohn-Sham orbitals. These Kohn-Sham orbitals are two component spinors for the system which includes SO coupling.

$$\psi_n(\mathbf{r}) = e^{ik_y y} \begin{pmatrix} \varphi_{n,k_y}(x, \uparrow) \\ \varphi_{n,k_y}(x, \downarrow) \end{pmatrix}$$

Using the Kohn-Sham orbitals, we can define the electron density by

$$\rho(\mu, \beta; \mathbf{r}) = \sum_n \frac{L}{2\pi} \int dk \langle \psi_{n,k} | \delta(\mathbf{r}' - \mathbf{r}) | \psi_{n,k} \rangle_{\mathbf{r}'} f_\mu(\epsilon_{nk}) \quad (4.3.24)$$

At finite temperature ($T = 1/(k_B\beta)$), the occupation numbers in Eq. (4.3.24) can be chosen according to the Fermi-Dirac distribution function

$$f_\mu(\epsilon_{nk}) = \frac{1}{(1 + e^{(\epsilon_{nk} - \mu)/k_B T})} \quad (4.3.25)$$

where μ is the chemical potential.

Translational invariance along the wire refers to all densities - actually all physical variables- only depend on x . Therefore, electron density of this physical system

depends on x and it can be written as

$$\rho(x) = \sum_n \frac{1}{2\pi} \int dk_y \left[|\varphi_{n,k_y}(x, \uparrow)|^2 + |\varphi_{n,k_y}(x, \downarrow)|^2 \right] f_\mu(\epsilon_{nk}) \quad (4.3.26)$$

The one-dimensional electron density along the QWR is the integral of $\rho(x)$ over x .

$$\rho_{1D} = \int dx \rho(x) \quad (4.3.27)$$

The spin magnetization that is used to calculate of the spin orientation at a given point can be defined as in the following equation:

$$m_a(\mathbf{r}) = \sum_n \frac{L}{2\pi} \int dk \langle \psi_{n,k} | \delta(\mathbf{r}' - \mathbf{r}) \sigma_a | \psi_{n,k} \rangle_{\mathbf{r}'} f_\mu(\epsilon_{nk}) \quad (4.3.28)$$

where the subscript identify x, y, z

Therefore substituting each Pauli spin matrices into above equation, we can get the corresponding spin magnetization components as follows

$$m_x(x) = \sum_n \frac{1}{2\pi} \int dk_y 2\text{Re} \left[\varphi_{n,k_y}^*(x, \uparrow) \varphi_{n,k_y}(x, \downarrow) \right] f_\mu(\epsilon_{nk}) \quad (4.3.29)$$

$$m_y(x) = \sum_n \frac{1}{2\pi} \int dk_y 2\text{Im} \left[\varphi_{n,k_y}^*(x, \uparrow) \varphi_{n,k_y}(x, \downarrow) \right] f_\mu(\epsilon_{nk}) \quad (4.3.30)$$

$$m_z(x) = \sum_n \frac{1}{2\pi} \int dk_y \left(|\varphi_{n,k_y}(x, \uparrow)|^2 - |\varphi_{n,k_y}(x, \downarrow)|^2 \right) f_\mu(\epsilon_{nk}) \quad (4.3.31)$$

Kohn-Sham Hamiltonian involves the sum of all terms: kinetic energy and confining potential, zeeman effect contribution which arise from perpendicular magnetic field, SO interaction terms and exchange correlation energy.

$$\mathcal{H} = \mathcal{H}_0 + \mathcal{H}_Z + \mathcal{H}_R + \mathcal{H}_D + \mathcal{V}_{xc} \quad (4.3.32)$$

The exchange-correlation potential (\mathcal{V}_{xc}) is derived from exchange-correlation

energy functional (E_{xc}). Spin dependent exchange-correlation potential is defined as follows,

$$\mathcal{V}_{xc}^{\eta\eta'}(\mathbf{r}) \equiv \frac{\delta E_{xc}[\rho_{\eta\eta'}(\mathbf{r})]}{\delta \rho_{\eta\eta'}(\mathbf{r})} \quad (4.3.33)$$

Here, η subscript represents spin up case (\uparrow), η' represents the down spin (\downarrow). The density matrix $\rho(\mathbf{r})$ is generally assumed to be diagonal for all \mathbf{r} . This indicates that the direction of the magnetization is considered to be constant and hence only up- and down-spin densities are used in Kohn-Sham equations (Heinonen, Kinaret, & Johnson, 1999). We need to know the exchange-correlation energy of a uniform system as a function of density ($\rho(\mathbf{r})$) and polarization ($\zeta(\mathbf{r})$) for LDA.

4.3.1.1 *Non-collinear Local-Spin Density Approximation*

There are multifarious spin-density functional calculations of the energy band structure and related electronic properties of spin polarized systems. Common to all of these theories and calculations is the treatment of the magnetic moment as having only two directions, namely up and down. These moment arrangements are entitled “*collinear*”. If the magnetic moments of atoms in a system are oriented in different directions, this case is called “*non-collinear magnetism*”.

For the systems whose magnetization direction changes in space, the approximation of constant magnetization direction no longer valid. A generalization of local spin density functional (Barth & Hedin, 1972) theory in which electron density is replaced by the single-particle density matrix to non-collinear magnetism was implemented by Kübler and co-workers (Kübler, Höck, Sticht, & Williams, 1988a,b, Sticht, Höck, & Kübler, 1989) for the first time. The main idea is to locally rotate the spin quantization axis to obtain a representation that locally diagonalizes the single-particle density matrix (Kübler et al., 1988a, Heinonen et al., 1999).

Here, we use the approximation which was developed by Kübler and co-workers to locally find $\mathcal{V}_{xc}^{\eta\eta'}$. Since exchange-correlation energy functional is a function of up-spin and down-spin electron densities, according to chain rule we can write the spin

dependent exchange-correlation potential term as

$$\mathcal{V}_{xc}^{\eta\eta'} = \frac{\delta E_{xc}[n_{\uparrow}, n_{\downarrow}]}{\delta n_{\uparrow}} \frac{\partial n_{\uparrow}}{\partial \rho_{\eta\eta'}} + \frac{\delta E_{xc}[n_{\uparrow}, n_{\downarrow}]}{\delta n_{\downarrow}} \frac{\partial n_{\downarrow}}{\partial \rho_{\eta\eta'}} \quad (4.3.34)$$

The density matrix denoted by $\rho_{\eta\eta'}$ can be defined in terms of particle and magnetization densities in the non-collinear case such as following equation.

$$\begin{aligned} \rho_{\eta\eta'}(x) &= \sum_n \frac{1}{2\pi} \int dk_y \varphi_{nk_y}^*(x, \eta) \varphi_{n, k_y}(x, \eta') f_{\beta}(\epsilon_{n, k_y}) \\ &\Rightarrow \begin{pmatrix} \rho_{\uparrow\uparrow} & \rho_{\uparrow\downarrow} \\ \rho_{\downarrow\uparrow} & \rho_{\downarrow\downarrow} \end{pmatrix} = \frac{1}{2} \begin{pmatrix} \rho + m_z & m_x + im_y \\ m_x - im_y & \rho - m_z \end{pmatrix} \end{aligned} \quad (4.3.35)$$

The density matrix can be diagonalized by means of local unitary transformation matrix.

$$U\rho(x)U^{\dagger} = n \equiv \begin{pmatrix} n_{\uparrow} & 0 \\ 0 & n_{\downarrow} \end{pmatrix} \quad (4.3.36)$$

where the local unitary transformation matrix is given by

$$U = \begin{pmatrix} e^{i\phi(x)/2} \cos(\theta(x)/2) & e^{-i\phi(x)/2} \sin(\theta(x)/2) \\ -e^{i\phi(x)/2} \sin(\theta(x)/2) & e^{-i\phi(x)/2} \cos(\theta(x)/2) \end{pmatrix} \quad (4.3.37)$$

where ϕ and θ are local spin rotation angles.

During the diagonalization process of the density matrix $\rho(x)$, local spin rotation angles that give the orientation of the spin are obtained as

$$\tan \phi(x) = -\frac{m_y(x)}{m_x(x)} \quad (4.3.38a)$$

$$\tan \theta(x) = \frac{\sqrt{m_x^2(x) + m_y^2(x)}}{m_z(x)} \quad (4.3.38b)$$

Also, we can derive the spin density terms n_{\uparrow} and n_{\downarrow} which are the diagonal elements

in Eq. (4.3.36)

$$\begin{aligned} n_{\uparrow} &= \rho_{\uparrow\uparrow} \cos^2(\theta/2) + \frac{1}{2} [\rho_{\uparrow\downarrow} e^{i\phi} + \rho_{\downarrow\uparrow} e^{-i\phi}] \sin(\theta) + \rho_{\downarrow\downarrow} \sin^2(\theta/2) \\ n_{\uparrow} &= \frac{1}{2} [\rho(x) + m_z(x) \cos(\theta)] + \text{Re} \{ \rho_{\uparrow\downarrow} e^{i\phi} \sin \theta \} \end{aligned} \quad (4.3.39)$$

$$\begin{aligned} n_{\downarrow} &= \rho_{\uparrow\uparrow} \sin^2(\theta/2) - \frac{1}{2} [\rho_{\uparrow\downarrow} e^{i\phi} + \rho_{\downarrow\uparrow} e^{-i\phi}] \sin(\theta) + \rho_{\downarrow\downarrow} \cos^2(\theta/2) \\ n_{\downarrow} &= \frac{1}{2} [\rho(x) - m_z(x) \cos(\theta)] - \text{Re} \{ \rho_{\uparrow\downarrow} e^{i\phi} \sin \theta \} \end{aligned} \quad (4.3.40)$$

We can use the familiar relations of collinear LSDA to compute the exchange-correlation potentials

$$\begin{pmatrix} v_{\uparrow} & 0 \\ 0 & v_{\downarrow} \end{pmatrix} \equiv \begin{pmatrix} \frac{\delta E_{xc}[n_{\uparrow}, n_{\downarrow}]}{\delta n_{\uparrow}} & 0 \\ 0 & \frac{\delta E_{xc}[n_{\uparrow}, n_{\downarrow}]}{\delta n_{\downarrow}} \end{pmatrix} \quad (4.3.41)$$

Using these descriptions, we can obtain the form of exchange correlation potential from Eq.(4.3.34).

$$\begin{aligned} \mathcal{V}_{xc}^{\uparrow\uparrow} &= v_{\uparrow} \frac{\partial n_{\uparrow}}{\partial \rho_{\uparrow\uparrow}} + v_{\downarrow} \frac{\partial n_{\downarrow}}{\partial \rho_{\uparrow\uparrow}} & \mathcal{V}_{xc}^{\uparrow\downarrow} &= v_{\uparrow} \frac{\partial n_{\uparrow}}{\partial \rho_{\uparrow\downarrow}} + v_{\downarrow} \frac{\partial n_{\downarrow}}{\partial \rho_{\uparrow\downarrow}} \\ \mathcal{V}_{xc}^{\downarrow\uparrow} &= v_{\uparrow} \frac{\partial n_{\uparrow}}{\partial \rho_{\downarrow\uparrow}} + v_{\downarrow} \frac{\partial n_{\downarrow}}{\partial \rho_{\downarrow\uparrow}} & \mathcal{V}_{xc}^{\downarrow\downarrow} &= v_{\uparrow} \frac{\partial n_{\uparrow}}{\partial \rho_{\downarrow\downarrow}} + v_{\downarrow} \frac{\partial n_{\downarrow}}{\partial \rho_{\downarrow\downarrow}} \end{aligned} \quad (4.3.42)$$

Derivatives of n_{\uparrow} and n_{\downarrow} with respect to $\rho_{\eta\eta'}$ give the terms that are related to local spin rotation angles θ and ϕ . As a result, formulation of the exchange correlation potential $\mathcal{V}_{xc}^{\eta\eta'}$ is obtained as (Malet et al., 2007, Gişi, 2012)

$$\mathcal{V}_{xc}^{\eta\eta'} = \begin{pmatrix} v_0 + \Delta v \cos \theta & \Delta v e^{i\phi} \sin \theta \\ \Delta v e^{-i\phi} \sin \theta & v_0 - \Delta v \cos \theta \end{pmatrix} \quad (4.3.43)$$

where $\nu_0 \equiv (\nu_\uparrow + \nu_\downarrow)/2$ and $\Delta\nu \equiv (\nu_\uparrow - \nu_\downarrow)/2$.

The relation between density and filling factor is $\nu(x) = 2\pi b_0^2 n(x)$ and we can write exchange-correlation energy

$$E_{xc} = \int dx n(x) \mathcal{E}_{xc}[\nu(x), \zeta(x)] \quad (4.3.44)$$

where \mathcal{E}_{xc} is the exchange-correlation energy per particle in an infinite, homogeneous system of filling factor $\nu(x) = 2\pi b_0^2 \rho(x)$ and polarization $\zeta = (n_\uparrow - n_\downarrow)/(n_\uparrow + n_\downarrow)$

Up- and down-spin electron densities may be defined in terms of polarization and total electron density

$$\rho(x) = n_\uparrow + n_\downarrow$$

$$\zeta = \frac{(n_\uparrow - n_\downarrow)}{\rho(x)} \Rightarrow n_\uparrow - n_\downarrow = \zeta \cdot \rho(x)$$

$$n_\uparrow = \frac{1}{2}\rho(x)[1 + \zeta] \quad (4.3.45)$$

$$n_\downarrow = \frac{1}{2}\rho(x)[1 - \zeta] \quad (4.3.46)$$

Once again we can write the Eq.(4.3.41):

$$\nu_\uparrow = \frac{\delta E_{xc}[n_\uparrow, n_\downarrow]}{\delta n_\uparrow} = \frac{\delta(\rho \cdot \mathcal{E}_{xc})}{\delta n_\uparrow}$$

$$\nu_\downarrow = \frac{\delta E_{xc}[n_\uparrow, n_\downarrow]}{\delta n_\downarrow} = \frac{\delta(\rho \cdot \mathcal{E}_{xc})}{\delta n_\downarrow}$$

derivatives with respect to up- and down-spin electron densities (n_\uparrow and n_\downarrow) can be defined as partial derivatives of total electron density and polarization.

$$\frac{\delta}{\delta n_\uparrow} = \frac{\partial}{\partial \rho} + \frac{1}{\rho} [1 - \zeta] \frac{\partial}{\partial \zeta} \quad (4.3.47)$$

$$\frac{\delta}{\delta n_\downarrow} = \frac{\partial}{\partial \rho} - \frac{1}{\rho} [1 + \zeta] \frac{\partial}{\partial \zeta} \quad (4.3.48)$$

Accordingly ν_{\uparrow} and ν_{\downarrow} can be defined as

$$\nu_{\uparrow} = \left[\frac{\partial}{\partial \rho} + \frac{1}{\rho} [1 - \zeta] \frac{\partial}{\partial \zeta} \right] (\rho \cdot \mathcal{E}_{xc}) \quad (4.3.49)$$

$$\nu_{\downarrow} = \left[\frac{\partial}{\partial \rho} - \frac{1}{\rho} [1 + \zeta] \frac{\partial}{\partial \zeta} \right] (\rho \cdot \mathcal{E}_{xc}) \quad (4.3.50)$$

Relation between the filling factor and electron density was denoted by $\nu(x) = 2\pi l_0^2 \rho(x)$. Therefore ν_{\uparrow} and ν_{\downarrow} can be written in terms of filling factor.

$$\nu_{\uparrow} = \left[\frac{\partial}{\partial \nu} + \frac{1}{\nu} [1 - \zeta] \frac{\partial}{\partial \zeta} \right] (\nu \cdot \mathcal{E}_{xc}) \quad (4.3.51)$$

$$\nu_{\downarrow} = \left[\frac{\partial}{\partial \nu} - \frac{1}{\nu} [1 + \zeta] \frac{\partial}{\partial \zeta} \right] (\nu \cdot \mathcal{E}_{xc}) \quad (4.3.52)$$

Exchange-correlation energy functional was taken from the work of Attaccalite and co-workers (Attaccalite et al., 2002).

4.4 Spin Orientation

The spin components of the eigenspinor $\varphi_n(k_y, x)$ in the n th subband are given by

$$s_j^n(k_y, x) = [\varphi_{n,\uparrow}^*(k_y, x) \quad \varphi_{n,\downarrow}^*(k_y, x)] \sigma_j [\varphi_{n,\uparrow}(k_y, x) \quad \varphi_{n,\downarrow}(k_y, x)]^T \quad (4.4.1)$$

where $j = (x, y, z)$ and $[\varphi_{n,\uparrow}(k_y, x) \quad \varphi_{n,\downarrow}(k_y, x)]^T$ is the spinor wave function in the n th spin-split level. And therefore we can define ‘‘spin density’’ components $S_j^n(k_y, x)$ for a given k_y in the n th level as (Upadhyaya et al., 2008b, Gujarathi et al., 2012)

$$S_j^n(k_y, x) = \frac{s_j^n(k_y, x)}{\sqrt{s_x^2(k_y, x) + s_y^2(k_y, x) + s_z^2(k_y, x)}} \quad (4.4.2)$$

The spin density components depend on wave vector k_y , the level index $n(\uparrow, \downarrow)$, and also confinement direction x . Consequently, for an electron belonging to a particular energy

level with certain wave vector k_y , spin orientations will vary with location along the width of the QWR. SO interaction-induced this spatial modulation of the spin density across the wire width is known as “spin texturing” (Upadhyaya et al., 2008b,a)

In order to calculate the real-space spin density ($S_j(x)$), we need to merge the spin density contribution from all occupied states:

$$S_j(x) = \sum_{n=1}^N \frac{\int_{k_{Fn}^-}^{k_{Fn}^+} S_j^n(k_y, x) dk_y}{k_{Fn}^+ - k_{Fn}^-} \quad j = (x, y, z) \quad (4.4.3)$$

where N is the number of occupied spin-split levels whose bottoms are below the Fermi energy. In Eqn. 4.4.3, intersection points between the Fermi energy and $E - k_y$ curve on the right (left) denote k_{Fn}^+ (k_{Fn}^-) wave vectors of the n th level (see Fig. 4.2(a)). For sake of simplicity, we assumed the low temperature limit which means that only the states below the Fermi level are fully occupied.

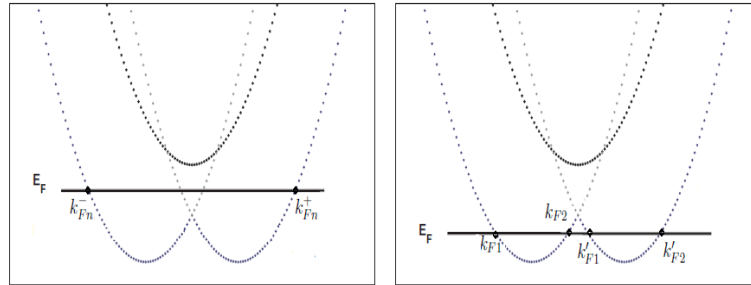


Figure 4.2 A representation for intersection points between the Fermi energy and $E - k_y$ curve.

The above definition (Eqn. 4.4.3) for real-space spin density can be used when the Fermi level intersects the subband only at two points, each of them locating at the opposite sides of the k_y axis. However in special case when $E - k_y$ curve has a camelback shape, Fermi level can intersect the same band at four different points (see Fig. 4.2(b)). Thereby Eqn. 4.4.3 needs to be adjusted as follows:

$$S_j(x) = \frac{\int_{k_{F1}}^{k_{F2}} S_j(k_y, x) dk_y}{k_{F2} - k_{F1}} + \frac{\int_{k'_{F1}}^{k'_{F2}} S_j(k_y, x) dk_y}{k'_{F2} - k'_{F1}} \quad (4.4.4)$$

Here k_{F1} , k_{F2} (k'_{F1} , k'_{F2}) are the wave vectors of intersection points between the Fermi level and the $E - k_y$ curve on the left (right) of the energy axis.

CHAPTER FIVE

RESULTS AND DISCUSSIONS

We consider a quasi-1D QWR with SO interaction in a perpendicular magnetic field. We assume that the wire material is GaAs so that the effective mass of electrons is 0.067 times the free electron mass ($m^* = 0.067m_0$) and the effective Lande-g factor $g^* = -0.44$. Both type of SO coupling constants (α, β) are chosen in the order of 10^{-11} eV m (Miller et al.,2003, Shafir, Shen, & Saikin,2004, Könemann, Haug, Maude, Fal'ko, & Altshuler,2005) which are in the same order of experimental values.

5.1 Numerical Results

The numerical results can be divided into three main parts. In the first part, we present energy eigenvalues and eigenfunctions for the physical system with/without SO coupling contribution and external magnetic field. In the second part, we exhibit spin texture figures and express the results. In the third and last part of numerical results we present the energy band dispersions and spin orientations for the system which includes exchange-correlation contribution.

5.1.1 Energy Bands

To clarify the interplay of different SO interaction contributions, first of all we calculate the energy dispersion relations of the subbands for a various strengths of Rashba and Dresselhaus SO couplings without magnetic field. Thereafter we take into consideration external magnetic field and calculate the energy bands to see how the magnetic field affects the subbands.

We can distinguish Rashba and Dresselhaus SO interactions into two regimes: weak $l_{so} \gg l_0$, and strong $l_{so} \lesssim l_0$ where $l_{so}^{R(D)} = \hbar^2/2m^* \alpha(\beta)$ is the length associated with SO couplings. In the presence of both types of SO couplings or only one type, the eigenenergies of the system are uniformly shifted downward by total characteristic SO

energy $\Delta_{so}^T = \Delta_{so}^R + \Delta_{so}^D$ where $\Delta_{so}^R = m^* \alpha^2 / 2\hbar^2$ and $\Delta_{so}^D = m^* \beta^2 / 2\hbar^2$ denote the Rashba and Dresselhaus SO couplings, respectively (Zhang et al., 2006, Knobbe & Schäpers, 2005).

5.1.1.1 Without Magnetic Field

With individual SO interaction ($\alpha \neq 0$ and $\beta = 0$): Initially, in order to identify the effect of individual SO coupling, in Fig. 5.1 we present the energy level spectrum of the QWR for different strengths of Rashba SO interaction in the absence of external magnetic field. Solid curves denote the energy dispersion with an individual mechanism of SO interaction whereas the dash-dot curves indicate the case for the absence of SO interaction.

When we calculate the energy dispersion for Rashba and Dresselhaus SO interaction individually, we get similar energy subband dispersions for each same characteristic SO energy. So, we show the case of which includes only Rashba SO coupling contribution in Fig. 5.1.

In case both external magnetic field and SO interaction terms are zero, all subbands are spin degenerate (the dash-dot curves in Fig. 5.1). As seen in Fig. 5.1(a), by inclusion of Rashba SO interaction spin-splitting occurs in doubly-degenerated energy bands at $k_y \neq 0$ and spin degeneracy is preserved only for eigenstates with $k_y = 0$. This can be explained on the basis of dependency of SO interaction to the electron momentum (Debald & Kramer, 2005). For a weak Rashba SO contribution, the coupling between different subbands does not take place clearly. As the Rashba SO interaction parameter is strengthened to a stronger value, coupling between spin-split levels causes an intraband mixing.

In order to illustrate to what extent the Rashba effect modifies the energy dispersion in a one-dimensional structure, in Fig. 5.1(b) and (c) we present the energy subband dispersions for two strong regimes of Rashba SO coupling, $\Delta_{so}^R / \hbar\omega_0 = 0.25$ and $\Delta_{so}^R / \hbar\omega_0 = 1$.

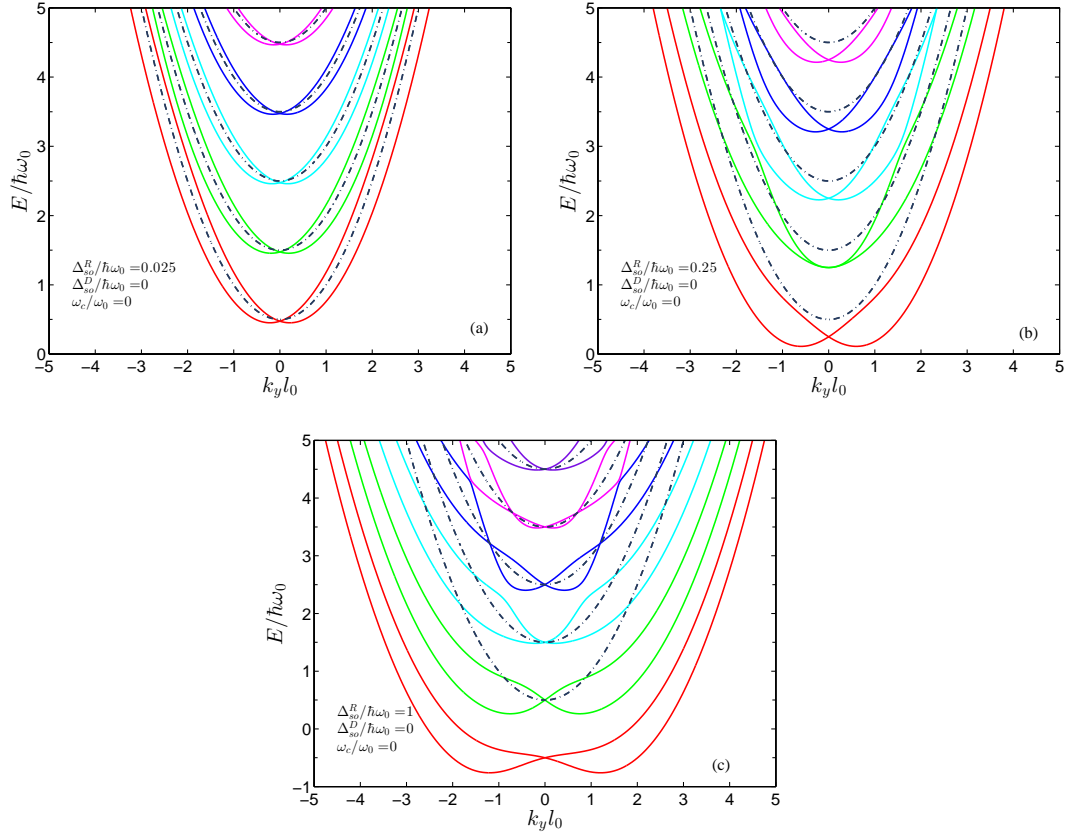


Figure 5.1 Quantum-wire energy dispersions with no Dresselhaus SO interaction term ($\Delta_{so}^D/\hbar\omega_0 = 0$) at zero magnetic field for three different Rashba SO strengths, (a) $\Delta_{so}^R/\hbar\omega_0 = 0.025$, (b) $\Delta_{so}^R/\hbar\omega_0 = 0.25$, and (c) $\Delta_{so}^R/\hbar\omega_0 = 1$. The dash-dot curves represent the energy subbands in the absence of both SO interaction and external magnetic field.

Deviation from the parabolicity and rising coupling between neighbouring subbands with increase of the characteristic Rashba SO energy ($\Delta_{so}^R/\hbar\omega_0$) is clearly visible. In the neighbourhood of $k_y = 0$ “camel-back” shape arises from the effect of SO coupling for spin branches of lower energy levels. For a stronger $\Delta_{so}^R/\hbar\omega_0$, described by the larger off-diagonal elements of the Hamiltonian matrix, significant coupling between neighbouring subbands leads to pronounced anticrossing (nonmonotonic portion) especially at higher levels. We should note that there is an energy shift in the subbands which is proportional with the magnitude of SO coupling energy.

Interplay of both SO interaction : We calculate the energy levels of the QWR for Rashba and Dresselhaus SO couplings to determine how the simultaneous contribution of both of SO interaction terms affect the energy dispersion.

$E - k_y$ curves for weak Rashba and Dresselhaus SO coupling regimes is given in Fig. 5.2(a). With inclusion of Dresselhaus term the spin degeneracy is removed except $k_y = 0$ point, as in the case for individual SO contribution (Fig. 5.1), and this term results in a downward energy shift at degeneracy point $k_y = 0$. In addition to this for weak Rashba and Dresselhaus SO interaction, the coupling between neighbouring subbands does not seen as clearly. In strong SO regimes, deviation from parabolicity of the subbands and anticrossing in higher subbands is visible.

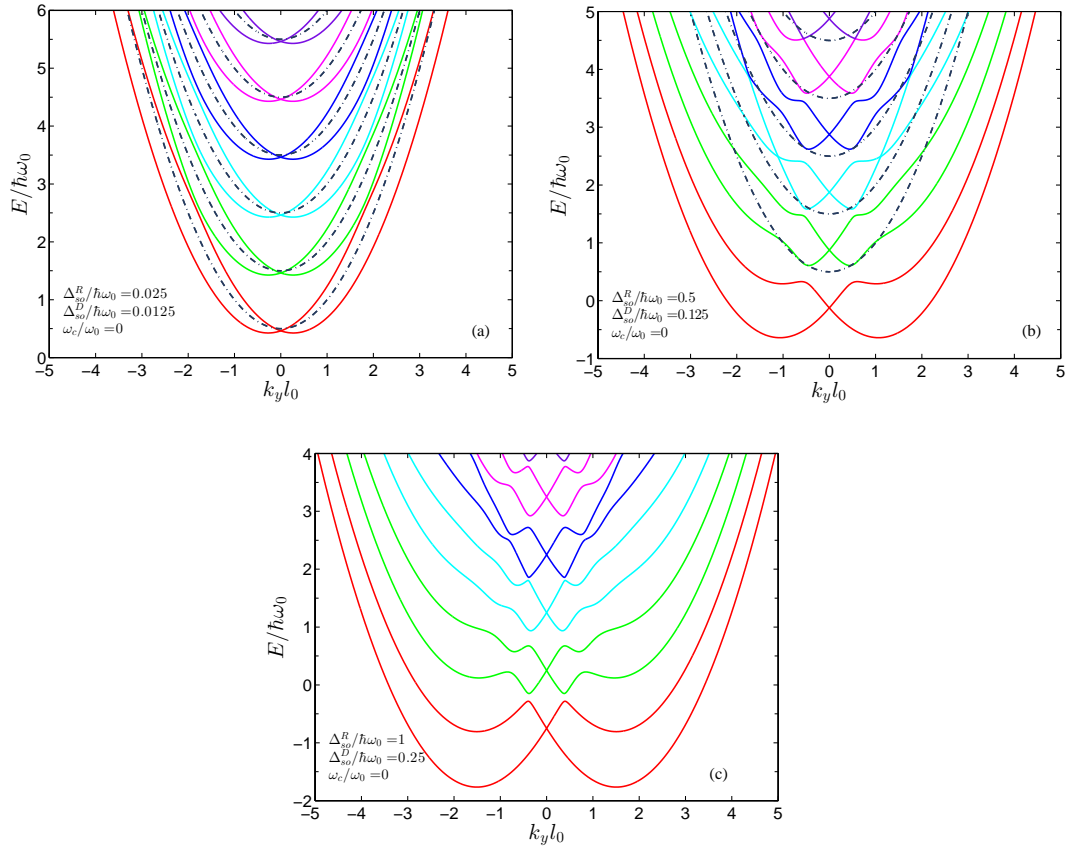


Figure 5.2 Subband energy spectra of QWR for various Rashba and Dresselhaus SO coupling strengths at $B = 0$. (a) $\Delta_{SO}^R/\hbar\omega_0 = 0.025$, $\Delta_{SO}^D/\hbar\omega_0 = 0.0125$, (b) $\Delta_{SO}^R/\hbar\omega_0 = 0.5$, $\Delta_{SO}^D/\hbar\omega_0 = 0.125$, (c) $\Delta_{SO}^R/\hbar\omega_0 = 1$, $\Delta_{SO}^D/\hbar\omega_0 = 0.25$

Comparison of the Figs. 5.1 and 5.2 reveals that more pronounced anticrossings occur between subbands of different levels in the vicinity of $k_y = 0$ when both of the SO interaction terms coexist. And we can say that amount of the downward shifting of energy increases with increasing total characteristic SO coupling energy ($\Delta_{SO}^T/\hbar\omega_0$) (Zhang et al., 2006).

5.1.1.2 With Magnetic Field

To elucidate the interplay of the SO interaction with magnetic field, at this part we consider QWR subjected to a perpendicular magnetic field. As can be seen in following figures, applying a magnetic field results in a subband separation and the degeneracy at $k_y = 0$ is removed.

In the absence of SO interaction : Fig. 5.3 shows the energy dispersion of electrons in a QWR without SO interactions for strong magnetic field values. When only the contribution of magnetic field is considered, one can argue that the magnetic field lifts the degeneracy in each energy band by the Zeeman effect. The energy spectrum in the absence of SO interaction and magnetic field is also given by dash-dot lines for comparison.

Increased magnetic field enhances the confinement potential which results in vertically upward shifting in the bottom of flattened energy subbands and increment in energy spacing between upper and lower level of each subband.

In the presence of SO interaction : Next, we consider the case when both SO interaction and magnetic field are present. In Fig. 5.4, we calculate the energy dispersion with a strong Rashba SO interaction under weak and strong magnetic fields. For weak magnetic field value, spin splitting which arose from Zeeman effect is imperceptible to the eye in Fig. 5.4(a) (especially between the lowest subbands). Moreover anticrossings between different energy subbands still exist as in zero magnetic field case.

From Fig. 5.4(b) and (c) we obviously see varying separation between each energy subband branches due by the effect of magnetic field as index of energy level increases. The degeneracy at the point $k_y = 0$ that has been removed with the effect of magnetic field is more evidently seen in strong B-field regime. Higher magnetic field values cause to negligible anticrossing between the subbands and extinguish the “camel-back” shape of the lower energy subbands.

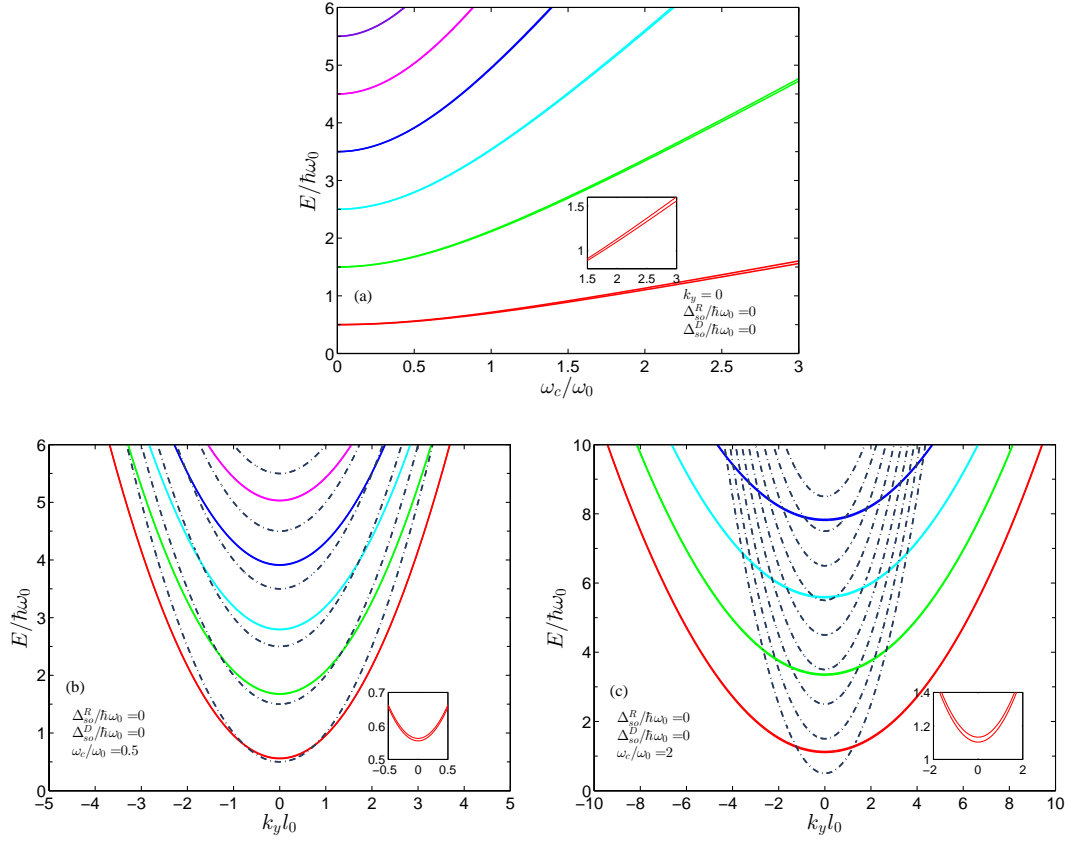


Figure 5.3 (a) Energy spectrum at $k_y = 0$ as a function of ω_c/ω_0 . (b)-(c) Energy dispersion of a QWR subjected to external magnetic field in the absence of SO interactions ($\omega_c/\omega_0 = 0.5$ and $\omega_c/\omega_0 = 2$, respectively)

In order to illustrate the competing effect between Rashba and Dresselhaus SO interaction, we plot Figs. 5.5 and 5.6. Figs. 5.5(a) and 5.6(a) represent the corresponding level spectrum with different and same SO coupling strengths. For different coupling strengths anticrossings between different subbands stand out whereas for the same SO interaction strengths crossings take place. In Figs. 5.5(b) and 5.6(b) variation of the energy with respect to ω_c/ω_0 at $k_y = 0$ is given. In both figures, different (same) amount of contribution of SO interaction gives rise to a remarkable (unremarkable) separation of spin-up and spin-down branches of the energy states. When the magnetic field increases, the subband separation becomes larger owing to an increasing $\hbar\omega_c$ for small-indexes of energy levels. We also calculate the energy bands for different and same Rashba and Dresselhaus SO coupling strengths in the presence of strong magnetic field (Figs. 5.5(c) and 5.6(c)). For a fixed magnetic field, the magnitude of

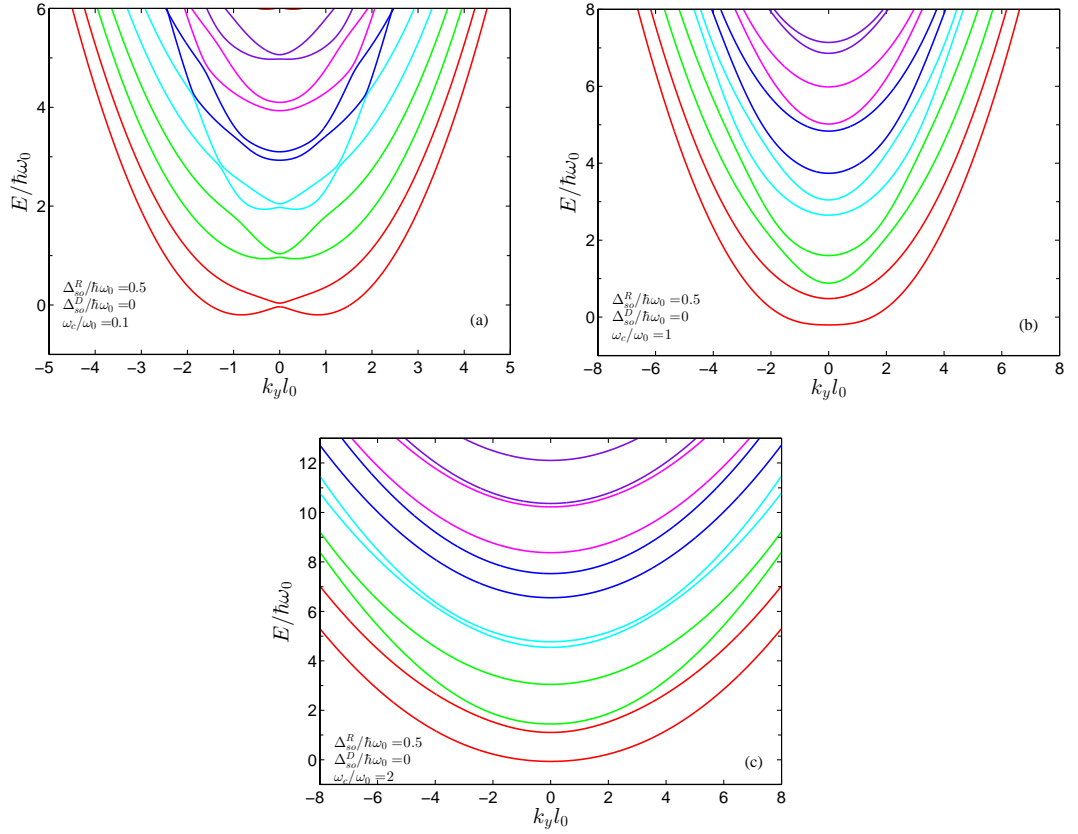


Figure 5.4 Energy dispersion of the spin-split subbands under the influence of external magnetic field and Rashba SO interaction ($\Delta_{SO}^R/\hbar\omega_0 = 0.5$) (a) $\omega_c/\omega_0 = 0.2$ (b) $\omega_c/\omega_0 = 1$ (c) $\omega_c/\omega_0 = 2$.

spin splitting between energy subbands of different states undergoes change depending on the interplay of SO coupling and external magnetic field. Based on this observation and looking the feature of Fig. 5.6(c) we can say that Rashba and Dresselhaus SO coupling terms can cancel each other by leading to a rather complex behavior in the energy dispersion in contrast with the different SO coupling strength case.

With the assumption of negligible intersubband crossing, the critical magnetic field for which the camelback shape cease to exist can be described as $B_c = 2m^*\eta_{SOI}/(|g|\mu_B\hbar^2)$ where η_{SOI} represent α or β (Gujarathi et al., 2012, Upadhyaya et al., 2008b). This fact reveals an important feature in energy dispersions: for cases with different SO interaction contributions, camelback shapes preserves when the total effective magnetic field corresponding to SO interactions is greater than the applied magnetic field.

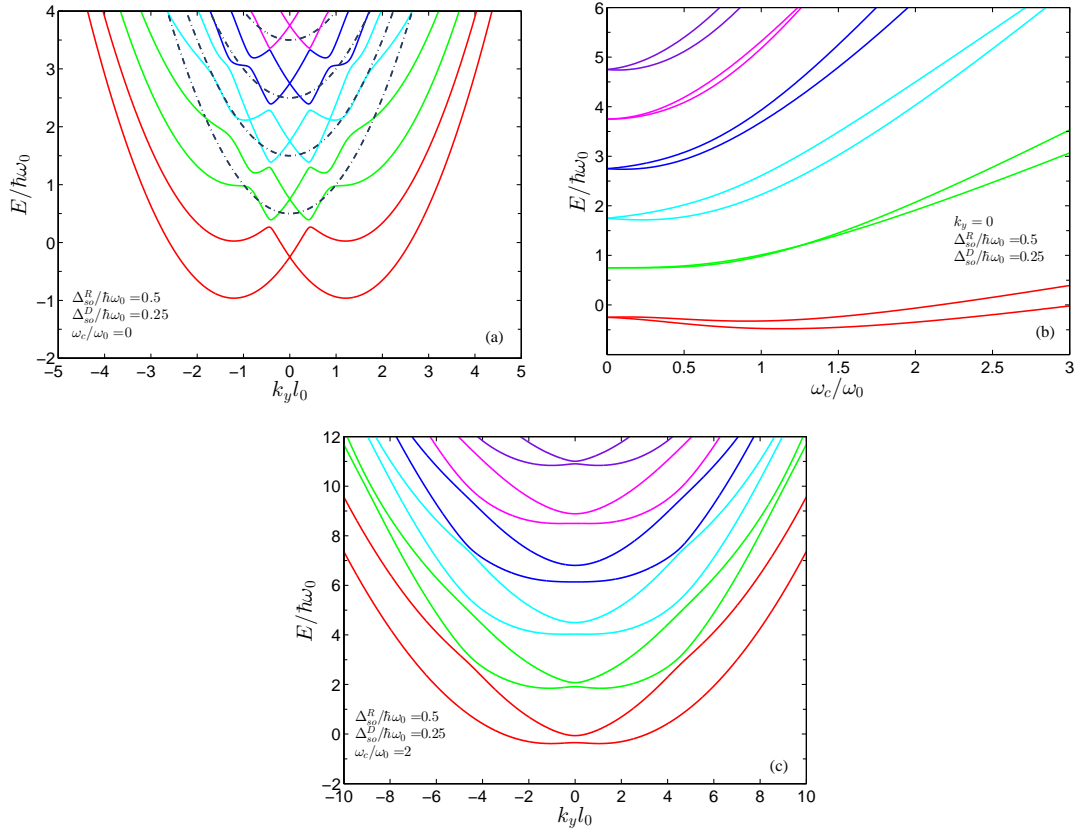


Figure 5.5 (a) Energy subband dispersion at $B = 0$ with Rashba ($\Delta_{so}^R/\hbar\omega_0 = 0.5$) and Dresselhaus ($\Delta_{so}^D/\hbar\omega_0 = 0.25$) SO coupling effect (b) Energy spectrum at $k_y = 0$ as a function of ω_c/ω_0 . (c) Energy dispersion of the wire at a finite magnetic field ($\omega_c/\omega_0 = 2$)

We obtain that the energy state spin-splitting strongly depends on the strengths of the Rashba and Dresselhaus SO coupling and also applied magnetic field.

5.1.2 Wave Functions

We plot the spinor components of the wave functions separately for the dimensionless wave vector values $k_y l_0$ for first lowest spin-split subband in the presence and also absence of SO interactions.

Fig. 5.7 shows the wave function of an electron in a finite magnetic field ($\omega_c/\omega_0 = 2$) without SO interaction. These spinor wave functions at $k_y l_0 = \pm 2$ correspond to the energy spectrum in Fig. 5.3(c).

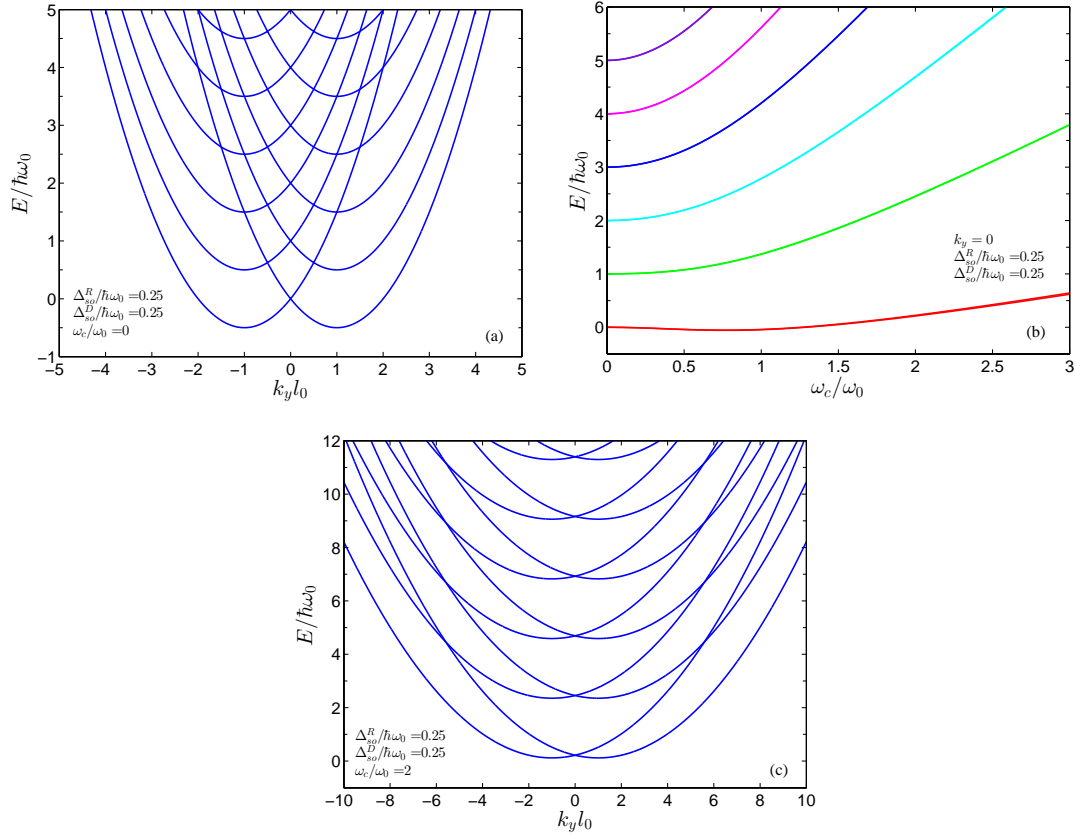


Figure 5.6 (a) Energy subband dispersion at $B = 0$ with the equal strength of Rashba and Dresselhaus SO interaction ($\Delta_{so}^R/\hbar\omega_0 = \Delta_{so}^D/\hbar\omega_0 = 0.25$) (b) Energy spectrum at $k_y = 0$ as a function of ω_c/ω_0 . (c) Energy dispersion of the wire at a finite magnetic field ($\omega_c/\omega_0 = 2$).

Skew direction of wave functions is determined by the Lorentz force associated with the magnetic field. Depending on whether the electrons are forward or backward traveling this force deflects electrons toward either the left or the right edge of the QWR (Pramanik et al., 2007).

By considering x dependency of the real and imaginary parts of the spinor wave function, Fig. 5.7 emphasizes that $[\varphi_\uparrow(k_y, x) \ \varphi_\downarrow(k_y, x)]^T$ can be separated in a spatial part and a space independent spinor part.

In Figs. 5.8-5.9, real and imaginary parts of the spinor wave function are plotted separately $[\varphi_\uparrow(k_y, x) \ \varphi_\downarrow(k_y, x)]^T$ for an electron in the lowest spin-split band under strong magnetic field.

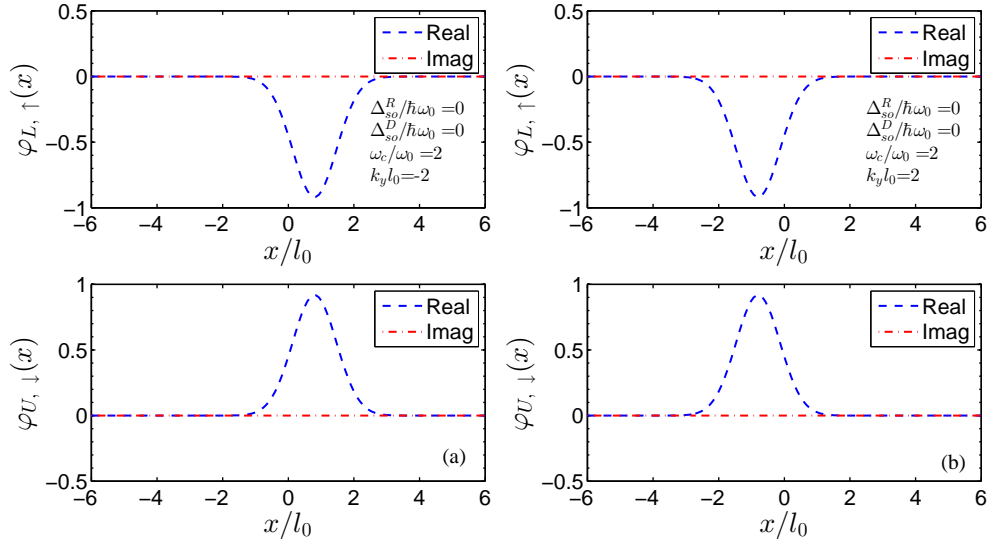


Figure 5.7 Real and imaginary parts of the spinor wave function as a function of x/l_0 in the first subband for the case of strong magnetic field ($\omega_c/\omega_0 = 2.0$) and the absence of SO interaction at $k_y l_0 = \pm 2$. The subscript $L(U)$ indicates the lower(upper) spin-split level of the first subband.

In the presence of Rashba and/or Dresselhaus SO coupling of any strength, emerged completely different situation imposes the fact that x dependent spinor wave function cannot be written as the product of space dependent and eigenspinor part. This observation is in accordance with previous works in literature (Pramanik et al., 2007, Moroz & Barnes, 1999, 2000, Gujarathi et al., 2012, Upadhyaya et al., 2008a).

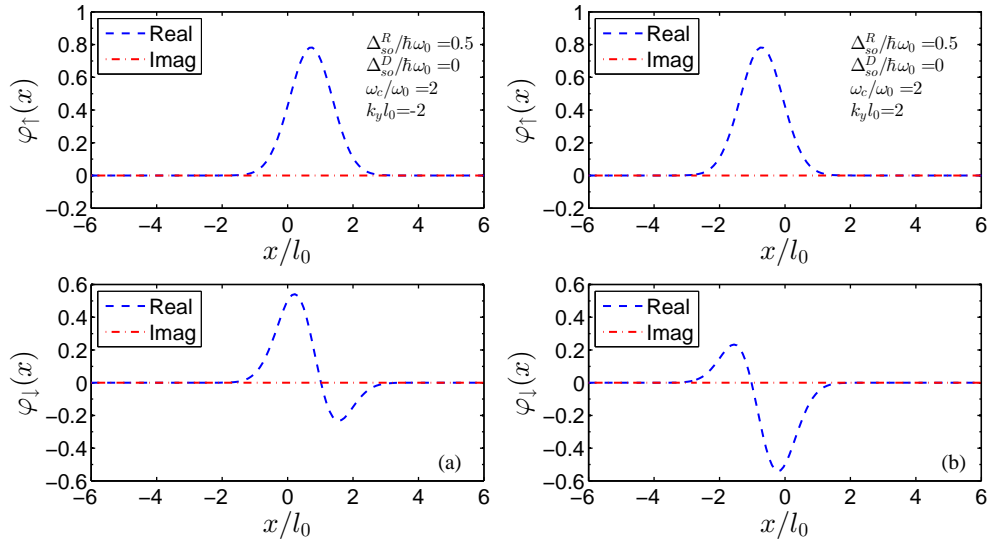


Figure 5.8 Real and imaginary parts of the spinor wave function as a function of x/l_0 in the first subband when the QWR is under the effect of Rashba SO interaction ($\Delta_{so}^R/\hbar\omega_0 = 0.5$) and external magnetic field ($\omega_c/\omega_0 = 2$).

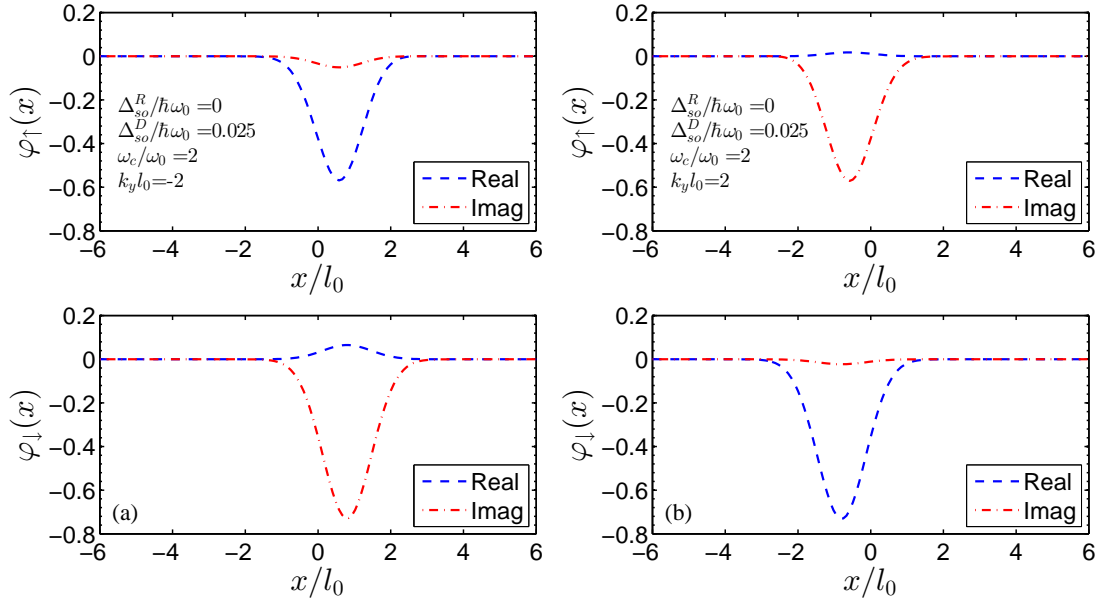


Figure 5.9 Spinor wave function components as a function of x/l_0 for the lowest spin-split level in the presence of weak Dresselhaus SO interaction ($\Delta_{so}^D/\hbar\omega_0 = 0.025$) and strong magnetic field ($\omega_c/\omega_0 = 2$).

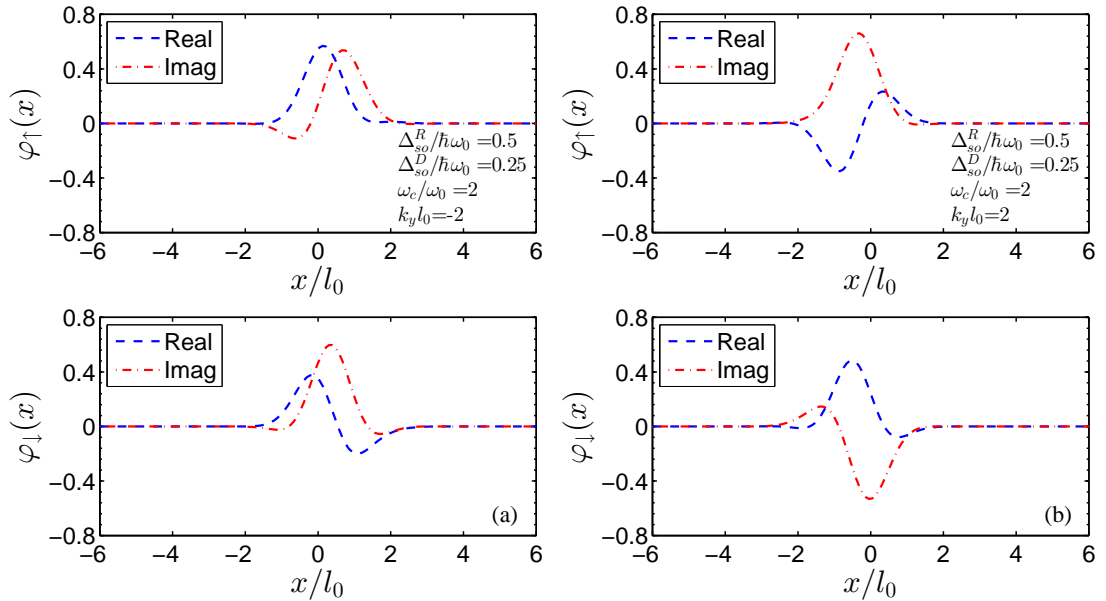


Figure 5.10 The components of the spinor wave function when both SO interaction ($\Delta_{so}^R/\hbar\omega_0 = 2 \Delta_{so}^D/\hbar\omega_0 = 0.5$) and external magnetic field ($\omega_c/\omega_0 = 2$) are present. Value of the wave vector is $k_y l_0 = \mp 2$.

5.1.3 Spin Orientation

In the following part, we present a detailed study of the spin texturing in a parabolically confined QWR with Rashba and/or Dresselhaus SO interaction and

external magnetic field. We express our results in terms of $\rho_{1D}l_0$ that is dimensionless form of the one-dimensional electron density (ρ_{1D}) across the wire and corresponding to densities in the range of $\sim 5 \times 10^6 - 2 \times 10^8 \text{ m}^{-1}$ (Malet, Pi, Barranco, & Lipparini, 2005).

5.1.3.1 Without Spin-Orbit Interaction

Initially we investigate the case when only the existence of external magnetic field causes vertical splitting of each subband. When only the lowest Zeeman-split band is occupied, one can foresee that \hat{x} and \hat{y} components ($S_x(x)$ and $S_y(x)$) of spin density will vanish even though \hat{z} component ($S_z(x)$) will take a nonzero positive value due to g -factor in case of strong magnetic field ($\omega_c/\omega_0 = 3.0$). x -independence of the magnetic field leads to no spatial modulation of spin density as seen in Fig. 5.11(a). We should state that if the system is under the effect of moderate external magnetic field such as $\omega_c/\omega_0 = 0.3$ and 0.6 , all components of $\mathbf{S}(x)$ are zero since the g -factor as small.

When we consider the case where the Fermi level is above the bottom of the upper spin-split level of first subband, the magnitude of the $S_z(x)$ will be almost zero according to Eqn. (4.4.3). In other words spins of the upper Zeeman branch are in the opposite direction with the lower Zeeman branch and therefore almost cancel each other.

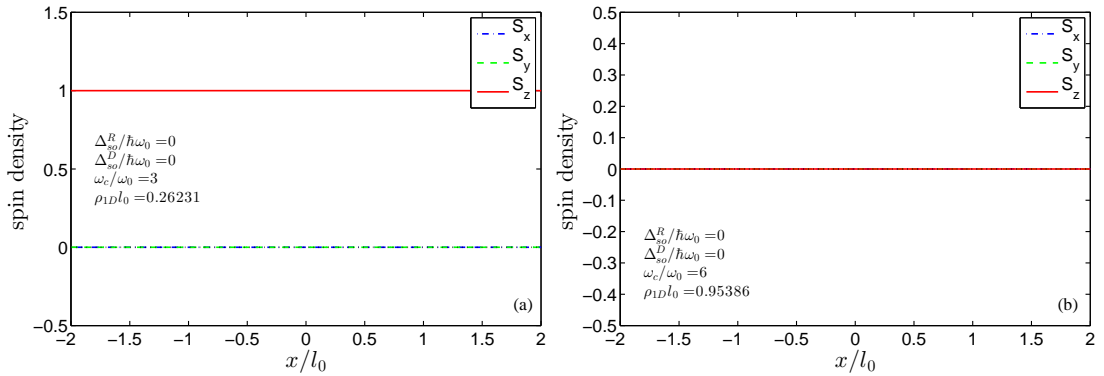


Figure 5.11 Spin density components in the absence of Rashba and Dresselhaus SO interactions at $\hbar\omega_0 = 2 \text{ meV}$ (a) low-density limit and $\omega_c/\omega_0 = 3$ (b) high-density limit and $\omega_c/\omega_0 = 6$.

5.1.3.2 Without External Magnetic Field

Next, we want to illustrate to what extent the Rashba and Dresselhaus SO interaction effect modify the spin orientation. For this purpose, we calculate the spin textures for weak and strong SO interaction regimes. In this case spin-degenerate band is splitted into two horizontally displaced branches under the influence of SO coupling terms and the system has a degeneracy point at $k_y = 0$ (see Fig. 5.1).

In connection with the Rashba and Dresselhaus SO coupling effects, there exist effective Rashba (\mathbf{B}_R) and Dresselhaus (\mathbf{B}_D) pseudomagnetic fields, respectively, that give contribution to the net magnetic field. The direction of Rashba magnetic field is perpendicular to the \hat{y} directed electron velocity and electric field associated with Rashba effect that is in \hat{z} direction (Upadhyaya et al., 2008a,b, Cummings, 2009, Camenzind, 2012). The effective Dresselhaus magnetic field is k_y dependent and oriented along the wire axis (\hat{y}) (Gujarathi et al., 2012, Meier, Salis, Gini, Shorubalko, & Ensslin, 2008, Studer, Walser, Baer, Rusterholz, Schön, Schuh, & et al., 2010).

When only the lowest spin-split band is occupied (small electron density limit) and weak SO interaction regime is considered, we see that there is not any spatial modulation because of the weak coupling effects between the spin-split subbands. The Fig. 5.12(a) shows spin components for the case of one type of SO coupling. For weak Rashba (Dresselhaus) SO interaction there is no magnetic field along \hat{y} or \hat{z} (\hat{x} or \hat{z}) so $\mathbf{S}(x)$ components along these directions are zero. On the other hand nonmagnetic feature of the material also results in zero $S_x(x)$ ($S_y(x)$).

In Fig. 5.12(b) similar behavior is obtained when both SO interaction terms are taken into account that can be explained by the afore mentioned reasons.

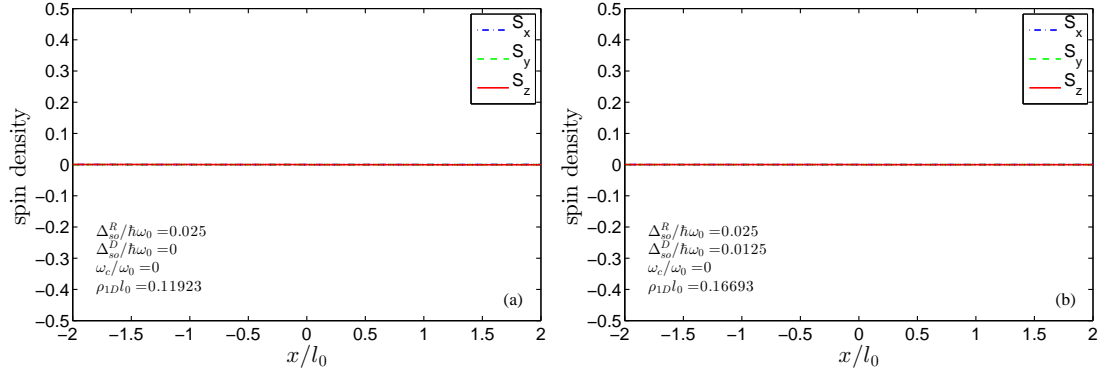


Figure 5.12 Spin densities under the influence of weak SO couplings at $\omega_c/\omega_0 = 0$ and $\hbar\omega_0 = 2 \text{ meV}$.

(a) $\Delta_{so}^R/\hbar\omega_0 = 0.025$, $\Delta_{so}^D/\hbar\omega_0 = 0$, (b) $\Delta_{so}^R/\hbar\omega_0 = 0.025$, $\Delta_{so}^D/\hbar\omega_0 = 0.0125$.

5.1.3.3 In The Presence of Both Spin-Orbit Interaction and External Magnetic Field

In the present case, the system is under the influence of \hat{x} and \hat{y} directed effective magnetic fields caused by Rashba and Dresselhaus SO interaction terms in addition to applied external magnetic field. As a consequence of that components of $\mathbf{S}(x)$ have nonzero values along all three different ($\hat{x}, \hat{y}, \hat{z}$) directions. The spin orientation will vary based on the relative values of characteristic Rashba and Dresselhaus SO energies, and also external magnetic field. Pseudomagnetic fields due to SO interactions are k_y dependent (Upadhyaya et al., 2008b, Gujarathi et al., 2012, Meier et al., 2008, Studer et al., 2010).

Low electron densities : This density limit means that only the lowest spin-split subband of the first energy level lies below the Fermi energy. For different magnetic field values we get real-space spin textures in the presence of weak Rashba and Dresselhaus SO coupling strengths as shown in Fig. 5.13.

The \hat{x} and \hat{y} components of $\mathbf{S}(x)$ are zero at the center of the wire since they experience no \mathbf{B}_R and \mathbf{B}_D , and they take different signs at opposite edges of the wire. The \hat{z} component has minimum values near the two edges and reaches a maximum value at the center of the wire in that the net magnetic field is \hat{z} directed. The magnitude of all spin components increases with increasing external magnetic field.

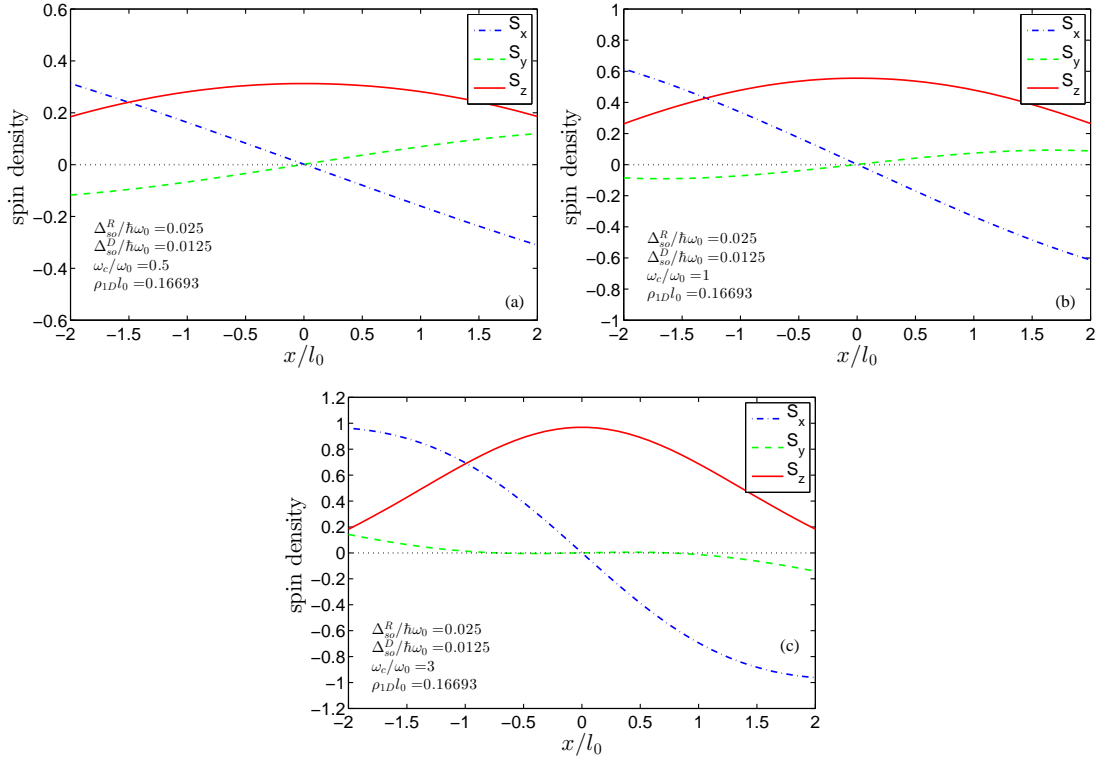


Figure 5.13 Spatial variation of spin density components in the presence of weak Rashba and Dresselhaus SO coupling strengths ($\Delta_{so}^R/\hbar\omega_0 = 0.025$, $\Delta_{so}^D/\hbar\omega_0 = 0.0125$) at different magnetic fields. (a) $\omega_c/\omega_0 = 0.5$, (b) $\omega_c/\omega_0 = 1$, and (c) $\omega_c/\omega_0 = 3$. We consider the case when only the lowest spin-split band is occupied.

In the strong Rashba and Dresselhaus SO coupling regime, at first we consider that the external magnetic field effect is weak ($\omega_c/\omega_0 = 0.05$). As one can see in Fig. 5.14(a), \hat{x} and \hat{y} components of $\mathbf{S}(x)$ are zero at the center of the wire and both of them have opposite signs at the two edges. The \hat{z} component of spin has minimum values near the edges and reaches a maximum value in the region close to the wire-center. On the other hand, with stronger SO interaction strengths spin distribution behaves more oscillatory that causes shortening in the "wavelength" of the standing wave of spin components as can be seen from Fig. 5.13(b) and Fig. 5.14(c).

Qualitative explanation of the features in Fig. 5.14 can be as follows. Pseudomagnetic Rashba field is proportional to translational velocity of electrons whereas Dresselhaus field is \mathbf{k}_y dependent. So, centrally localized electrons will experience neither Rashba nor Dresselhaus effective magnetic field. The only field exerted on the electrons at the center is the external one that leads to only one nonzero valued spin component

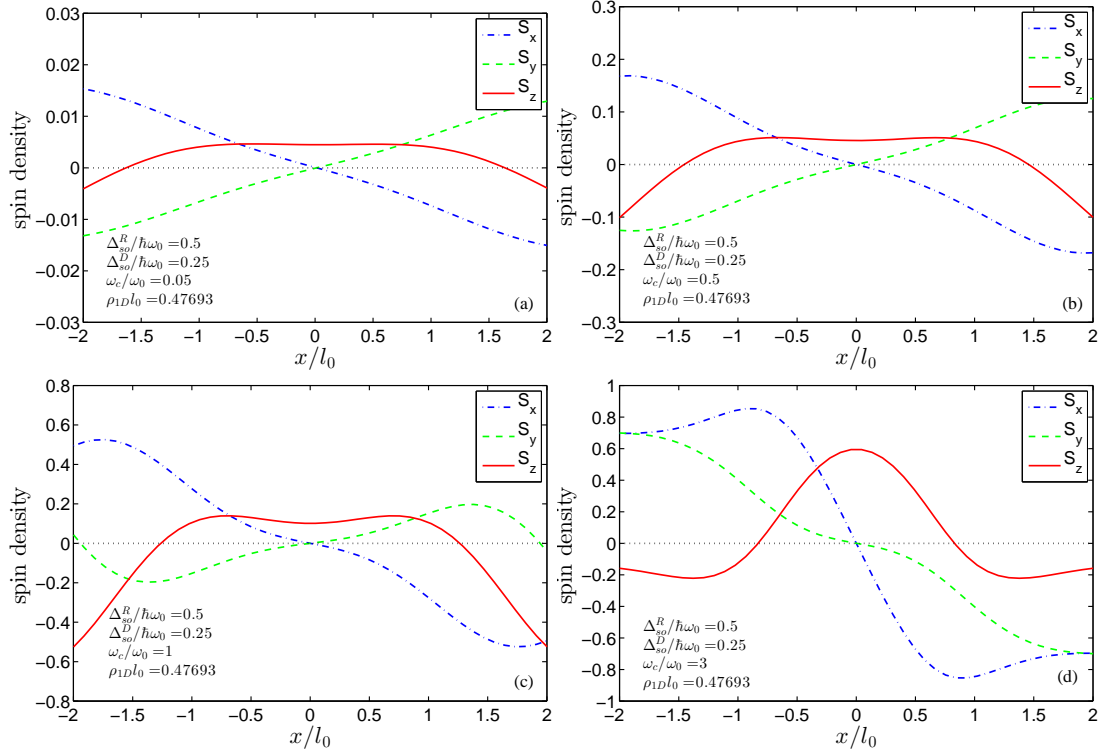


Figure 5.14 Spin texture for the strong Rashba and Dresselhaus SO couplings ($\Delta_{so}^R/\hbar\omega_0 = 0.5$, $\Delta_{so}^D/\hbar\omega_0 = 0.25$). Magnetic field is varied from weak to strong limit. (a) $\omega_c/\omega_0 = 0.05$, (b) $\omega_c/\omega_0 = 0.5$, (c) $\omega_c/\omega_0 = 1$, and (d) $\omega_c/\omega_0 = 3$, respectively. The lowest spin-split band at $\hbar\omega_0 = 2$ meV is occupied in all cases.

($S_z(x)$). In spite of that different situation come out at the edges of the wire where anymore $\mathbf{B}_R(x)$ and $\mathbf{B}_D(x)$ are different than zero. Electrons located near the different edge points have oppositely directed translational velocities. Furthermore, $S_x(x)$ and $S_y(x)$ spin components will line up parallel to $\mathbf{B}_R(x)$ and $\mathbf{B}_D(x)$ to produce maximums with opposite signs at opposite edges of the wire.

If we consider the system when it is under the effect of strong magnetic field ($\omega_c/\omega_0 = 1.0, 3.0$), we can get the spin textures as shown in Figs. 5.14(c)-(d). $S_x(x)$ has similar feature with the weak B case whereas the $S_y(x)$ component undergoes a sign reversal. This behavior can be attributed to the flattening of the camelback shape in the energy spectrum with increasing external field.

Another important observation is that in the presence of both SO coupling terms S_z component of spin orientation shows positional variation with respect to x

regardless of SO coupling strengths. Meanwhile stronger SO interaction limits cause more pronounced modulation both in spatial behavior and sign reversal of all spin components.

High electron densities : In this case, we analyze the treatment of the spin components when both of the lower and the upper spin-split branches of the lowest subband are occupied.

In Fig. 5.15 we show the spin distribution for strong SO interaction for different magnetic fields ($\omega_c/\omega_0 = 0.5 - 3$). At the center of the wire, electrons are oriented along the external magnetic field because the fact that the net field comprises only of the applied magnetic field. Therefore, the \hat{z} component of $\mathbf{S}(x)$ takes a higher values at the wire center. Besides $S_x(x)$ and $S_y(x)$ have zero value at the wire center and take opposite signs at different edge points since the values of \mathbf{B}_R and \mathbf{B}_D effective magnetic fields will increase for the electrons that are far away from the center of the wire. The magnitude of all spin components takes greater values when the applied magnetic field increases. The common feature in Fig. 5.15 reveals the fact that competing effects between different magnetic fields lead to more complicated oscillating behavior in spin distribution. Comparison between different density cases shows that for the high density limit rapid spatial variation of all spin components is more evident than the low density case.

5.1.4 Effects of Exchange-Correlation Energy

We investigate the exchange-correlation effects on energy dispersion relations of the subbands in addition to the contributions of SO interaction terms and externally applied magnetic field by using non-collinear local spin density approximation. We solve Kohn-Sham equations of our physical system in a self-consistent scheme which was previously described in Fig. 3.1. We assume that harmonic oscillator energy is $\hbar\omega_0 = 2 \text{ meV}$ which specify the strength of the parabolic confinement potential. To compare the differences in the energy subband dispersion we plot each subband energy spectra

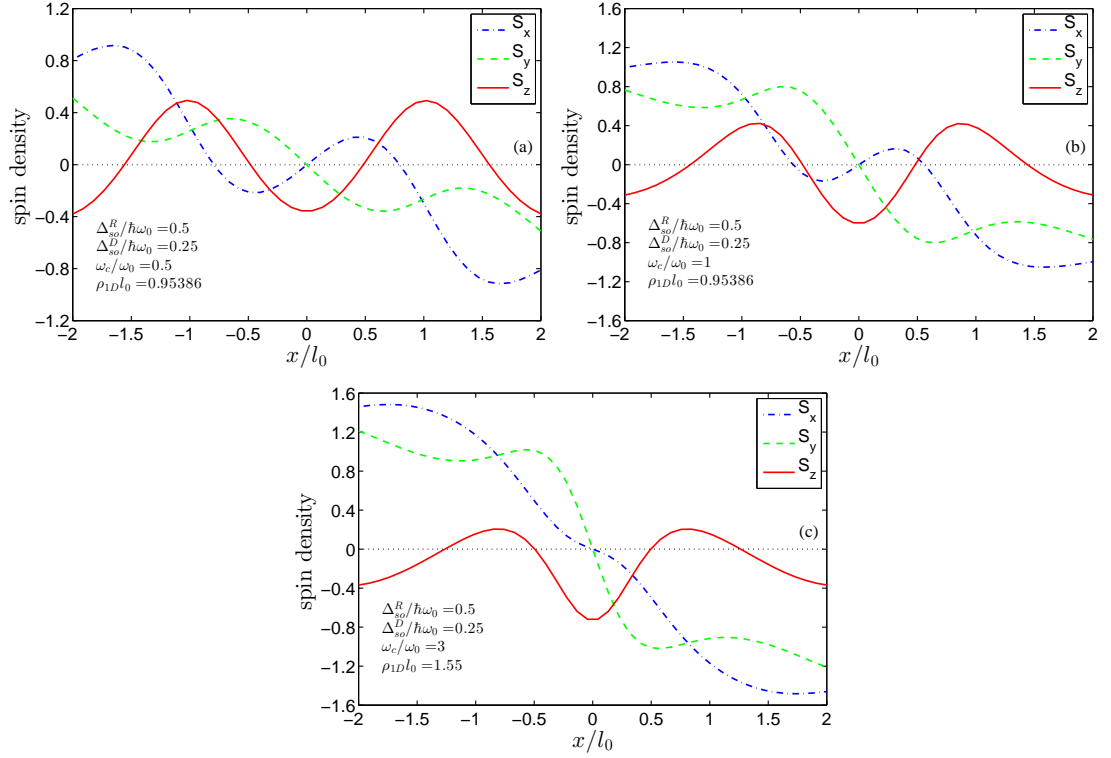


Figure 5.15 Spin texture for the case when both spin-split branches of the lowest subband are occupied. Strong Rashba and Dresselhaus SO couplings case ($\Delta_{so}^R/\hbar\omega_0 = 0.5$, $\Delta_{so}^D/\hbar\omega_0 = 0.25$) is considered for three different values of magnetic field: (a) $\omega_c/\omega_0 = 0.5$, (b) $\omega_c/\omega_0 = 1$, and (c) $\omega_c/\omega_0 = 3$.

of the QWR both in the presence and absence of the exchange-correlation effect. In all figures solid curves indicate the energy dispersions of subbands in the absence of exchange correlation interaction ($\mathcal{V}_{xc} = 0$) while the dashed curves represent the situation which includes the exchange-correlation contributions ($\mathcal{V}_{xc} \neq 0$). The Fermi energy level has also been drawn on all figures for either case.

5.1.4.1 Energy Bands Without Magnetic Field

In the first instance, we analyse the energy subband structures for taking only Rashba SO interaction term into account when the magnetic field is zero and the value of electron density is low. Fig. 5.16 shows the energy subband dispersion for three different Rashba SO strengths at $\rho_{1D}l_0 \approx 0.24$ and zero magnetic field case. As one can see in this figure, the exchange-correlation interaction term causes a downward shift in the energy subbands. As the strength of Rashba SO interaction increases

($\Delta_{so}^R/\hbar\omega_0 = 0.5$), one can see a noticeable increment in the amount of separation between the branches of each spin-split subbands near $k_y = 0$ point.

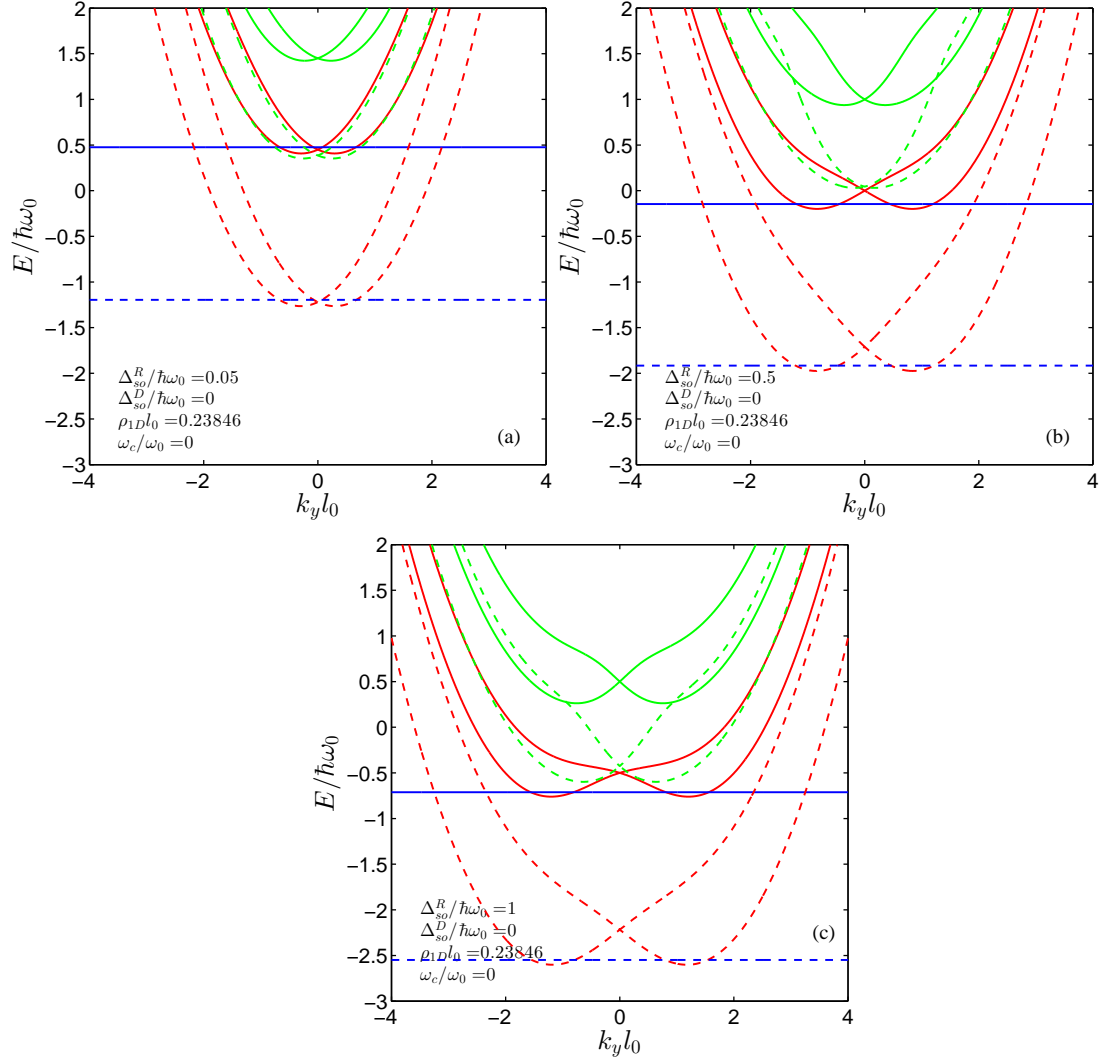


Figure 5.16 Exchange-correlation effect on the energy subband structure of the QWR in the absence of Dresselhaus SO interaction term at zero magnetic field for low density regime ($\rho_{1D}l_0 \simeq 0.24$). (a) $\Delta_{so}^R/\hbar\omega_0 = 0.05$, (b) $\Delta_{so}^R/\hbar\omega_0 = 0.5$, (c) $\Delta_{so}^R/\hbar\omega_0 = 1$.

In Fig. 5.17(a) and (b), we present energy dispersions of the QWR for the case of different contributions of both Rashba and Dresselhaus SO coupling terms coexist (weak and strong, respectively). In this case, exchange-correlation effects are also obvious. For strong Dresselhaus SO coupling term, the band bending in spin branches of each level in the neighbourhood of $k_y = 0$ becomes more smoothly by the effect of exchange-correlation energy term.

We also calculate the energy dispersion of the subbands with strong Rashba and Dresselhaus SO interactions to determine how the exchange-correlation contribution affects on the energy subbands for different electron density values at zero magnetic field. The downward energy shift in the subbands increases slightly with increasing electron density as shown in Fig. 5.17(b)-(c).

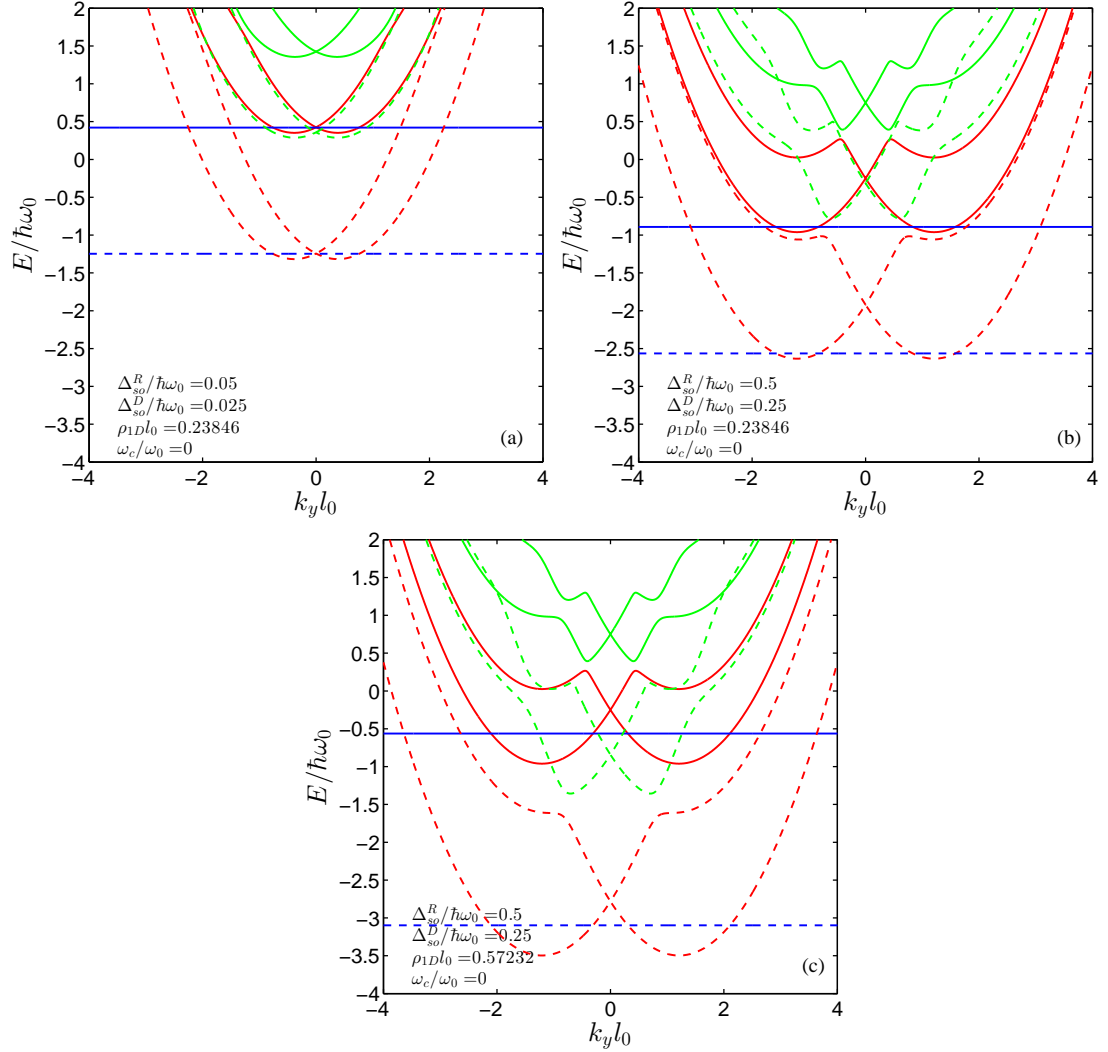


Figure 5.17 Energy dispersion relations of the subbands for weak and strong SO interactions at $B = 0$. (a) Weak regime of Rashba and Dresselhaus SO interaction such as $\Delta_{so}^R/\hbar\omega_0 = 0.05$ and $\Delta_{so}^D/\hbar\omega_0 = 0.025$ for low electron density limit $\rho_{1D}l_0 \approx 0.24$, (b) Strong regime of Rashba and Dresselhaus SO interaction such as $\Delta_{so}^R/\hbar\omega_0 = 0.5$ and $\Delta_{so}^D/\hbar\omega_0 = 0.25$ for the same density value as in (a), (c) The same energy subband dispersion as in (b) for different electron density value: $\rho_{1D}l_0 \approx 0.57$.

5.1.4.2 Energy Bands With Magnetic Field

Fig. 5.18 shows the exchange-correlation effect for strong Rashba SO interaction ($\Delta_{so}^R/\hbar\omega_0 = 0.5$) and various magnetic field values when any Dresselhaus SO interaction term does not exist. The exchange-correlation energy causes a shift in the energy subbands as in the case for zero magnetic field. In consideration of the effect of external magnetic field, asymmetries occur in the vicinity of $k_y = 0$ for the first lowest subbands of odd energy levels.

When only Rashba SO coupling is considered in the presence of a certain perpendicular magnetic field and exchange-correlation interaction, near the $k_y = 0$ point an asymmetry occurs conspicuously in the first lowest spin-split subband for higher magnetic field strengths ($\omega_c/\omega_0 = 1$ and 2) with respect to the case of that includes only Dresselhaus SO coupling contribution (compare Figs. 5.18(b)-(c) and 5.19(a)-(b)).

To determine the interplay of the different strengths of individual SO coupling with magnetic field when \mathcal{V}_{xc} term exists, in Fig. 5.20 and 5.21 we present the energy subband dispersions for three different values of characteristic Rashba and Dresselhaus SO energies under strong magnetic field, respectively. Since we obtain similar subband energy spectra for each same characteristic SO energy in weak SO regimes, we show the case for the existence of only weak Rashba SO coupling in Fig. 5.20(a). For a fixed magnetic field strength, the asymmetric feature of the lowest subband, which arises only in the existence of exchange-correlation energy, undergoes change depending on the strength of Rashba SO coupling as shown in Fig. 5.20. Comparison of the Figs. 5.20(b)-(c) and 5.21(a)-(b) brings out into open that the interplay between each type of SO interaction strength and external magnetic field shows an alteration under the effect of exchange-correlation.

As a common feature of individual mechanism of SO interaction, we can say that with inclusion of exchange-correlation interaction energy “camel-back” shape that arises at spin branches of the lowest energy level has remained in the neighbourhood

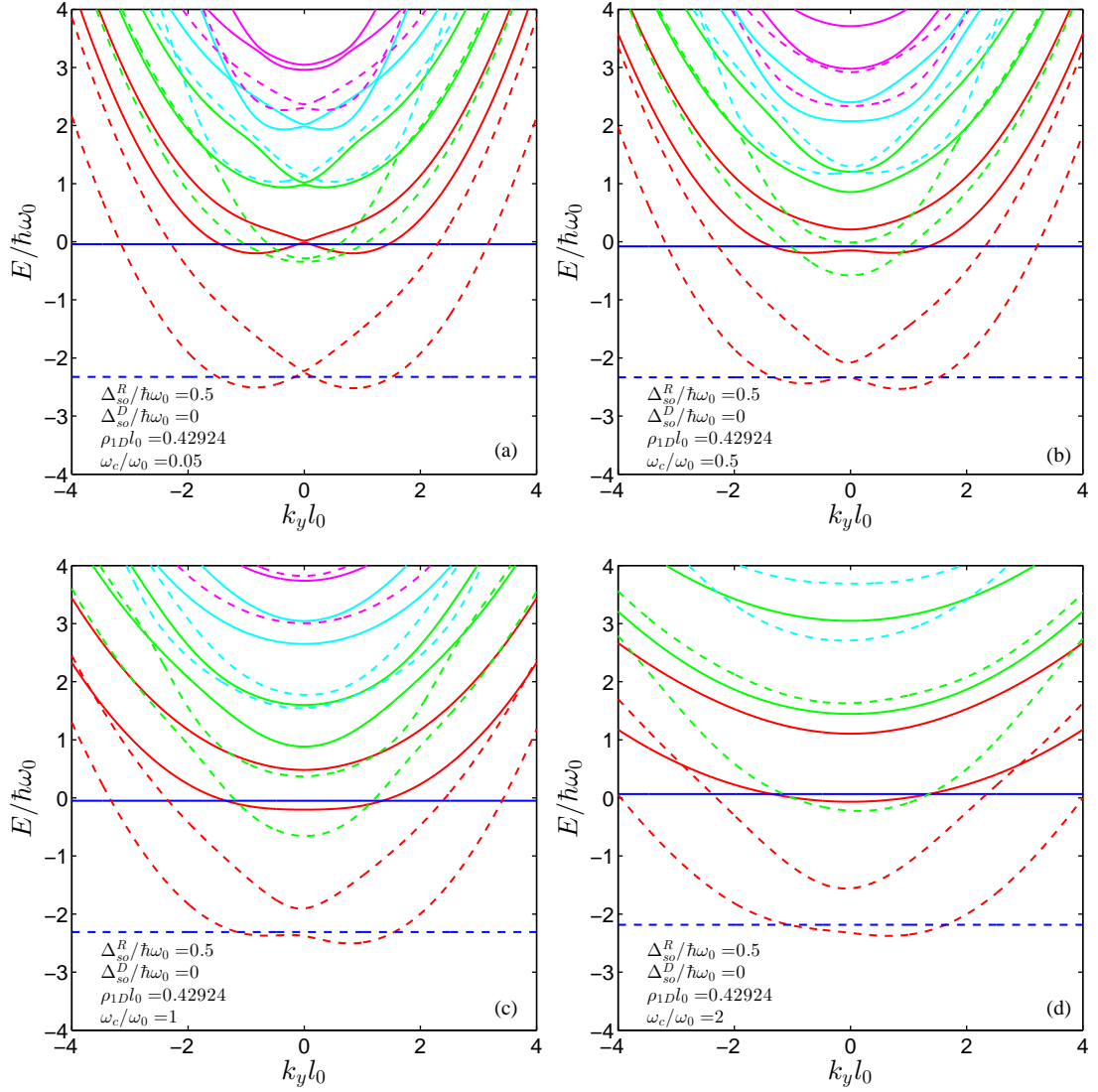


Figure 5.18 Energy subband dispersion at $\rho_{1D}l_0 \simeq 0.43$ with strong regime of Rashba SO coupling ($\Delta_{so}^R/\hbar\omega_0 = 0.5$) and zero Dresselhaus SO coupling ($\Delta_{so}^D/\hbar\omega_0 = 0$). The strength of the magnetic field is varied from weak to strong limit. (a) $\omega_c/\omega_0 = 0.05$, (b) $\omega_c/\omega_0 = 0.5$, (c) $\omega_c/\omega_0 = 1$, (d) $\omega_c/\omega_0 = 2$

of $k_y = 0$ even though the QWR is under the effect of external magnetic field. On the other hand when exchange-correlation contribution is not considered, magnetic field leads to flattening of the camelback shape in the lower energy subbands as previously described in Section 5.1.1.

Moreover, the asymmetry in the lowest subband changes markedly with increasing magnetic field. In connection with this result, one can consider that exchange-correlation interaction contributes to the lowest energy subbands as if there has been

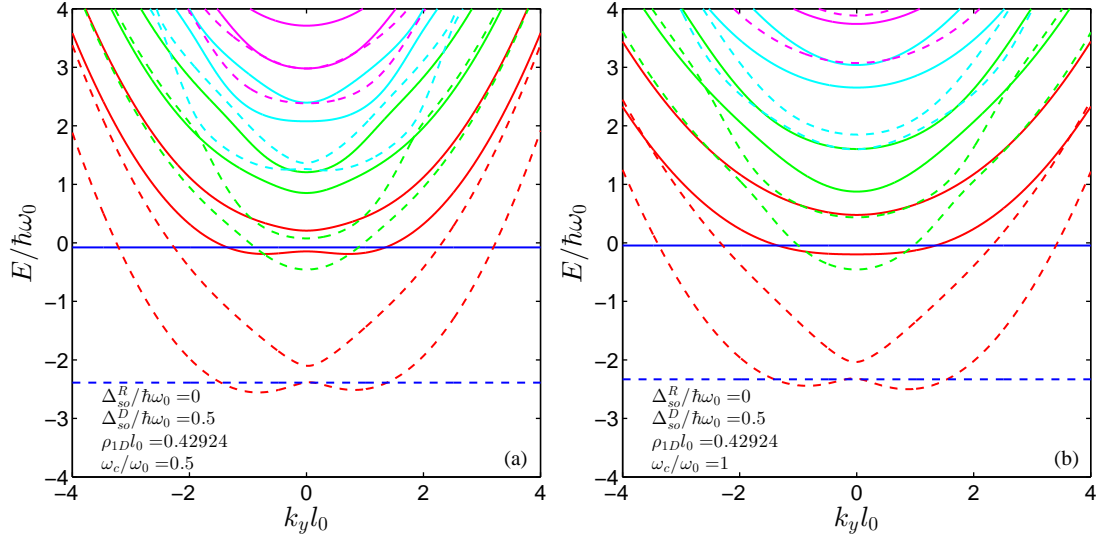


Figure 5.19 Energy subband dispersion at $\rho_{1D}l_0 \simeq 0.43$ with zero Rashba SO coupling ($\Delta_{so}^R/\hbar\omega_0 = 0$) and strong regime of Dresselhaus SO coupling ($\Delta_{so}^D/\hbar\omega_0 = 0.5$) for two different values of magnetic field. (a) $\omega_c/\omega_0 = 0.5$, (b) $\omega_c/\omega_0 = 1$.

an additional effective pseudomagnetic field for certain external magnetic fields and this interaction term has different influences on the energy subbands for each type of SO coupling term. Stronger magnetic field values cause the flattening of camelback shape in the subband structure in a similar manner as in the case for the no exchange-correlation energy is taken into account.

As can be seen in Figs. 5.22(a) and (b), with inclusion of weak Dresselhaus contribution in addition to strong Rashba SO effect and different magnetic field strengths, the asymmetry in the first lowest subband no longer exists for the case of exchange-correlation interaction is considered (see also Figs. 5.18(b) and (c)). The contributions from Dresselhaus SO coupling tend to extinguish the asymmetry in the lowest subband.

In order to analyze the effect of both electron density and exchange-correlation energy, we calculate the energy spectrum of the QWR which is under the influence of external magnetic field and different regimes of Rashba and Dresselhaus SO coupling contributions. In Fig. 5.23, we present the energy subband dispersion for weak regime of both SO coupling. When electron density is varied from low to high limit, separation between spin-split subbands of same energy level decreases and the amount

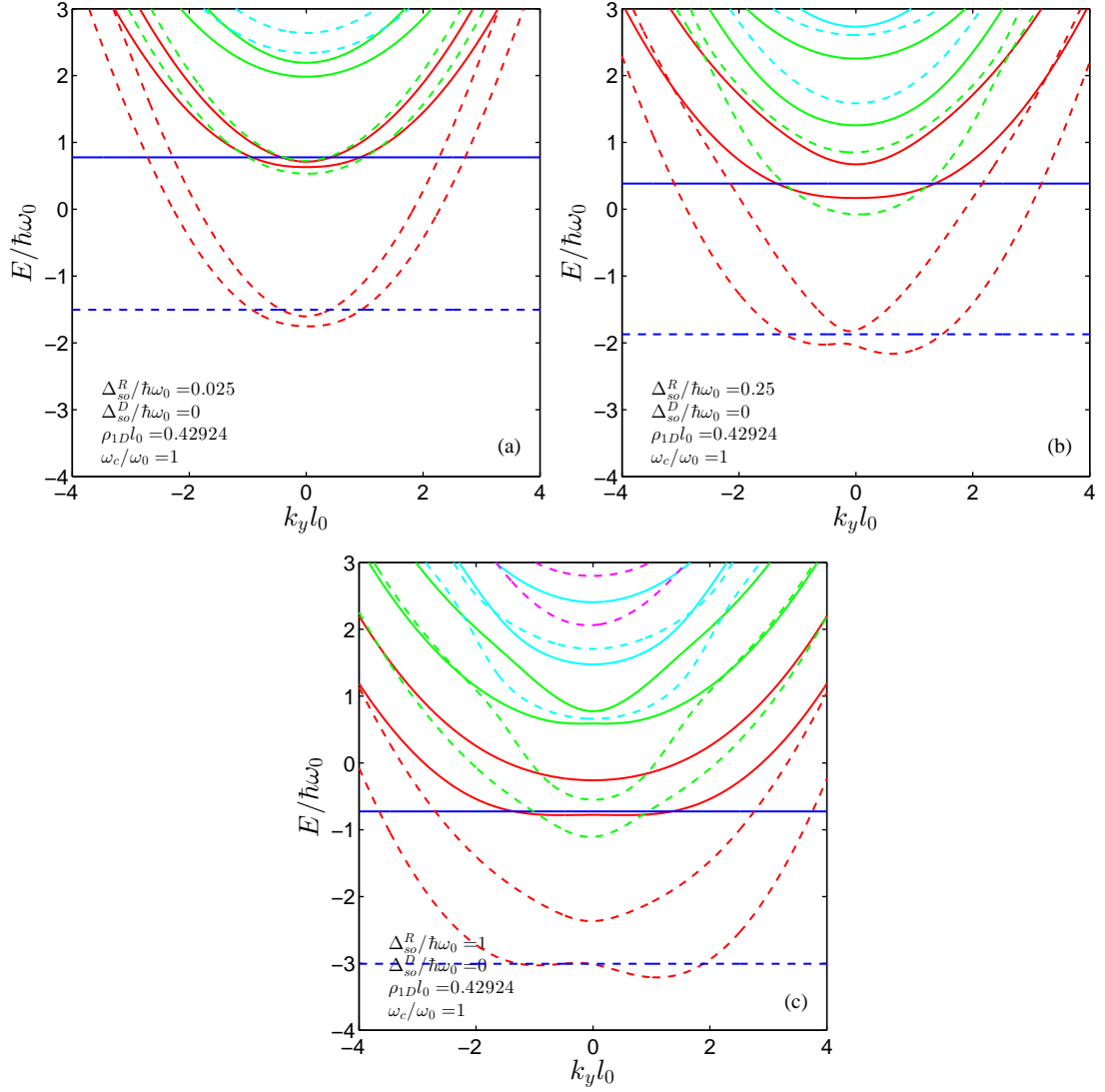


Figure 5.20 Subband energy spectra of the QWR with no Dresselhaus SO interaction term ($\Delta_{so}^D/\hbar\omega_0 = 0$) at strong magnetic field ($\omega_c/\omega_0 = 1$) and low electron density ($\rho_{1D}l_0 \approx 0.43$). Rashba SO coupling strength is varied from weak to strong regime. (a) $\Delta_{so}^R/\hbar\omega_0 = 0.025$, (b) $\Delta_{so}^R/\hbar\omega_0 = 0.25$, (c) $\Delta_{so}^R/\hbar\omega_0 = 1$

of downward energy shifting to lower energies increases at $k_y = 0$ point in the presence of \mathcal{V}_{xc} .

Fig. 5.24 represents the energy level spectrum for equal strength of both SO coupling terms and different values of electron density in the presence of external magnetic field. Similar to the previous ones, for weak SO regime and low electron density limit (Fig. 5.24(a)) the increment of spin-splitting between lowest energy subbands can be seen clearly when exchange-correlation contribution is taken into account. On the contrary, for high electron density limit spin splitting is imperceptible

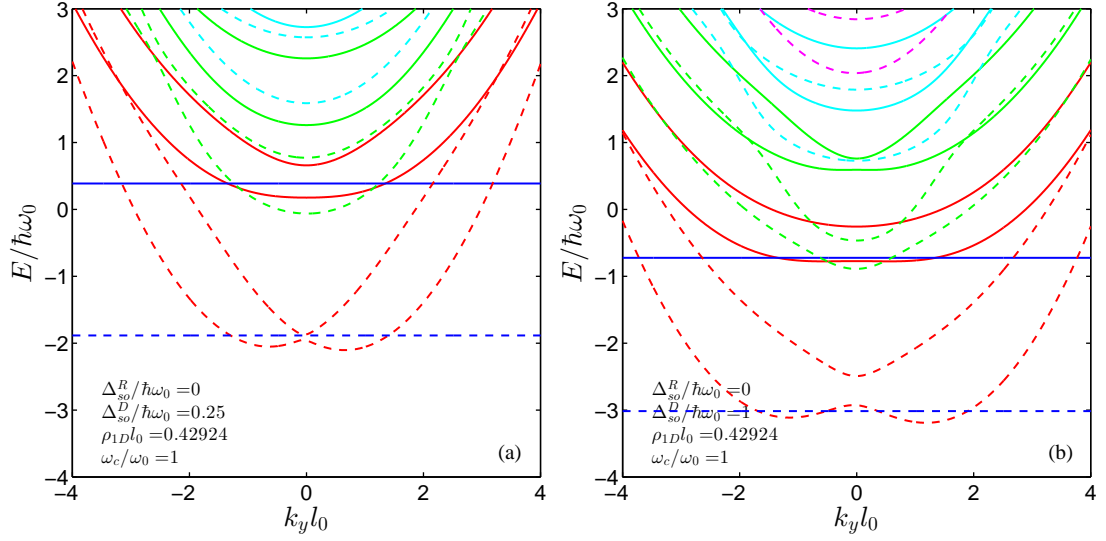


Figure 5.21 Subband energy spectra of QWR with no Rashba SO interaction term ($\Delta_{so}^R/\hbar\omega_0 = 0$) at strong magnetic field ($\omega_c/\omega_0 = 1$) and low electron density ($\rho_{1D}l_0 \simeq 0.43$) for two different values of Dresselhaus SO coupling strength. (a) $\Delta_{so}^D/\hbar\omega_0 = 0.25$, (b) $\Delta_{so}^D/\hbar\omega_0 = 1$.

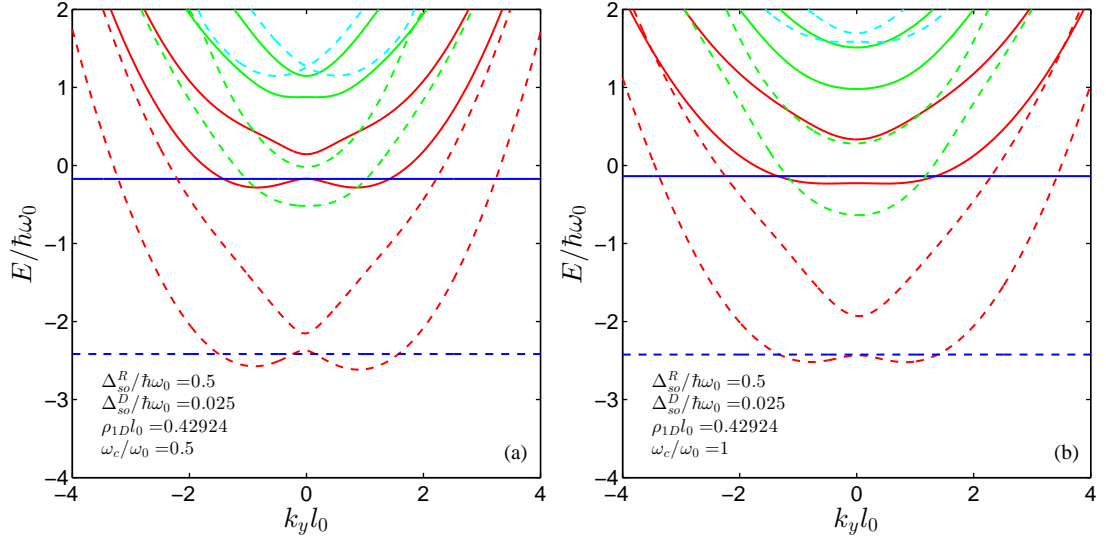


Figure 5.22 Energy dispersion of the spin-split subbands at $\rho_{1D}l_0 \simeq 0.43$ for two different values of magnetic field when Rashba SO interaction is strong ($\Delta_{so}^R/\hbar\omega_0 = 0.5$) and Dresselhaus SO interaction is weak ($\Delta_{so}^D/\hbar\omega_0 = 0.025$). (a) $\omega_c/\omega_0 = 0.5$, (b) $\omega_c/\omega_0 = 1$.

to the eye in the existence of the exchange-correlation effect at $k_y = 0$ point. Furthermore, at low electron density limit there exists an asymmetry in the lower spin-split subband of the even energy level which includes the exchange-correlation contribution (inset in Fig. 5.24(a)). In either case, degeneracy has remained at $k_y = 0$ point in the presence or absence of exchange-correlation energy as shown in

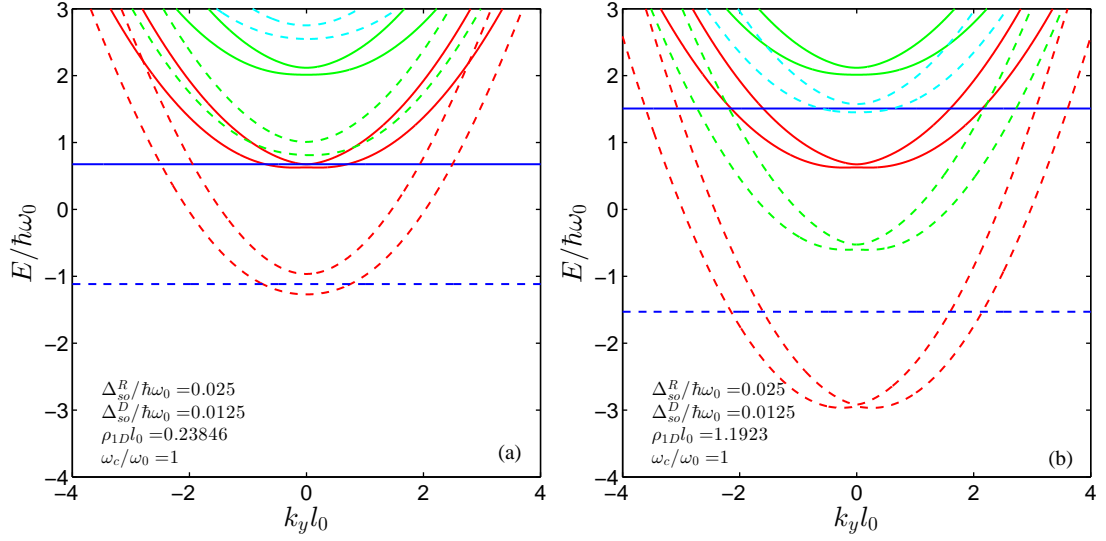


Figure 5.23 Energy subband dispersion for weak strength of Rashba and Dresselhaus SO interactions ($\Delta_{so}^R/\hbar\omega_0 = 0.025$, $\Delta_{so}^D/\hbar\omega_0 = 0.0125$) at a finite magnetic field ($\omega_c/\omega_0 = 1$). (a) $\rho_{1D}l_0 \simeq 0.24$, (b) $\rho_{1D}l_0 \simeq 1.19$.

Figs. 5.24(c) and (d).

For low electron density case, increasing SO coupling strength leads to an asymmetry in the energy subband as shown in Fig. 5.25(a). The asymmetry in the lowest subband is more pronounced for strong Dresselhaus SO coupling case rather than strong Rashba SO coupling (compare Fig. 5.25(a) with Fig. 5.25(c)). As a consequence we can say that this asymmetry depends on which type of SO coupling term is effective according to another (Rashba or Dresselhaus). Decreasing spin-splitting between energy subbands and disappearance of asymmetric shape in the lowest subband is clearly visible with increasing electron density as seen in Fig 5.25(b). The feature of Fig. 5.25(d) states that with the increment of SO coupling strength, asymmetry in the lowest subband varies due to the interplay between SO coupling strength and exchange-correlation energy under a certain magnetic field.

When strong regime of both characteristic Rashba and Dresselhaus SO coupling energies is considered, energy subband distributions are similar to each other for the same density limits (compare Fig. 5.26(a) with (c) for low density limit, Fig. 5.26(b) with (d) for high density limit)

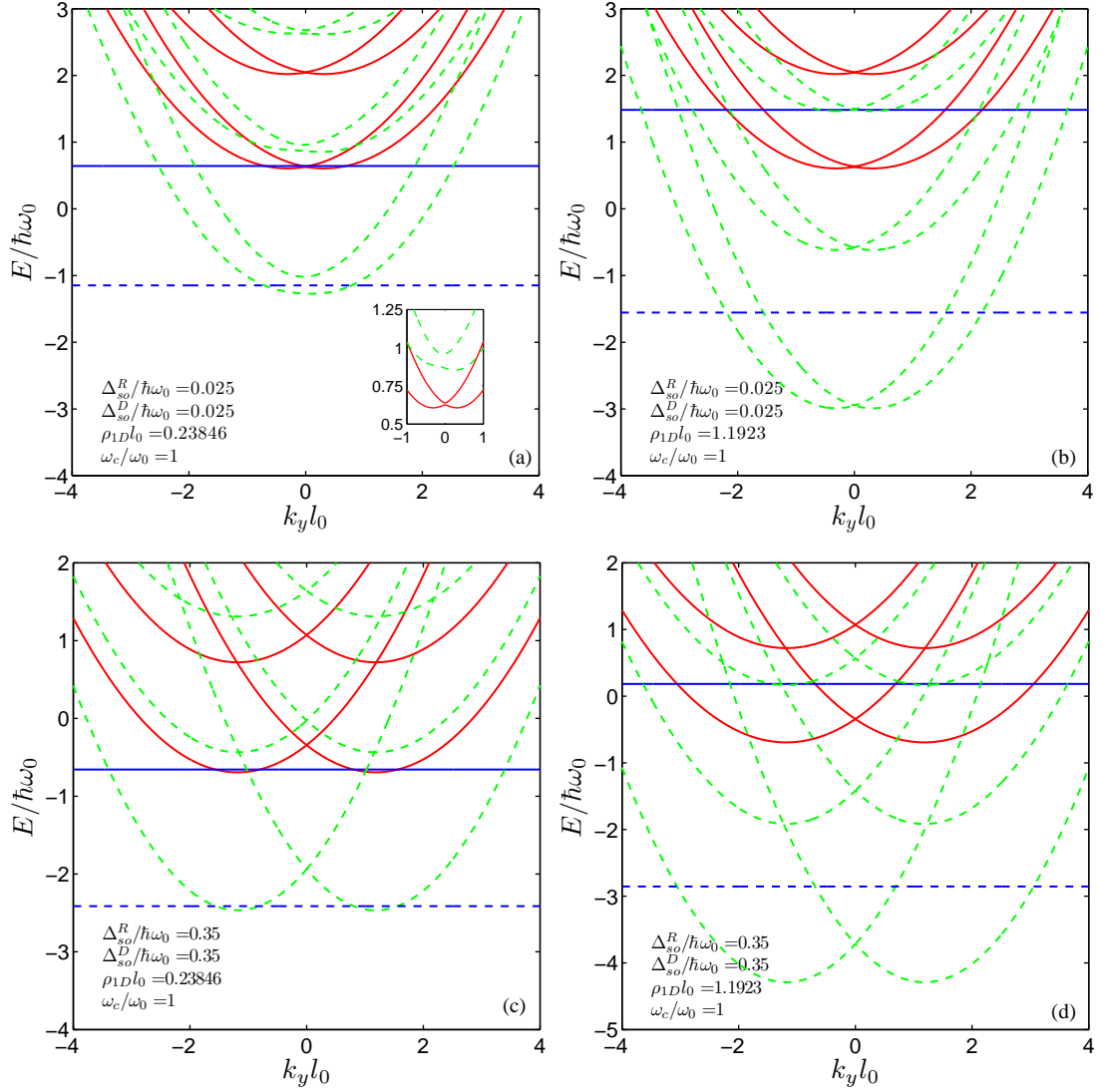


Figure 5.24 Energy subband dispersion for equal strength of weak and strong SO interactions at a finite magnetic field ($\omega_c/\omega_0 = 1$). (a) Weak SO regime: $\Delta_{so}^R/\hbar\omega_0 = \Delta_{so}^D/\hbar\omega_0 = 0.025$ in low electron density ($\rho_{1D}l_0 \approx 0.24$) limit. The inset shows the asymmetry in the lower spin-split subband of the even energy level. (b) The same energy subband dispersion as in (a) with high electron density ($\rho_{1D}l_0 \approx 1.19$) limit. (c)-(d) The same energy subband dispersion as in (a) for strong SO regime: $\Delta_{so}^R/\hbar\omega_0 = \Delta_{so}^D/\hbar\omega_0 = 0.35$ with low density ($\rho_{1D}l_0 \approx 0.24$) and high density ($\rho_{1D}l_0 \approx 1.19$) limits, respectively.

5.1.4.3 Spin Orientation Without Spin-Orbit Interaction

At first, we calculate the spin textures when only the contribution of magnetic field is considered in the presence of exchange-correlation effect. As shown in Fig. 5.27(a), the spin component $S_z(x)$ is different from zero for non-small values of the magnetic field at low electron density limit. There is no spatial modulation of spin density due

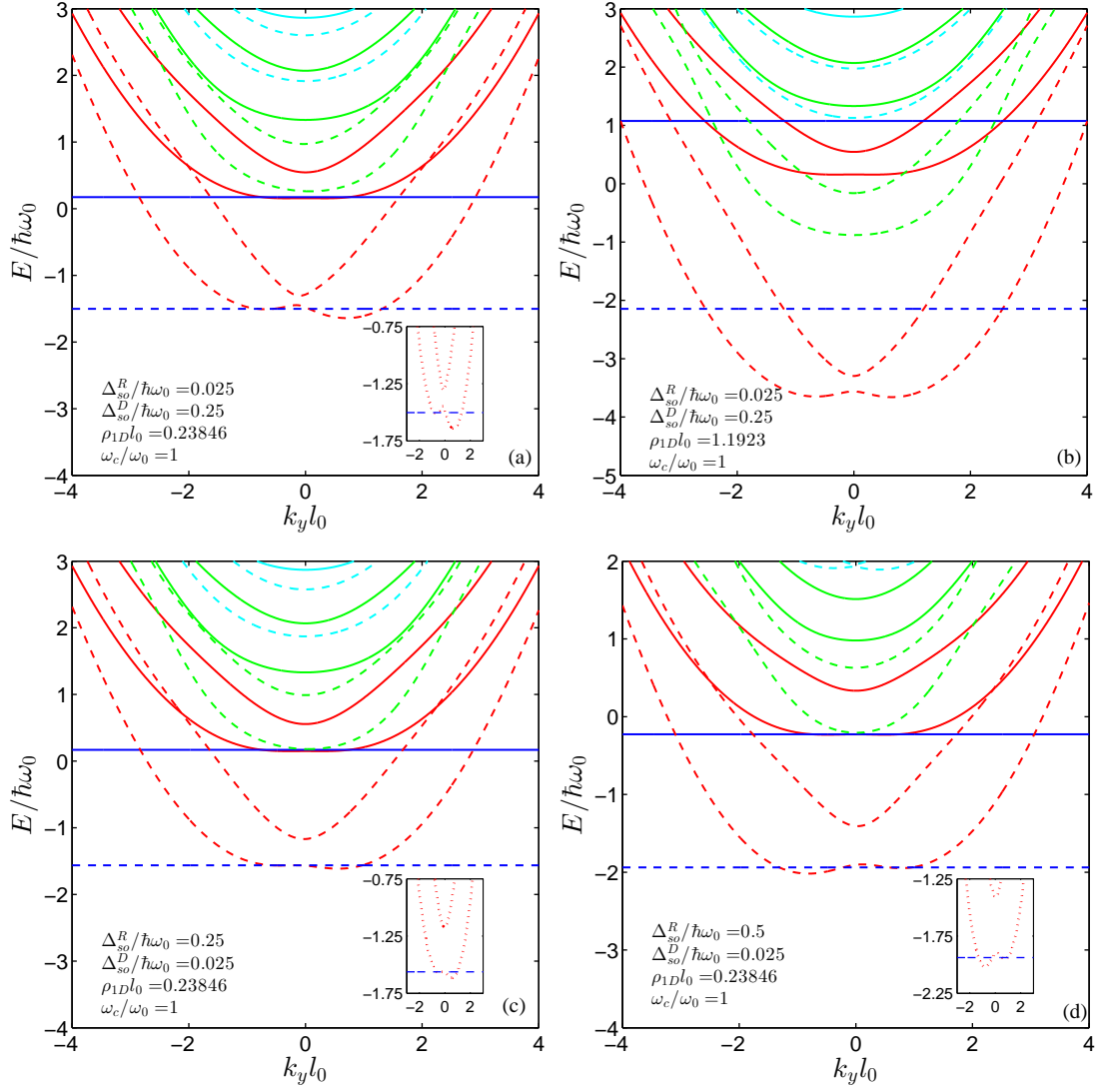


Figure 5.25 Energy subband dispersion for different mechanism of Rashba and Dresselhaus SO interactions. (a) $\Delta_{so}^R/\hbar\omega_0 = 0.025$ and $\Delta_{so}^D/\hbar\omega_0 = 0.25$ at a finite magnetic field ($\omega_c/\omega_0 = 1$) for low density limit ($\rho_{1D}l_0 \simeq 0.24$), (b) Same SO coupling strengths as in (a) with high density limit ($\rho_{1D}l_0 \simeq 1.19$), (c)-(d) same energy subband dispersion as in (a) with strong Rashba ($\Delta_{so}^R/\hbar\omega_0 = 0.25$ and $\Delta_{so}^R/\hbar\omega_0 = 0.5$, respectively) and weak Dresselhaus ($\Delta_{so}^D/\hbar\omega_0 = 0.025$) SO coupling.

to the fact that externally applied magnetic field has no x-dependency. For the high density limit, the magnitude of $S_z(x)$ becomes zero (see section 5.1.3.1).

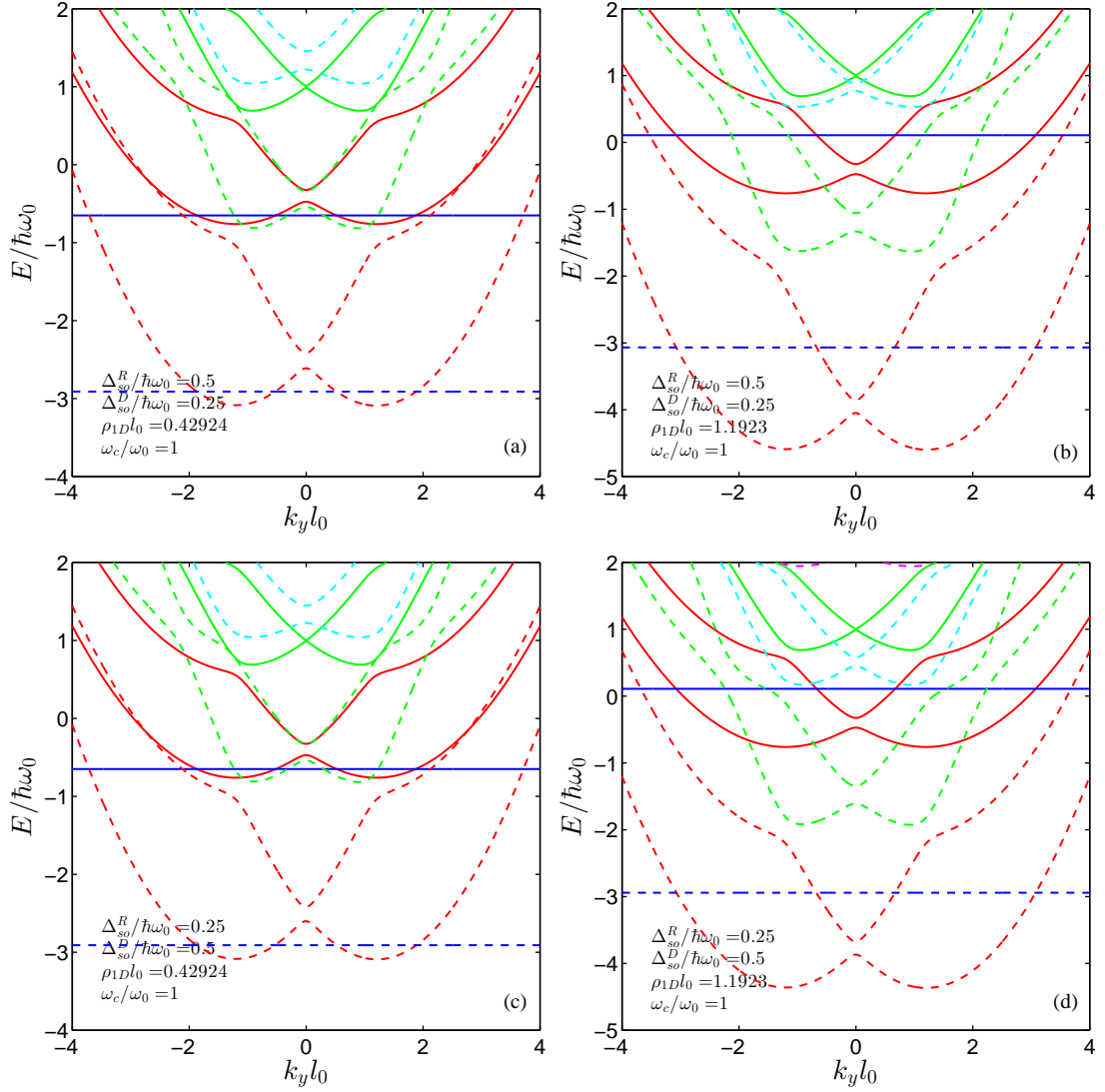


Figure 5.26 Subband energy spectra of QWR with strong SO coupling strengths for two density limits at a finite magnetic field ($\omega_c/\omega_0 = 1$). (a) $\Delta_{so}^R/\hbar\omega_0 = 0.5$, $\Delta_{so}^D/\hbar\omega_0 = 0.25$ low density $\rho_{1D}l_0 \approx 0.43$, (b) $\Delta_{so}^R/\hbar\omega_0 = 0.5$, $\Delta_{so}^D/\hbar\omega_0 = 0.25$ high density ($\rho_{1D}l_0 \approx 1.19$), (c) $\Delta_{so}^R/\hbar\omega_0 = 0.25$, $\Delta_{so}^D/\hbar\omega_0 = 0.5$ low density $\rho_{1D}l_0 \approx 0.43$ (d) $\Delta_{so}^R/\hbar\omega_0 = 0.25$, $\Delta_{so}^D/\hbar\omega_0 = 0.5$ high density ($\rho_{1D}l_0 \approx 1.19$).

5.1.4.4 Spin Orientation Without Magnetic Field

To identify the effect of Rashba and Dresselhaus SO interaction on spin orientation in the presence of exchange-correlation contribution, we calculate the spin textures for weak SO interaction regimes at zero magnetic field. For low electron density limit, we obtain that there is no spatial modulation due to aforementioned reasons in section (5.1.3.2) and also weak interaction between SO coupling and exchange-

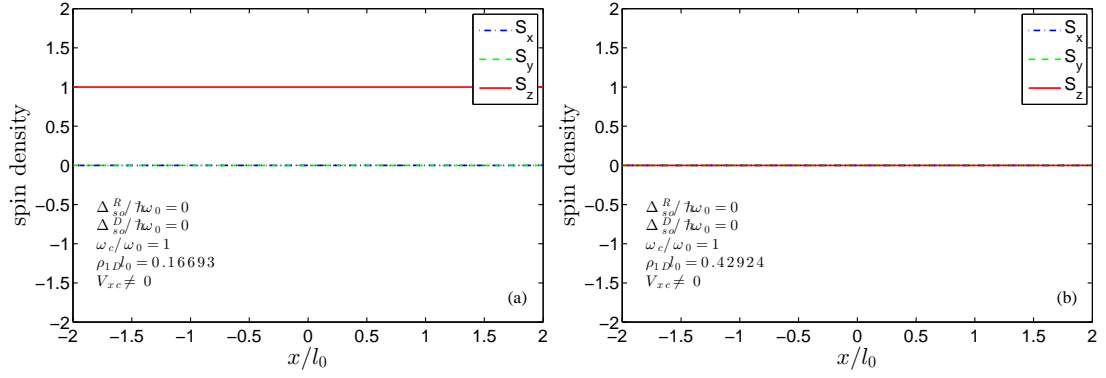


Figure 5.27 Spin density components in the absence of both SO coupling terms at $\omega_c/\omega_0 = 1$ for different density limits. (a) low-density limit (b) high-density limit.

correlation (see Fig. 5.17(a)). This behavior in spin distribution is similar with the case for no exchange-correlation effect is considered (see Fig. 5.12).

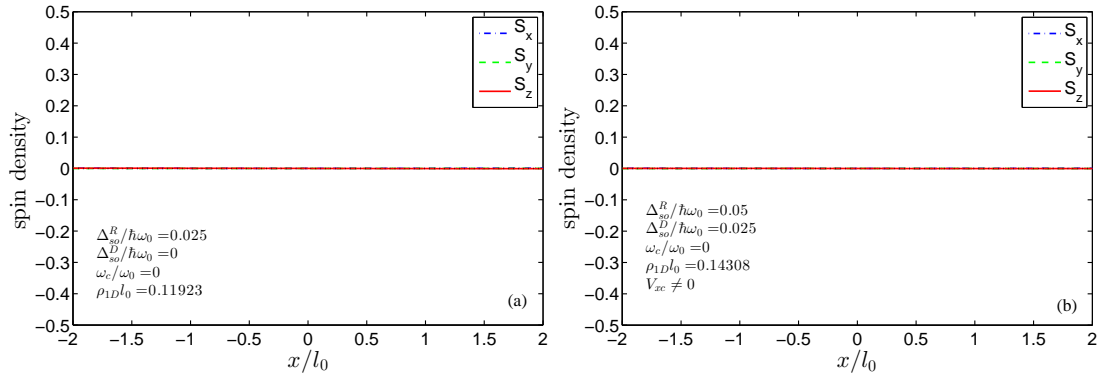


Figure 5.28 Spin densities under the influence of exchange-correlation and weak SO couplings at $\omega_c/\omega_0 = 0$ and $\hbar\omega_0 = 2 \text{ meV}$. (a) $\Delta_{so}^R/\hbar\omega_0 = 0.025$, $\Delta_{so}^D/\hbar\omega_0 = 0$, (b) $\Delta_{so}^R/\hbar\omega_0 = 0.05$, $\Delta_{so}^D/\hbar\omega_0 = 0.025$.

5.1.4.5 Spin Orientation In The Presence of Both Spin-Orbit Interaction and Magnetic Field

Previously (in section 5.1.3.3), we obtained that spin components had non-zero values along $\hat{x}, \hat{y}, \hat{z}$ directions by inclusion of both type of SO coupling term and external magnetic field. This spatial dependency of spin components remains when the effect of exchange-correlation contribution is considered as can be seen in Fig. 5.29. In this figure, we get spin textures in the absence/presence of exchange-correlation contribution for different strengths of SO interaction. The spin components $S_x(x)$ and

$S_y(x)$ are zero at the center of the wire in the absence/presence of exchange-correlation effect. Both symmetric and parabolic behavior of spin components are destroyed with the effect of exchange-correlation contribution.

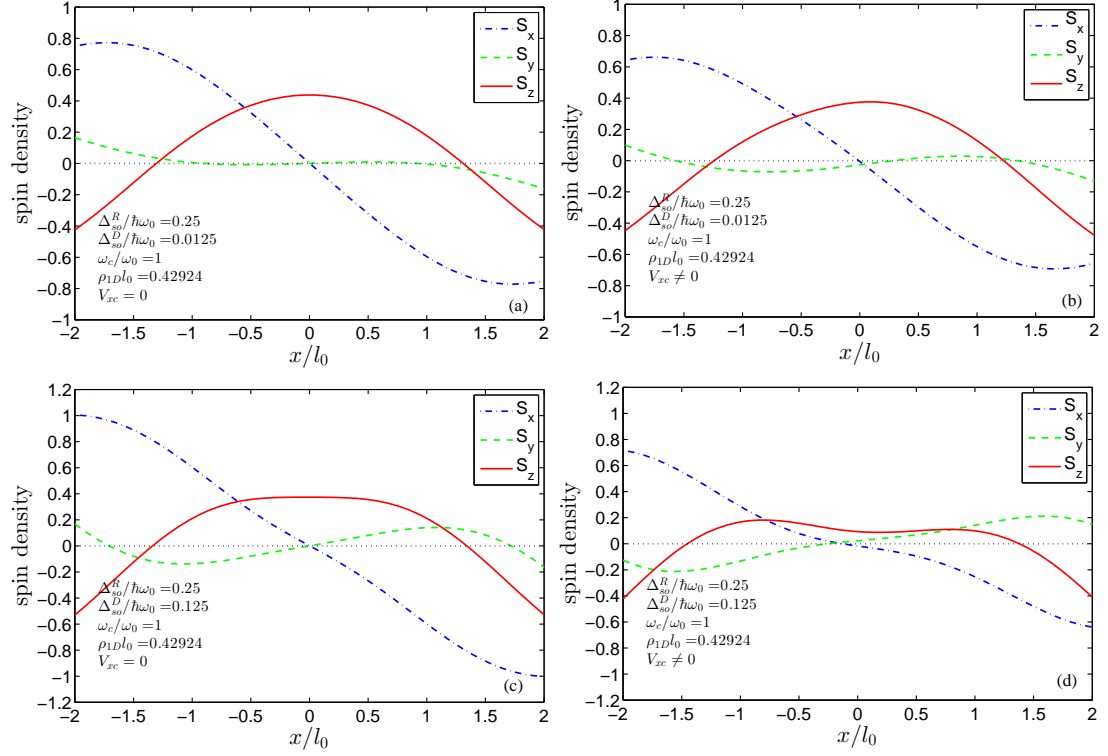


Figure 5.29 Spatial variation of spin density components for the case of different SO coupling strengths at a finite magnetic field value ($\omega_c/\omega_0 = 1$) and low density regime ($\rho_{1D}l_0 \simeq 0.43$). (a) $\Delta_{so}^R/\hbar\omega_0 = 0.25$, $\Delta_{so}^D/\hbar\omega_0 = 0.0125$ with no exchange-correlation effect, (b) The same SO coupling strengths as in (a) with nonzero exchange-correlation contribution (c)-(d) $\Delta_{so}^R/\hbar\omega_0 = 0.25$, $\Delta_{so}^D/\hbar\omega_0 = 0.125$ in the absence and presence of the exchange-correlation contribution, respectively.

To determine how the magnitude of external magnetic field modify the spin distribution, we calculate the spin orientations for different strengths of magnetic field which is varied from weak to strong limit. At the center of the wire, electrons are only under the influence of external magnetic field. So the spin component $S_z(x)$ has a maximum value at this point. At the edges of the wire, effective Rashba and Dresselhaus pseudo-magnetic fields give contribution to the net magnetic field. So, $S_x(z)$ and $S_y(x)$ spin components are different than zero and they take different signs at opposite edges of the wire. As the magnetic field strengthen to a stronger value, the magnitude of all spin components change.

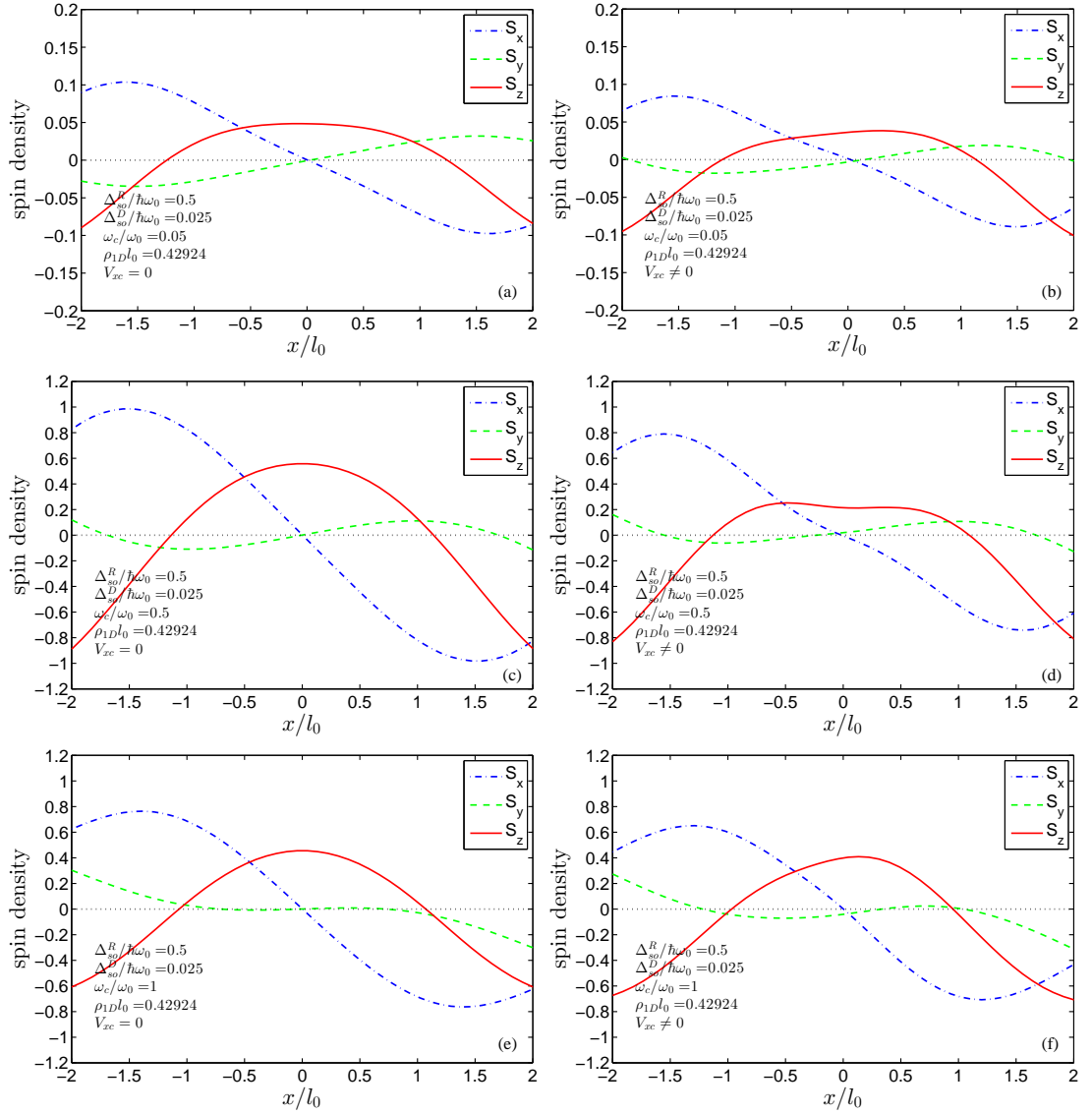


Figure 5.30 Spin texture for the strong Rashba and Dresselhaus SO couplings ($\Delta_{so}^R/\hbar\omega_0 = 0.5$, $\Delta_{so}^D/\hbar\omega_0 = 0.25$) in the absence/presence of the exchange-correlation effect. The lowest spin-split band is occupied in all cases. The figures in the left side refers to the condition that the contribution of the exchange-correlation effect is not considered. The figures in the right side stands for the case of nonzero exchange-correlation effect. Magnetic field is varied from weak to strong limit. (a)-(b) $\omega_c/\omega_0 = 0.05$, (c)-(d) $\omega_c/\omega_0 = 0.5$, (e)-(f) $\omega_c/\omega_0 = 1$

CHAPTER SIX

CONCLUSION

In this thesis, we have investigated electronic properties of parabolically confined quasi-1D QWR that is subjected to an externally applied perpendicular magnetic field and also under the effect of both Rashba and/or Dresselhaus SO couplings and taking into account the exchange-correlation interaction. We have calculated numerically energy subband dispersions, wavefunctions and also spin texturing by using the FEM.

We have begun our study by considering the contribution of only SO interaction for the physical system without a magnetic field to determine the SO coupling effects on the energy dispersion. In this context, we have investigated the subband energy spectra for different regimes of characteristic SO coupling energies. For comparison we have also calculated the energy eigenvalues in the absence of SO interaction at zero magnetic field. All energy subbands are spin degenerate when SO coupling terms and magnetic field are zero. The presence of Rashba and/or Dresselhaus SO coupling lifts the degeneracy in the spin-split bands except $k_y = 0$ point. Energy dispersion of the spin-split subbands is symmetric throughout the k_y axis. Increasing the SO coupling strength leads to pronounced deviation from the parabolicity of energy subbands and anticrossing has been seen between neighbouring subbands with opposite spin indices. In the neighbourhood of $k_y = 0$, “camel-back” shape arises from the effect of SO coupling for spin branches of lower energy levels. Additionally the amount of the downward shifting of energy increases with increasing total characteristic SO coupling energy.

We have also studied the effect of perpendicular magnetic field on the subband structure of QWR with/without Rashba and/or Dresselhaus SO couplings. When only the external magnetic field is present, the degeneracy has been removed in each energy subband for all k_y points. In other words, each energy band splits up into a doublet in the presence of external magnetic field and the amount of splitting is proportional to the magnitude of this applied magnetic field. For the case of nonzero magnetic field and the existence of SO interaction, we have observed that the magnitude of spin

splitting between energy subbands of different states undergoes change depending on the interplay of SO coupling with the external magnetic field. Increased magnetic field enhances the confinement potential which results in vertically upward shifting in the bottom of flattened energy subbands and increment in energy spacing between upper and lower level of each subband. For different SO interaction contributions, camel-back shapes preserves under certain conditions.

Afterwards, we have investigated the effect of a perpendicular magnetic field on the spin texturing of a parabolically confined QWR taking into account Rashba and Dresselhaus SO couplings. Our results show that competing effects between magnetic field and SO interactions introduce complex features in spin texturing. By comparing different SO coupling regimes, we can say that energy subband dispersion and spin orientation for the strong SO coupling regime are more intricate than for the case of weak SO regime.

In addition to understanding the interplay of Rashba and/or Dresselhaus SO coupling with external magnetic field and the effect of these contributions on energy subband structure and spin orientation, another purpose of this thesis is to obtain the influence of exchange-correlation interaction on subband energy spectra of the QWR. In order to handle the QWR system with exchange-correlation interaction, we have used the noncollinear local-spin density approximation within the framework of density functional theory. We have used Attacalite formalism (Attacalite et al., 2002) for exchange-correlation energy functional.

The subband separation, which is produced by the effect of external magnetic field, remains when exchange-correlation interaction has been taken into account. When both SO coupling strengths are equal, the inclusion of V_{xc} does not change the crossing properties of the subbands and that it only induces a small subband splitting.

With inclusion of exchange-correlation interaction the energy subbands are shifted to lower energies in the absence/presence of SO interactions and/or external magnetic field. The magnitude of the energy shift increases with increasing electron density.

The effect of exchange-correlation at low density limit leads to an asymmetric double minimum in the lowest subbands when the QWR is under the effect of external magnetic field and SO coupling term.

If we want to emphasize the results of this thesis, in a nutshell we can argue the following: We find that the interplay between the magnetic field and SO couplings affects strongly the energy subband dispersion of the QWR. Energy subband structure varies depending on which type of SO coupling strength is considered and also the magnitude of SO coupling. Our numerical calculations show that the spatial distribution of spin components can be modulated by SO coupling, external magnetic field and carrier concentration of the system. We expect that these observations can assist in understanding of transport and optical properties of quasi-1D quantum structures.

REFERENCES

- Arakawa, Y., Nagamune, Y., Nishioka, M., & Tsukamoto, S. (1993). Fabrication and optical properties of GaAs quantum wires and dots by MOCVD selective growth. *Semiconductor Science and Technology*, 8(6), 1082.
- Asahi, H. (1997). Self-organized quantum wires and dots in III-V semiconductors. *Advanced Materials*, 9(13), 1019–1026.
- Attacalite, C., Moroni, S., Gori-Giorgi, P., & Bachelet, G. B. (2002). Correlation energy and spin polarization in the 2D electron gas. *Physical Review Letters*, 88(25), 256601.
- Attacalite, C., Moroni, S., Gori-Giorgi, P., & Bachelet, G. B. (2003). Erratum: Correlation energy and spin polarization in the 2D electron gas [physical review letters 88, 256601 (2002)]. *Physical Review Letters*, 91(10), 109902.
- Bader, S. D., & Parkin, S. S. P. (2010). Spintronics. *Annual Review of Condensed Matter Physics*, 1, 71–88.
- Banerjee, S., Dan, A., & Chakravorty, D. (2002). Review: Synthesis of conducting nanowires. *Journal of Materials Science*, 37(20), 4261–4271.
- Barth, U. V., & Hedin, L. (1972). A local exchange-correlation potential for the spin polarized case. i. *Journal of Physics C: Solid State Physics*, 5(13), 1629–1642.
- Bin, S. Z. (2010). *Transport in nanostructures with spin orbit interaction*. Master's Thesis, National University of Singapore.
- Born, M., & Oppenheimer, J. R. (1927). On the quantum theory of molecules. *Annalen der Physik*, 389(20), 457–484.
- Bransden, B. H., & Joachain, C. J. (1990). *Physics of atoms and molecules*. (2nd ed.). Prentice Hall.
- Bulaev, D. V., & Loss, D. (2005). Spin relaxation and anticrossing in quantum dots: Rashba versus Dresselhaus spin-orbit coupling. *Physical Review B*, 71, 205324.

- Burk, K. (2003). The abc of DFT. Department of Chemistry, Rutgers University. Retrieved May 3, 2013, from <http://dft.rutgers.edu/kieron/beta>.
- Bychkov, Y. A., & Rashba, E. I. (1960). Oscillatory effects and the magnetic susceptibility of carriers in inversion layers. *Journal of Physics C: Solid State Physics*, 17(33), 6039.
- Camenzind, L. (2012). *Quantum transport signatures of electric dipole spin resonance near the persistent spin helix in GaAs quantum wells*. Master's Thesis, University Of Basel.
- Ceperley, D. M., & Alder, B. J. (1980). Ground state of the electron gas by a stochastic method. *Physical Review Letters*, 45(7), 566–569.
- Chang, M.-C. (2005). Effect of in-plane magnetic field on the spin hall effect in a Rashba-Dresselhaus system. *Physical Review B*, 71, 085315.
- Chang, R. S., Chu, C. S., & Mal'shukov, A. G. (2009). Competing interplay between Rashba and cubic-k Dresselhaus spin-orbit interactions in spin-hall effect. *Physical Review B*, 79, 195314.
- Cummings, A. W. (2009). *The spin Hall effect in quantum wires*. Ph.D. Thesis, Arizona State University.
- Datta, S. (1995). *Electronic transport in mesoscopic systems*. (1st ed.). Cambridge: Cambridge University Press.
- Debald, S., & Kramer, B. (2005). Rashba effect and magnetic field in semiconductor quantum wires. *Physical Review B*, 71, 115322.
- Dirac, P. A. M. (1930). Note on exchange phenomena in the thomas atom. *Mathematical Proceedings of the Cambridge Philosophical Society*, 26(3), 376–385.
- Doğan, Ü. (2009). *Mesh generation and electronic structure of quantum wires*. Ph.D. Thesis, Dokuz Eylül University.

- Dresselhaus, G. (1955). Spin-orbit coupling effects in zinc blende structures. *Physical Review*, 100(2), 580–586.
- Dyakonov, M. I., & Kachorovskii, V. Y. (1986). Spin relaxation of two-dimensional electrons in noncentrosymmetric semiconductors. *Soviet Physics: Semiconductors*, 20, 110.
- Erlingsson, S. I., Egues, J. C., & Loss, D. (2010). Energy spectra for quantum wires and two-dimensional electron gases in magnetic fields with Rashba and Dresselhaus spin-orbit interactions. *Physical Review B*, 82(15), 155456.
- Fabian, J., Matos-Abiaguea, A., Ertlera, C., Stano, P., & Zutic, I. (2007). Semiconductor spintronics. *Acta Physica Slovaca*, 57(4& 5), 565–907.
- Fermi, E. (1928). Eine statistische methode zur bestimmung einiger eigenschaften des atoms und ihre anwendung auf die theorie des periodischen systems der elemente. *Zeitschrift Für Physik*, 48(1-2), 73–79.
- Fert, A. (2007). Nobel lecture: The origin, development and future of spintronics. The Nobel Foundation 2007. Retrieved May 25, 2013, from <http://www.nobelprize.org/nobelprizes/physics/laureates/2007/fert-lecture.html>.
- Fock, V. (1930). Approximation method for the solution of the quantum mechanical more-particle problem. *Zeitschrift für Physik*, 61(1), 126–148.
- Gáspár, R. (1954). On an approximation of Hartree-Fock potentials through a universal potential. *Acta Physica Hungarica*, 3, 263.
- Gharaati, A., & Khordad, R. (2012). Effects of magnetic field and spin-orbit interaction on energy levels in 1D quantum wire: Analytical solution. *Optical and Quantum Electronics*, 44(8–9), 425–436.
- Giglberger, S., Golub, L. E., Bel'kov, V. V., Danilov, S. N., Schuh, D., Gerl, C., & et al. (2007). Rashba and Dresselhaus spin splittings in semiconductor quantum wells measured by spin photocurrents. *Physical Review B*, 75, 035327.

- Gişi, B. (2012). *Electronic structure of the quantum wires with spin-orbit interactions under the influence of in-plane magnetic fields*. Master's Thesis, Dokuz Eylül University.
- Gori-Giorgi, P., Attaccalite, C., Moroni, S., & Bachelet, G. B. (2003). Two dimensional electron gas: Correlation energy versus density and spin polarization. *International Journal of Quantum Chemistry*, 91(2), 126–130.
- Governale, M., & Zülicke, U. (2002). Spin accumulation in quantum wires with strong Rashba spin-orbit coupling. *Physical Review B*, 66(7), 073311.
- Governale, M., & Zülicke, U. (2004). Rashba spin splitting in quantum wires. *Solid State Communications*, 131, 581.
- Grünberg, P. (2007). Nobel lecture: From spinwaves to giant magnetoresistance (GMR) and beyond. The Nobel Foundation 2007. Retrieved May 25, 2013, from <http://www.nobelprize.org/nobelprizes/physics/laureates/2007/grunberg-lecture.html>.
- Gujarathi, S., Alam, K. M., & Pramanik, S. (2012). Magnetic-field-induced spin texture in a quantum wire with linear Dresselhaus spin-orbit coupling. *Physical Review B*, 85(4), 045413.
- Gunnarsson, O., & Lundqvist, B. I. (1976). Exchange and correlation in atoms, molecules, and solids by the spin-density-functional formalism. *Physical Review B*, 13, 4274–4298.
- Gunnarsson, O., & Lundqvist, B. I. (1977). Erratum: Exchange and correlation in atoms, molecules, and solids by the spin-density-functional formalism. *Physical Review B*, 15(12), 6006.
- Guzenko, V. A., Bringer, A., Knobbe, J., Hardtdegen, H., & Schäpers, T. (2007). Rashba effect in $Ga_xIn_{1-x}As/InP$ quantum wire structures. *Applied Physics A*, 87(3), 577–584.

- Hartree, D. R. (1928). The wave mechanics of an atom with a non-coulomb central field. part i. theory and methods, part ii. some results and discussions. *Mathematical Proceedings of the Cambridge Philosophical Society*, 24, 89–110.
- Heinonen, O., Kinaret, J. M., & Johnson, M. D. (1999). Ensemble density-functional approach to charge-spin textures in inhomogeneous quantum hall systems. *Physical Review B*, 59(12), 8073–8083.
- Herman, M. A. (1994). Semiconductor quantum wire structures: MBE growth and application perspectives in optoelectronic devices. *Opto-Electronics Review*, 2(3), 55.
- Hohenberg, P., & Kohn, W. (1964). Inhomogeneous electron gas. *Physical Review*, 136(520), B864–871.
- Hutton, D. V. (2004). *Fundamentals of finite element analysis*. (1st ed.). New York: McGraw-Hill.
- Kaneko, T., Koshino, M., & Ando, T. (2008). Numerical study of spin relaxation in quantum wire with spin-orbit interaction. *Physical Review B*, 78, 245303.
- Kantser, V. G. (2006). Materials and structures for semiconductor spintronics. *Journal of Optoelectronics and Advanced Materials*, 8(2), 425–438.
- Kash, K., Scherer, A., M. Worklock, J., Craighead, H. G., & Tamargo, M. C. (1986). Optical spectroscopy of ultrasmall structures etched from quantum wells. *Applied Physics Letters*, 49, 1043.
- Khordad, R. (2013). Optical properties of quantum wires: rashba effect and external magnetic field. *Journal of Luminescence*, 134(201–207).
- Knobbe, J., & Schäpers, T. (2005). Magnetosubbands of semiconductor quantum wires with Rashba spin-orbit coupling. *Physical Review B*, 71(3), 035311.
- Kohanoff, J. (2006). *Electronic structure calculations for solids and molecules, theory and computational methods*. (1st ed.). Cambridge: Cambridge University Press.

- Kohn, W., & Sham, L. J. (1965). Self-consistent equations including exchange and correlation effects. *Physical Review*, *140*(4A), A1133–A1138.
- Könemann, J., Haug, R. J., Maude, D. K., Fal’ko, V. I., & Altshuler, B. L. (2005). Spin-orbit coupling and anisotropy of spin splitting in quantum dots. *Physical Review Letters*, *94*(22), 226404.
- Krich, J. J., & Halperin, B. I. (2007). Cubic dresselhaus spin-orbit coupling in 2D electron quantum dots. *Physical Review Letters*, *98*, 226802.
- Kübler, J., Höck, K.-H., Sticht, J., & Williams, A. R. (1988a). Density functional theory of non-collinear magnetism. *Journal of Physics F: Metal Physic*, *18*, 469–483.
- Kübler, J., Höck, K.-H., Sticht, J., & Williams, A. R. (1988b). Local spin-density functional theory of noncollinear magnetism (invited). *Journal of Applied Physics*, *63*(8), 3482–3486.
- Kumar, M., Lahon, S., Jha, P. K., & Mohan, M. (2013). Energy dispersion and electron g-factor of quantum wire in external electric and magnetic fields with rashba spin orbit interaction. *Superlattices and Microstructures*, *57*, 11–18.
- Kwon, Y. W., & Bang, H. (1997). *The finite element method using MATLAB*. (2nd ed.). United States of America: CRC Press.
- Malet, F., Pi, M., Barranco, M., & Lipparini, E. (2005). Ground state structure and conductivity of quantum wires of infinite length and finite width. *Physical Review B*, *72*(20), 205326.
- Malet, F., Pi, M., Barranco, M., Serra, L., & Lipparini, E. (2007). Exchange-correlation effects on quantum wires with spin-orbit interactions under the influence of in-plane magnetic fields. *Physical Review B*, *76*, 115306.
- Martin, R. M. (2004). *Electronic structure: Basic theory and practical methods*. (1st ed.). New York: Cambridge University Press.

- Meier, L., Salis, G., Gini, E., Shorubalko, I., & Ensslin, K. (2008). Two-dimensional imaging of the spin-orbit effective magnetic field. *Physical Review B*, *77*(3), 035305.
- Meier, L., Salis, G., Shorubalko, I., Gini, E., Schön, S., & Ensslin, K. (2007). Measurement of Rashba and Dresselhaus spin-orbit magnetic fields. *Nature Physics*, *3*(9), 650–654.
- Miller, J. B., Zumbühl, D. M., Marcus, C. M., Lyanda-Geller, Y. B., Goldhaber-Gordon, D., Campman, K., & et al. (2003). Gate-controlled spin-orbit quantum interference effects in lateral transport. *Physical Review Letters*, *90*(7), 076807.
- Mireles, F., & Kirczenow, G. (2001). Ballistic spin-polarized transport and Rashba spin precession in semiconductor nanowires. *Physical Review B*, *64*(2), 024426.
- Moroz, A. V., & Barnes, C. H. W. (1999). Effect of the spin-orbit interaction on the band structure and conductance of quasi-one-dimensional systems. *Physical Review B*, *60*(20), 14272–14285.
- Moroz, A. V., & Barnes, C. H. W. (2000). Spin-orbit interaction as a source of spectral and transport properties in quasi-one-dimensional systems. *Physical Review B*, *61*(4), R2464–R2467.
- Nitta, J. (2004). Selected papers: Semiconductor spintronics. *Nippon Telegraph And Telephone Corporation Technical Review*, *2*(6), 31–36.
- Nitta, J., Akazaki, T., Takayanagi, H., & Enoki, T. (1997). Gate control of spin-orbit interaction in an inverted $\text{In}_{0.53}\text{Ga}_{0.47}\text{As}/\text{In}_{0.52}\text{Al}_{0.48}\text{As}$ heterostructure. *Physical Review Letters*, *78*(7), 1335–1338.
- Nix, M. B. (2006). Fabrication of spin valves using soft lithography techniques. *Caltech Undergraduate Research Journal*, *7*(1).
- Parr, R. G., & Yang, W. (1989). *Density-functional theory of atoms and molecules*. (1st ed.). New York: Oxford University Press.
- Pask, J. E., Klein, B. M., Sterne, P. A., & Fong, C. Y. (2001). Finite-element methods in electronic-structure theory. *Computer Physics Communications*, *135*, 1–34.

- Perdew, J. P., & Wang, Y. (1992). Accurate and simple analytic representation of the electron-gas correlation energy. *Physical Review B*, *45*(23), 13244–13249.
- Perroni, C. A., Bercioux, D., Ramaglia, V. M., & Cataudella, V. (2007). Rashba quantum wire: exact solution and ballistic transport. *Journal of Physics: Condensed Matter*, *19*(18), 186227.
- Petro, P. M., Gossard, A. C., Logan, R. A., & Wiegmann, W. (1982). Toward quantum well wires: Fabrication and optical properties. *Applied Physics Letters*, *41*, 635.
- Picciotto, R. D., Stormer, H. L., Pfeiffer, L. N., Baldwin, K. W., & West, K. W. (2001). Four-terminal resistance of a ballistic quantum wire. *Nature*, *411*, 51–54.
- Pramanik, S., Bandyopadhyay, S., & Cahay, M. (2007). Energy dispersion relations of spin-split subbands in a quantum wire and electrostatic modulation of carrier spin polarization. *Physical Review B*, *76*(15), 155325.
- Quay, C. H. L., Hughes, T. L., Sulpizio, J. A., Pfeiffer, L. N., Baldwin, K. W., West, K. W., & et al. (2010). Observation of a one-dimensional spin-orbit gap in a quantum wire. *Nature Physics*, *6*(5), 336–339.
- Rahman, S. S. (2007). *Spontaneous spin polarization due to lateral spin-orbit coupling in InAs quantum point contacts*. Ph.D. Thesis, University of Cincinnati.
- Ram-Mohan, L. R. (2002). *Finite element and boundary element applications in quantum mechanics*. (1st ed.). Oxford: Oxford University Press.
- Räsänen, E. (2004). *Electronic properties of non-circular quantum dots*. Ph.D. Thesis, Helsinki University of Technology.
- Rashba, E. (1960). Properties of semiconductors with an extremum loop. 1. cyclotron and combinational resonance in a magnetic field perpendicular to the plane of the loop. *Soviet Physics: Solid State*, *2*(6), 1109–1122.
- Rashba, E. I. (2007). *Semiconductor spintronics: Progress and challenges, in future trends in microelectronic*. (1st ed.). Canada: John Wiley & Sons, Inc.

- Reddy, J. N. (1993). *An introduction to the finite element method*. (2nd ed.). McGraw-Hill.
- Sakurai, J. J. (1967). *Advanced quantum mechanics*. (1st ed.). Addison-Wesley.
- Schäpers, T., Guzenko, V. A., Bringer, A., Akabori, M., Hagedorn, M., & Hardtdegen, H. (2009). Spin-orbit coupling in $Ga_xIn_{1-x}As/InP$ two-dimensional electron gases and quantum wire structures. *Semiconductor Science and Technology*, 24(6), 064001.
- Schäpers, T., Knobbe, J., & Guzenko, V. A. (2004a). Effect of Rashba spin-orbit coupling on magnetotransport in InGaAs/InP quantum wire structures. *Physical Review B*, 69(23), 235323.
- Schäpers, T., Knobbe, J., Guzenko, V. A., & van der Hart, A. (2004b). Rashba effect in gated InGaAs/InP quantum wire structures. *Physica E: Low-dimensional Systems and Nanostructures*, 21(2–4), 933–936.
- Schliemann, J., Egues, J. C., & Loss, D. (2003). Nonballistic spin-field-effect transistor. *Physical Review Letters*, 90, 146801.
- Schöll, E. (1998). *Theory of transport properties of semiconductor nanostructures*. (1st ed.). London: Chapman & Hall.
- Serra, L., Sanchez, D., & Lopez, R. (2005). Rashba interaction in quantum wires with in-plane magnetic fields. *Physical Review B*, 72, 235309.
- Shafir, E., Shen, M., & Saikin, S. (2004). Modulation of spin dynamics in a channel of a nonballistic spin field effect transistor. *Physical Review B*, 70(24), 241302.
- Shik, A. (1998). *Quantum wells: Physics and electronics of two-dimensional systems*. (1st ed.). Singapore: World Scientific Publishing.
- Singh, J. (2003). *Electronic and optoelectronic properties of semiconductor structures*. (1st ed.). Cambridge: Cambridge University Press.
- Slater, J. C. (1928). The self consistent field and the structure of atoms. *Physical Review*, 32(3), 339–348.

- Slater, J. C. (1951a). Magnetic effects and the Hartree-Fock equation. *Physical Review*, 82(4), 538–541.
- Slater, J. C. (1951b). A simplification of the Hartree-Fock method. *Physical Review*, 81(3), 385–390.
- Stern, N. P. (2008). *Electrical spin generation by the spin Hall effect in semiconductors*. Ph.D. Thesis, University of California, Santa Barbara.
- Sticht, J., Höck, K.-H., & Kübler, J. (1989). Non-collinear itinerant magnetism: The case of Mn₃Sn. *Journal of Physics: Condensed Matter*, 1(43).
- Studer, M., Walser, M. P., Baer, S., Rusterholz, H., Schön, S., Schuh, D., & et al. (2010). Role of linear and cubic terms for drift-induced Dresselhaus spin-orbit splitting in a two-dimensional electron gas. *Physical Review B*, 82(23), 235320.
- Sugahara, S., & Nitta, J. (2010). Spin-transistor electronics: An overview and outlook. *Proceedings of the Institute of Electrical and Electronics Engineers*, 98(12), 2124–2154.
- Sun, Y. (1995). *Theory of semiconductor quantum wires*. Ph.D. Thesis, Simon Fraser University.
- Szabo, A., & Ostlund, N. S. (1996). *Modern quantum chemistry: Introduction to advanced electronic structure theory*. (2nd ed.). New York: Dover Publications.
- Tanatar, B., & Ceperley, D. M. (1989). Ground state of the two-dimensional electron gas. *Physical Review B*, 39(8), 5005–5016.
- Thijssen, J. M. (1999). *Computational physics*. (1st ed.). Cambridge: Cambridge University Press.
- Thomas, L. H. (1927). The calculation of atomic fields. *Mathematical Proceedings of the Cambridge Philosophical Society*, 23(05), 542–548.
- Thompson, A. G. (1997). MOCVD technology for semiconductors. *Materials Letters*, 30, 255–263.

- Toffoli, H. (2009). *Summer school on modeling nanostructures using density functional theory: Lecture notes*. Izmir Institute Of Technology. Retrieved April 20, 2013, from <http://nanodft09.iyte.edu.tr/pdf/HT-L2.pdf>.
- Upadhyaya, P., Pramanik, S., & Bandyopadhyay, S. (2008a). Optical transitions in a quantum wire with spin-orbit interaction and its applications in terahertz electronics: Beyond zeroth-order theory. *Physical Review B*, 77(15), 155439.
- Upadhyaya, P., Pramanik, S., Bandyopadhyay, S., & Cahay, M. (2008b). Magnetic field effects on spin texturing in a quantum wire with Rashba spin-orbit interaction. *Physical Review B*, 77(4), 045306.
- Wagner, R. (2009). *G-factor, effective mass and spin susceptibility of a 2-dimensional electron gas*. Master's Thesis, University of Basel.
- Wang, X.-L., & Voliotis, V. (2006). Epitaxial growth and optical properties of semiconductor quantum wires. *Journal of Applied Physics*, 99, 121301.
- Weisbuch, C., & Vinter, B. (1991). *Quantum semiconductor structures: Fundamentals and applications*. (1st ed.). California: Academic Press.
- Wigner, E. (1934). On the interaction of electrons in metals. *Physical Review*, 46(11), 1002–1011.
- Winkler, R. (2003). *Spin-orbit coupling effects in two-dimensional electron and hole systems*. (1st ed.). Berlin: Springer.
- Wolf, S. A., Awschalom, D. D., Buhrman, R. A., Daughton, J. M., von Molnár, S., Roukes, M. L., & et al. (2001). Spintronics: A spin-based electronics vision for the future. *Science*, 294(5546), 1488–1495.
- Zhang, S., Liang, R., Zhang, E., Zhang, L., & Liu, Y. (2006). Magnetosubbands of semiconductor quantum wires with Rashba and Dresselhaus spin-orbit coupling. *Physical Review B*, 73, 155316.
- Zhang, T.-Y., Zhao, W., & Li, X.-M. (2009). Energy dispersion of the electrosubbands in parabolic confining quantum wires: interplay of Rashba, Dresselhaus, lateral

spin-orbit interaction and the Zeeman effect. *Journal of Physics: Condensed Matter*, 21(33), 335501.

Zieliński, T. G. (2012). *Introductory Course on Modelling of Multiphysics Problems*. Retrieved April 17, 2013, from <http://www.ippt.gov.pl/tzielins/index.php?im=1&id=lectures.html>.

Zutic, I., Fabian, J., & Sarma, S. D. (2004). Spintronics: Fundamentals and applications. *Reviews of Modern Physics*, 76(2), 323–410.